27
4-27-80
NTIS
MMB

LBL-10837
GSRMP-8

Detailed Report on Tested Models Companion Report 2 to Simulation of Geothermal Subsidence (LBL-10571)

MASTER

I. Miller, W. Dershowitz, K. Jones,
L. Myer, K. Roman, and M. Schauer

Golder Associates, Inc.

Geothermal Subsidence Research Management Program

March 1980

Earth Sciences Division
Lawrence Berkeley Laboratory
University of California

DISTRIBUTION OF THIS DOCUMENT IS UNLIMITED

Prepared for the U.S. Department of Energy under Contract W-7405-ENG-48

DISCLAIMER

This report was prepared as an account of work sponsored by an agency of the United States Government. Neither the United States Government nor any agency Thereof, nor any of their employees, makes any warranty, express or implied, or assumes any legal liability or responsibility for the accuracy, completeness, or usefulness of any information, apparatus, product, or process disclosed, or represents that its use would not infringe privately owned rights. Reference herein to any specific commercial product, process, or service by trade name, trademark, manufacturer, or otherwise does not necessarily constitute or imply its endorsement, recommendation, or favoring by the United States Government or any agency thereof. The views and opinions of authors expressed herein do not necessarily state or reflect those of the United States Government or any agency thereof.

DISCLAIMER

Portions of this document may be illegible in electronic image products. Images are produced from the best available original document.

LEGAL NOTICE

This book was prepared as an account of work sponsored by an agency of the United States Government. Neither the United States Government nor any agency thereof, nor any of their employees, makes any warranty, express or implied, or assumes any legal liability or responsibility for the accuracy, completeness, or usefulness of any information, apparatus, product, or process disclosed, or represents that its use would not infringe privately owned rights. Reference herein to any specific commercial product, process, or service by trade name, trademark, manufacturer, or otherwise, does not necessarily constitute or imply its endorsement, recommendation, or favoring by the United States Government or any agency thereof. The views and opinions of authors expressed herein do not necessarily state or reflect those of the United States Government or any agency thereof.

Printed in the United States of America
Available from
National Technical Information Service
U.S. Department of Commerce
5285 Port Royal Road
Springfield, VA 22161
Price Code: A10

DETAILED REPORT ON TESTED MODELS
COMPANION REPORT 2
TO
SIMULATION OF GEOTHERMAL SUBSIDENCE
(LBL 10571)

PREPARED FOR LAWRENCE BERKELEY LABORATORY
by GOLDER ASSOCIATES
UNDER SUBCONTRACT 3730302

Prepared by: I. Miller, W. Dershowitz, K. Jones,
L. Meyer, K. Roman, and M. Schauer

78304D
D/81

March 1980

DISCLAIMER

This book was prepared as an account of work sponsored by an agency of the United States Government. Neither the United States Government nor any agency thereof, nor any of their employees, makes any warranty, express or implied, or assumes any legal liability or responsibility for the accuracy, completeness, or usefulness of any information, apparatus, product, or process disclosed, or represents that its use would not infringe privately owned rights. Reference herein to any specific commercial product, process, or service by trade name, trademark, manufacturer, or otherwise, does not necessarily constitute or imply its endorsement, recommendation, or favoring by the United States Government or any agency thereof. The views and opinions of authors expressed herein do not necessarily state or reflect those of the United States Government or any agency thereof.

DISTRIBUTION OF THIS DOCUMENT IS UNLIMITED

This report is the second in a series of three companion reports presenting the results of an investigation into the use of mathematical models for predicting subsidence caused by geothermal extraction. The simulation of results of the investigation are summarized in the report, "Simulation of "Geothermal Subsidence" (LBL 10571). The titles of the supporting reports are listed below.

Report No.	Title	
1	Physical Processes of Compaction	LBL-10838
3	Case Study Data Base	LBL-10839

An additional report on the subject of reservoir models was generated as part of this project. The report was produced in 1979 by Dr. George F. Pinder under subcontract to Golder Associates and is titled "State-of-the-Art Review of Geothermal Reservoir Modelling" (LBL 9093).

ABSTRACT

The Lawrence Berkeley Laboratory of the University of California is conducting an ongoing research program aimed at improved understanding and control of ground movements caused by geothermal power production. As part of this research program, Golder Associates, acting under subcontract to the University, performed an assessment of existing mathematical models for subsidence simulation and prediction. This report presents detailed analyses of the theory, power, usability, and performance of the seven models used in conjunction with this research. The models used were:

- Hand-calculation techniques
- The nucleus-of-strain method
- The one-dimensional Terzaghi consolidation method
- The two-dimensional boundary-integral-equation method
- Two-dimensional finite-element coupled fluid flow and deformation
- Three-dimensional integrated finite difference, coupled fluid flow, heat flow, and porosity change
- The three-dimensional displacement discontinuity method.

TABLE OF CONTENTS

		Page
ABSTRACT		iii
1.0	INTRODUCTION	1
	1.1 REFERENCES	11
2.0	HAND CALCULATIONS	13
	2.1 INTRODUCTION	13
	2.2 SOLUTION METHOD - GENERAL THEORY	13
	2.3 CAPABILITIES AND LIMITATIONS	20
	2.4 USABILITY	20
	2.5 PERFORMANCE ON SAMPLE TEST PROBLEMS	21
	2.6 CONCLUSIONS	30
	2.7 REFERENCES	30
3.0	NUCLEUS-OF-STRAIN MODEL "SUBSID"	31
	3.1 INTRODUCTION	31
	3.2 SOLUTION METHOD - GENERAL THEORY	31
	3.3 CAPABILITIES AND LIMITATIONS	35
	3.4 USABILITY	36
	3.5 PERFORMANCE ON SAMPLE PROBLEMS	39
	3.6 CONCLUSIONS	46
	3.7 LIST OF SYMBOLS	46
	3.8 REFERENCES	48
4.0	ONE-DIMENSIONAL CONSOLIDATION MODEL "UPDOWN"	49
	4.1 INTRODUCTION	49
	4.2 SOLUTION METHOD - GENERAL THEORY	49
	4.3 CAPABILITIES AND LIMITATIONS	50
	4.4 USABILITY	53
	4.5 PERFORMANCE ON SAMPLE PROBLEMS	55
	4.6 CONCLUSIONS	58
	4.7 LIST OF SYMBOLS	58
	4.8 REFERENCES	59
5.0	BOUNDARY-ELEMENT MODEL "BIEM2D"	61
	5.1 INTRODUCTION	61
	5.2 SOLUTION METHOD - GENERAL THEORY	61
	5.3 CAPABILITIES AND LIMITATIONS	67
	5.4 USABILITY	68
	5.5 PERFORMANCE ON SAMPLE PROBLEMS AND CASE STUDIES	71
	5.6 CONCLUSION	81
	5.7 LIST OF SYMBOLS	81
	5.8 REFERENCES	82

TABLE OF CONTENTS (Cont.)

		Page
6.0	FINITE-ELEMENT STRESS-STRAIN FLOW MODEL "CONSOL3"	83
6.1	INTRODUCTION	83
6.2	SOLUTION METHOD - GENERAL THEORY	83
6.3	CAPABILITIES AND LIMITATIONS	84
6.4	USABILITY	86
6.5	PERFORMANCE ON SAMPLE PROBLEMS AND CASE STUDIES	90
6.6	CONCLUSIONS	94
6.7	REFERENCES	97
7.0	MASS-AND-HEAT FLOW MODEL "CCC"	99
7.1	INTRODUCTION	99
7.2	SOLUTION METHOD - GENERAL THEORY	99
7.3	CAPABILITIES AND LIMITATIONS	105
7.4	USABILITY	108
7.5	PERFORMANCE ON TEST PROBLEMS AND CASE STUDIES	112
7.6	CONCLUSIONS	118
7.7	LIST OF SYMBOLS	120
7.8	REFERENCES	122
8.0	THREE-DIMENSIONAL DISPLACEMENT-DISCONTINUITY MODEL "NFOLD"	125
8.1	INTRODUCTION	125
8.2	SOLUTION METHOD - GENERAL THEORY	126
8.3	CAPABILITIES AND LIMITATIONS	128
8.4	USABILITY	133
8.5	PERFORMANCE ON SAMPLE PROBLEMS AND CASE STUDIES	135
8.6	CONCLUSIONS	139
8.7	REFERENCES	139
APPENDIX A -	USERS' MANUAL - PROGRAM "SUBSID"	A-1
A.1	INTRODUCTION	A-3
A.2	INPUT	A-5
A.3	OUTPUT	A-10
A.4	SAMPLE PROBLEM	A-10
A.5	MODELING A CYLINDER WITH SPHERES	A-16
A.6	CHANGING THE PROGRAM	A-17
A.7	SOURCE LISTING FOR SUBSID	A-20

TABLE OF CONTENTS (Cont.)

	Page
APPENDIX B - USERS' MANUAL - PROGRAM "BIEM2D"	B-1
B.1 INTRODUCTION	B-3
B.2 DISCUSSION OF INPUT PARAMETERS	B-4
B.3 INPUT	B-12
B.4 OUTPUT	B-17
B.5 SAMPLE PROBLEM	B-17
B.6 SOURCE LISTING FOR BIEM2D	B-23

LIST OF TABLES

Table		Page
1-1	Material Properties	8
1-2	Sample Problem Summary	9
2-1	Values of A for Ranges of Values of $\rho = r/R$ and $\eta = D/R$	19
2-2	Values of B for Ranges of Values of $\rho = r/R$ and $\eta = D/R$	19
3-1	Comparison of Vertical and Horizontal Surface Displacement, Sample Problem 1	40
3-2	Comparison of Vertical and Horizontal Surface Displacement, Sample Problem 5	43
4-1	UPDOWN Solution Efficiency	54
6-1	CONSOL3 Solution Efficiency	89
8-1	NFOLD Element Types	130
A-1	Cylinders Modeled with Spheres	A-4

LIST OF FIGURES

Figure		Page
1-1	Sample Problem 1, Infinite Confined Reservoir	2
1-2	Sample Problem 2, Infinite Leaky Reservoir	3
1-3	Sample Problem 3, Finite Confined Reservoir	4
1-4	Sample Problem 4, Finite Leaky Reservoir	5
1-5	Sample Problem 5, Thick Finite Confined Reservoir	6
1-6	Sample Problem 6, Finite Confined Wedge-Shaped Reservoir	7
2-1	Hand-Calculation Method, Surface Subsidence Sample Problem 3	25
2-2	Hand-Calculation Method, Surface Subsidence Sample Problem 4	25
2-3	Hand-Calculation Method, Surface Subsidence Sample Problem 5 (Single Disk and 10-Disk Stack)	27
2-4	Hand-Calculation Method, Surface Subsidence Sample Problem 6	29
3-1	Nucleus-of-Strain Model, Solution Time as a Function of Number of Source Spheres and Number of Observation Points	38
3-2	Nucleus-of-Strain Model, Surface Subsidence Using 9, 25, and 169 Spheres, Sample Problem 3	41
3-3	Nucleus-of-Strain Model, Horizontal Deformation of the Surface Using 9, 25 and 169 Spheres, Sample Problem 3	42
3-4	Nucleus-of-Strain Model, Surface Subsidence Using 4 and 100 Spheres, Sample Problem 5	44
3-5	Nucleus-of-Strain Model, Horizontal Deformation of the Surface Using 4 and 100 Spheres, Sample Problem 5	44
3-6	Nucleus-of-Strain Model, Contours of Surface Subsidence, Sample Problem 5	47
4-1	One-Dimensional Consolidation Model, Finite Difference Grid in Time and Space	51
4-2	One-Dimensional Consolidation Model Set Up for Sample Problem 2	52

LIST OF FIGURES (Cont.)

Figure		Page
4-3	One-Dimensional Consolidation Model, Variation in Effective Stress with Time, Sample Problem 2	57
4-4	One-Dimensional Consolidation Model, Aquitard Compaction as a Function of Time, Sample Problem 2	57
5-1	Boundary-Integral-Equation Method, Theoretical Development	63
5-2	Boundary-Integral-Equation Method, Solution Efficiency	70
5-3	Boundary-Integral-Equation Method, Element Configuration of Sample Problem 1	72
5-4	Boundary-Integral-Equation Method, Variation in Vertical Displacement with Depth, Sample Problem 1	74
5-5	Boundary-Integral-Equation Method, Element Configuration of Sample Problem 3	75
5-6	Boundary-Integral-Equation Method, Vertical Displacement of Ground Surface and Reservoir Top and Bottom, Sample Problem 3	75
5-7	Boundary-Integral-Equation Method, Element Configuration of Sample Problem 5	77
5-8	Boundary-Integral-Equation Method, Vertical Displacement of Ground Surface and Reservoir Top and Bottom, Sample Problem 5	77
5-9	Boundary-Integral-Equation Method, Element Configuration of Sample Problem 6	78
5-10	Boundary-Integral-Equation Method Vertical Displacement of Ground Surface and Reservoir Top and Bottom, Sample Problem 6	79
6-1	Two-Dimensional Finite-Element Model, Solution Efficiency as a Function of Number of Elements	88

LIST OF FIGURES (Cont.)

Figure		Page
6-2	Two-Dimensional Finite-Element Model, Formulation for Sample Problem 2	91
6-3	Two-Dimensional Finite-Element Model, Formulation for Sample Problem 4	93
6-4	Two-Dimensional Finite-Element Model, Pore-Pressure Decrease on Vertical Axis of Symmetry, Sample Problem 4	95
6-5	Two-Dimensional Finite-Element Model, Pore-Pressure Decrease at Lower Boundary of Aquifer, Sample Problem 4	95
6-6	Two-Dimensional Finite-Element Model, Vertical Displacement at Ground Surface and Upper Boundary of Aquitard, Sample Problem 4	96
7-1	Heat-and-Mass Flow Model, Solution Efficiency as a Function of Number of Nodes	111
7-2	Heat-and-Mass Flow Model, Element Layout for Sample Problem 2	113
7-3	Heat-and-Mass Flow Model, Pore-Pressure Drop with Time, Sample Problem 2	115
7-4	Heat-and-Mass Flow Model, Reservoir Compaction With Constant and Void Ratio Dependent Permeability, Sample Problem 2	115
7-5	Heat-and-Mass Flow Model, Element Layout for Sample Problem 4	116
7-6	Heat-and-Mass Flow Model, Pore-Pressure Profile at 5 Years, Sample Problem 4	117
7-7	Heat-and-Mass Flow Model, Pore-Pressure Drop in Axisymmetric and 2-D Planar Flow Models After 5 Years, Sample Problem 4	117
7-8	Heat-and-Mass Flow Model, Reservoir Compaction After 5 Years, Planar Flow Model of Sample Problem 4	119
8-1	Three-Dimensional Displacement-Discontinuity Model, Coupling of Elements and Element Groups	129
8-2	Three-Dimensional Displacement-Discontinuity Model, Nonlinear Stress-Strain Properties	132
8-3	Three-Dimensional Displacement-Discontinuity Model, Solution Efficiency	136

LIST OF FIGURES (Cont.)

Figure		Page
8-4	Three-Dimensional Displacement-Discontinuity Model for Sample Problem 3	138
8-5	Three-Dimensional Displacement-Discontinuity Model, Element Layout for Austin Bayou Case Study	140
A-1	SUBSID Users' Manual, Ordering of Nodal Points Within Rectangular Grids	A-11
A-2	SUBSID Users' Manual, Geometry of Spheres Representing Sample Problem Reservoir	A-11
A-3	SUBSID Users' Manual, Forming Model Cylinder With Spheres (N=4)	A-19
B-1	BIEM2D Users' Manual, Illustration of Straight-Line Boundary Element	B-5
B-2	BIEM2D Users' Manual, Illustration of Circular-Arc Boundary Elements	B-5
B-3	BIEM2D Users' Manual, Illustration of Elliptical-Arc Boundary Element	B-7
B-4	BIEM2D Users' Manual, Example of Use of Straight-Line, Circular-Arc, and Elliptical-Arc Boundary Elements	B-7
B-5	BIEM2D Users' Manual, Examples of Symmetry Conditions	B-10

1.0 INTRODUCTION

This report presents detailed analyses of the theory, power, usability, and performance of the seven models used in conjunction with the report, "Simulation of Geothermal Subsidence" (Miller et al. 1980). Each model has unique capabilities and each has value in the simulation of geothermal subsidence.

A chapter is devoted to the study of each model. The models are listed below.

Chapter	Model
2	Hand Calculations
3	SUBSID - Nucleus of Strain
4	UPDOWN - One-Dimensional Consolidation
5	BIEM2D - Boundary-Integral-Equation Method
6	CONSOL3 - Nonlinear Finite Element
7	CCC - Heat-and-Mass Flow
8	NFOLD - 3-D Displacement Discontinuities

In addition, two users' manuals for programs developed or modified by Golder Associates are included as appendices A and B. Appendix A is a users' manual for SUBSID, developed on the basis of nucleus-of-strain formulation. Appendix B is a users' manual for BIEM2D, a program developed by John W. Bray at University College, London, and modified by Golder Associates to solve geothermal problems.

Sample problems were used to test the facility of each model. Figures 1-1 through 1-6 present the sample problems. Material properties are summarized in Table 1-1. Table 1-2 is a summary of the sample problems. Solution efficiency is measured by the number of CPU seconds required to achieve solution. Values are for Boeing Computer Services' CDC Cyber A5 computers

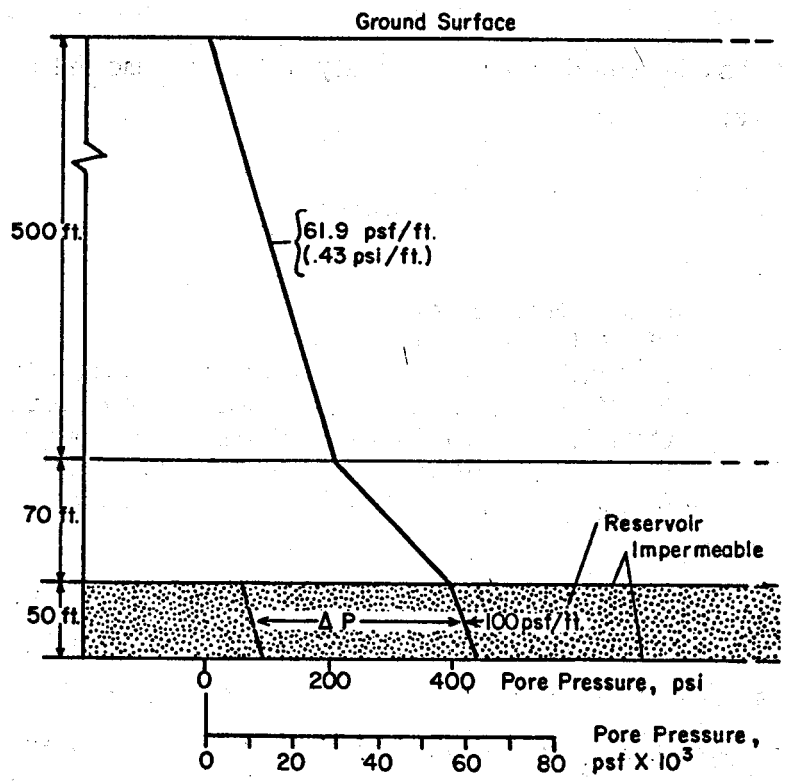

FIGURE 1-1
SAMPLE PROBLEM 1
INFINITE CONFINED RESERVOIR

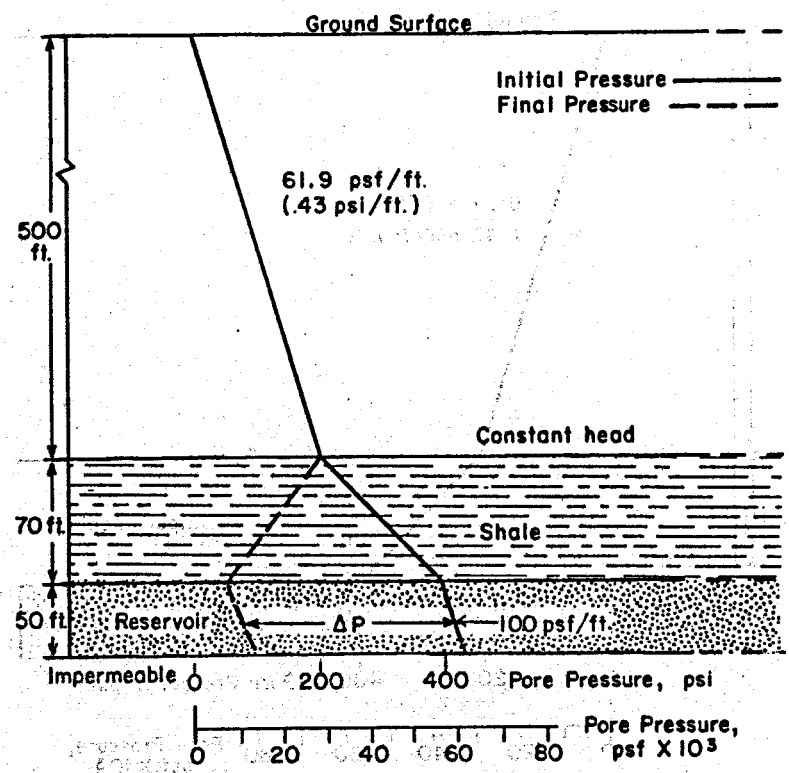

FIGURE 1-2
SAMPLE PROBLEM 2
INFINITE LEAKY RESERVOIR

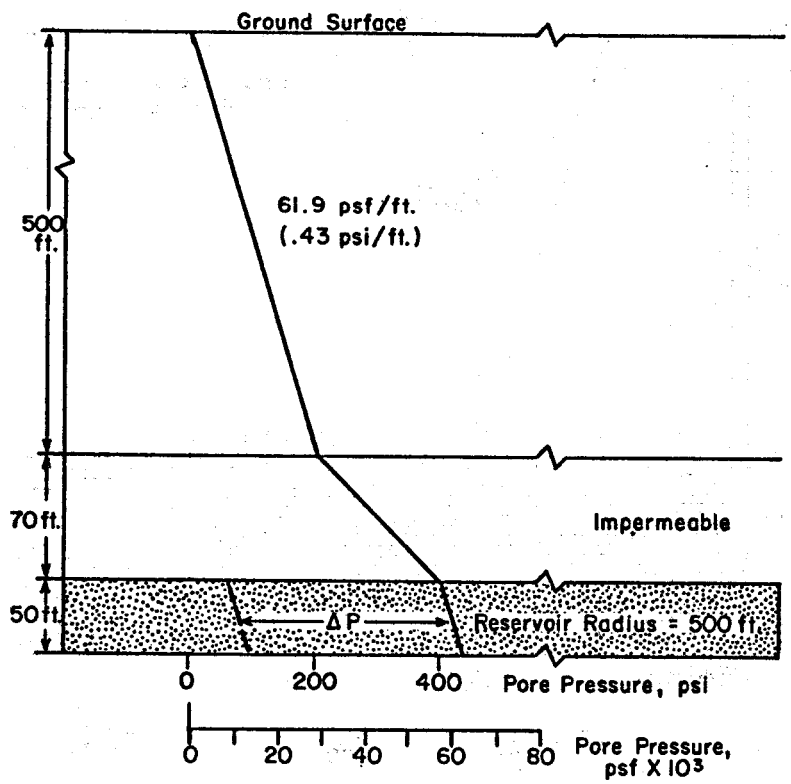

FIGURE 1-3
SAMPLE PROBLEM 3
FINITE CONFINED RESERVOIR

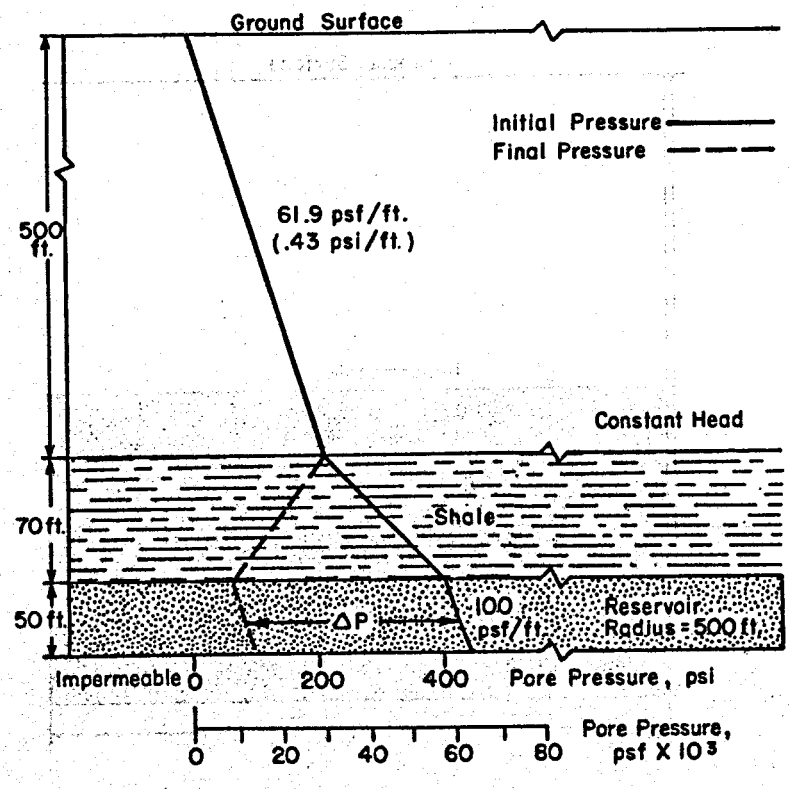

FIGURE 1-4
SAMPLE PROBLEM 4
FINITE LEAKY RESERVOIR

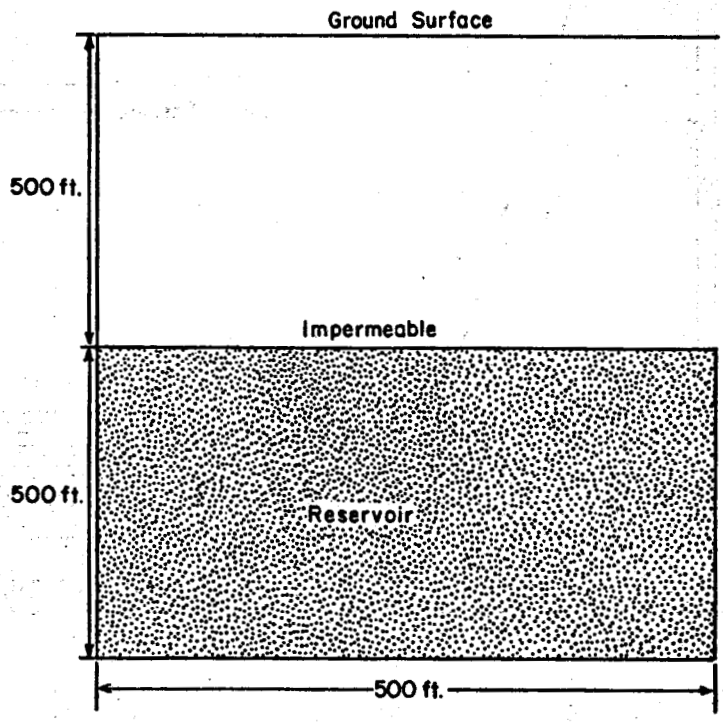

FIGURE 1-5
SAMPLE PROBLEM 5
THICK FINITE CONFINED RESERVOIR

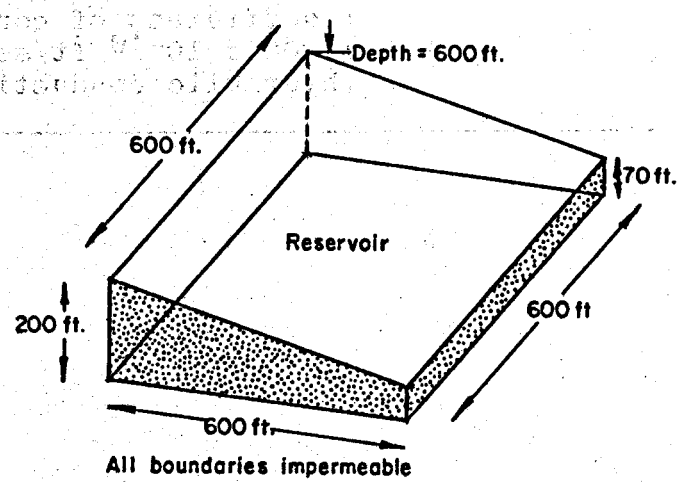

FIGURE 1-6
SAMPLE PROBLEM 6
FINITE CONFINED WEDGE-SHAPED RESERVOIR

TABLE 1-1
MATERIAL PROPERTIES

LINEAR ELASTIC	E-LOG P COMPRESSIBILITY
$K = 1.44 \times 10^{16}$ (bulk modulus)	$C_c = .15$ (compaction coefficient) $e = 0.3$ (void ratio)
$\nu = 0.25$ (Poisson's ratio)	$m_v = 1.111 \times 10^{-6}$ psf (coefficient of volume comp) $C_v = 1.736 \times 10^{-6}$ ft^2/sec (coefficient of consolidation) $k = 1.208 \times 10^{-10}$ ft/sec (hydraulic conductivity)

TABLE 1-2
SAMPLE PROBLEM SUMMARY
(from Miller et al. 1980)

PROBLEM	DESCRIPTION
1	Uniform linear elastic material properties throughout half-space. Rock mass saturated from surface downward. Reservoir interval bounded above and below by impermeable boundaries. Initial pore pressure distribution as shown in Figure 1-1. Uniform pressure drop of 5.04×10^4 psf in reservoir.
2	Linear elastic reservoir and elsewhere except shale layer; infinite reservoir. Shale layer e-log p compressibility. Impermeable boundary below reservoir. Constant head boundary at top of shale layer. Uniform pressure drop of 5.04×10^4 psf maintained in reservoir. Initial and final pore pressure distribution as shown.
3	Finite, thin reservoir of disk shape. Impermeable boundaries around reservoir. Uniform linear elastic material properties throughout. Initial pore pressure distribution as shown. Uniform pressure drop of 5.04×10^4 in reservoir.

TABLE 1-2 (Cont.)
SAMPLE PROBLEM SUMMARY

PROBLEM	DESCRIPTION
4	Same geometry as problem 3. Properties of shale layer above reservoir: e-log p compressibility. Impermeable boundary below reservoir. Constant head boundary at top of shale. Besides shale layer, material linear elastic. Uniform pressure drop of 5.04×10^4 psf maintained in reservoir. Initial and final pore pressure as shown.
5	Thick, cylindrically shaped reservoir. Uniform elastic material properties throughout. Uniform pressure drop of 2.16×10^4 psf in reservoir. Impermeable boundaries surrounding reservoir. Constant initial pore-pressure gradient of 61.92 psf from surface downward.
6	Wedge-shaped reservoir. Uniform elastic material properties throughout. Uniform pressure drop of 2.88×10^4 psf in reservoir. Impermeable boundaries surround reservoir. Constant initial pore pressure gradient of 61.92 psf/ft.

operating under EKS1. Cost (1979) is approximately $1 per CPU second.

1.1 REFERENCES

Miller, I., W. Dershowitz, K. Jones, L. Meyer, K. Roman, and M. Schauer (1980). "Simulation of Geothermal Subsidence," prepared for Lawrence Berkeley Laboratory, University of California, Berkeley, LBL 10571.

2.0 HAND CALCULATIONS

2.1 INTRODUCTION

There are a number of techniques available which allow an investigator to estimate subsidence in simple systems. For this study we have selected a hand-calculation technique that computes vertical compaction of the reservoir using one-dimensional equations. Propagation of the compaction to ground surface is modeled using a technique developed by Geertsma (1973) which treats the reservoir as an infinitely thin, horizontal disc. A relatively thick reservoir may be modeled using a stack of these disks.

2.2 SOLUTION METHOD - GENERAL THEORY

2.2.1 Theory

2.2.1.1 Compaction

The vertical compaction of the reservoir is computed assuming vertical strains with constant vertical stress. Companion Report 1 (Miller et al. 1980) presents the governing equations for this case. The compaction coefficient (Miller et al. 1980, equation [18]) is:

[2-1]

$$C_m = \frac{1 - K/K_s}{\lambda + 2G}$$

where: K is the bulk modulus of the reservoir material, which is assumed to be isotropic and elastic

K_s is the bulk modulus of the solid matrix

λ is Lame's elastic coefficient or the reservoir material

G is the shear modulus of the reservoir material.

It is commonly assumed that K_s is much greater than K, which gives C_m the same value as used in the conventional (Terzaghi) effective stress law: $C_m = \frac{1}{\lambda+2G}$

The amount of compaction in a layer due to pressure drop ΔP is:

[2-2a] $$\int_{Z_b}^{Z_t} C_m \Delta P dZ$$

where Z_b, Z_t are the elevations at the base and top of the layer.

The amount of compaction due to temperature drop ΔT is:

[2-2b] $$\int_{Z_b}^{Z_t} \frac{3K\alpha}{\lambda+2G} \Delta T dZ$$

where α is the coefficient of isotropic linear thermal expansion of the reservoir material.

If the reservoir is homogeneous and of thickness H, then the total compaction is:

[2-3] $$C = H\left(C_m \Delta P + \frac{3K\alpha}{\lambda+2G} \Delta T\right)$$

where ΔP and ΔT are vertically averaged. In order to use equation [2-3], it is necessary to know ΔP and ΔT from reservoir-flow modeling calculations.

An alternative means of computing the one-dimensional compaction is based on knowing the volume of fluid produced. The resulting equation is based on adding a term for the thermal expansion of the fluid to equation [2-3] of Companion Report 1 (Miller et al. 1980):

[2-4]
$$C = H\left[\frac{\frac{\Delta V_w}{V} - n\alpha_f \Delta T}{1 + \frac{4}{3}\frac{G}{K_s} + \frac{n}{C_m}\left(\frac{1}{K_f} - \frac{1}{K_s}\right)} + \frac{3K\alpha}{\lambda + 2G}\Delta T\right]$$

where ΔV_w is the volume of fluid produced divided by the total

V is reservoir volume

n is the porosity

α_f is the coefficient of volumetric thermal expansion for the reservoir fluid

K_f is the bulk modulus (1/compressibility) of the reservoir fluid.

Equation [2-4] assumes that the bulk modulus of the fluid is constant and thus is not appropriate for steam-dominated reservoirs.

If the assumption is made that the bulk modulus of the matrix material, K_s, is much greater than the other elastic parameters (λ, G, K_s, K_f), then equation [2-4] becomes simpler.

[2-5]
$$C = HC_m \left[\frac{\frac{\Delta V_w}{V} - n\alpha_f \Delta T}{C_m + \frac{n}{K_f}} + 3K\alpha \Delta T \right]$$

A common nonlinear approach to estimating compaction is based on Terzaghi's one-dimensional e-log p relationship. The relationship is in terms of the void ratio e:

[2-6]
$$e = e_o - C_c \log_{10} \left(\frac{P_o + \Delta P}{P_o} \right)$$

where: e is the void ratio $\left(\frac{\text{volume of voids}}{\text{volume of solids}} \right)$

P is the effective vertical compressive stress = overburden weight minus the pore pressure

C_c is the compression index, a material property

e_o, P_o are the initial state.

Assuming that the volume of solids is constant, the vertical compressive strain is:

[2-7]
$$\varepsilon_z = \frac{e - e_o}{1 + e_o}$$

Two alternate forms of the relationship are based on differentiating it and are only valid for small changes in P:

[2-8]
$$e = e_o + a_v \Delta P$$

or
$$\varepsilon_v = \frac{-a_v \Delta P}{1 + e_o}$$

where: $a_v = \frac{de}{dP} = \frac{-.434C_c}{P_o}$

and

[2-9] $\varepsilon_v = -m_v \Delta P$

where: $m_v = \frac{1}{1+e_o}\frac{de}{dP} = \frac{-.434C_c}{P_o(1+e_o)}$

The reservoir compaction is found by integrating ε_v:

$$C = -\int_{z_b}^{z_t} \varepsilon_v \, dz$$

2.2.1.2 <u>Subsidence</u>

Geertsma (1973) presented a simple and powerful technique for computing the ground surface deformations due to an infinitely thin, disk-shaped reservoir. The reservoir and the surrounding material were assumed to be of identical materials with isotropic linear elastic properties. The following presentation is adapted directly from Geertsma.

The disk-shaped reservoir is assumed to be of radius R and buried at depth D. The ground movements at a radius r from the point overlying the center of the reservoir are:

[2-10] $$u_z = -2C\,\frac{2G+\lambda}{2G+2\lambda}\,R\int_0^\infty e^{-D\theta} J_1(\theta R) J_0(\theta r)\, d\theta$$

[2-11] $$u_r = 2C\,\frac{2G+\lambda}{2G+2\lambda}\,R\int_0^\infty e^{-D\theta} J_1(\theta R) J_1(\theta r)\, d\theta$$

where J_o and J_1 are Bessel functions of zero and first order, respectively.

Geertsma (1973) went on to tabulate specific values of the integrals in equations [2-10] and [2-11] in terms of specific values of the radius ratio $\rho = r/R$ and the depth-to-radius aspect ratio of the reservoir $\eta = D/R$. The tabular values are used in the following equations.

[2-12] $$u_z = -2C \frac{2G+\lambda}{2G+2\lambda} A(\rho,\eta)$$

[2-13] $$u_r = 2C \frac{2G+\lambda}{2G+2\lambda} B(\rho,\eta)$$

Specific values of A and B are given in tables 2-1 and 2-2.

Note that the ratio $\frac{2G+\lambda}{2G+2\lambda}$ equals $1-\nu$ where ν = Poisson's ratio. If the method is used for cases where the reservoir properties are different from the overburden properties, the compaction C should be computed using reservoir properties, but the Poisson's ratio for the overburden should be used when computing $\frac{2G+\lambda}{2G+2\lambda}$.

2.2.2 Numerical Methods

Application of the technique is straightforward. The reservoir compaction is determined using equations [2-3], [2-4], or [2-5]. The surface deformations are then computed using equations [2-12] and [2-13] and tables 2-1 and 2-2.

TABLE 2-1 VALUES OF A FOR RANGES OF VALUES OF $\rho = r/R$ AND $\eta = D/R$

ρ	0.0	0.2	0.4	0.6	0.8	1.0	1.2	1.4	1.6	1.8	2.0	3.0
0.0	1.0000	0.8039	0.6286	0.4855	0.3753	0.2929	0.2318	0.1863	0.1520	0.1258	0.1056	0.0513
0.2	1.0000	0.7983	0.6201	0.4771	0.3683	0.2876	0.2279	0.1835	0.1500	0.1244	0.1045	0.0510
0.4	1.0000	0.7789	0.5924	0.4508	0.3473	0.2720	0.2167	0.1754	0.1442	0.1202	0.1014	0.0502
0.6	1.0000	0.7349	0.5377	0.4043	0.3124	0.2470	0.1989	0.1628	0.1351	0.1135	0.0965	0.0488
0.8	1.0000	0.6301	0.4433	0.3368	0.2658	0.2147	0.1762	0.1465	0.1234	0.1049	0.0901	0.0470
1.0	0.5000	0.3828	0.3105	0.2559	0.2130	0.1787	0.1510	0.1286	0.1102	0.0951	0.0827	0.0449
1.2	0.0000	0.1544	0.1871	0.1795	0.1621	0.1453	0.1257	0.1103	0.0965	0.0848	0.0748	0.0424
1.4	0.0000	0.0717	0.1101	0.1216	0.1197	0.1120	0.1024	0.0925	0.0831	0.0744	0.0667	0.0398
1.6	0.0000	0.0400	0.0682	0.0829	0.0876	0.0865	0.0824	0.0768	0.0707	0.0646	0.0589	0.0370
1.8	0.0000	0.0249	0.0449	0.0580	0.0647	0.0668	0.0659	0.0633	0.0597	0.0557	0.0516	0.0343
2.0	0.0000	0.0168	0.0312	0.0418	0.0485	0.0519	0.0528	0.0520	0.0502	0.0477	0.0450	0.0315
3.0	0.0000	0.0042	0.0082	0.0118	0.0149	0.0174	0.0193	0.0207	0.0216	0.0221	0.0222	0.0198

TABLE 2-2 VALUES OF B FOR RANGES OF VALUES OF $\rho = r/R$ AND $\eta = D/R$

ρ	0.0	0.2	0.4	0.6	0.8	1.0	1.2	1.4	1.6	1.8	2.0	3.0
0.0	0.0000	0.0000	0.0000	0.0000	0.0000	0.0000	0.0000	0.0000	0.0000	0.0000	0.0000	0.0000
0.2	0.1015	0.0954	0.0804	0.0628	0.0472	0.0350	0.0259	0.0194	0.0147	0.0113	0.0089	0.0032
0.4	0.2134	0.1979	0.1622	0.1238	0.0917	0.0675	0.0500	0.0375	0.0285	0.0220	0.0173	0.0062
0.6	0.3530	0.3163	0.2443	0.1789	0.1298	0.0949	0.0703	0.0529	0.0405	0.0314	0.0248	0.0090
0.8	0.5721	0.4573	0.3151	0.2197	0.1570	0.1147	0.0854	0.0648	0.0500	0.0391	0.0311	0.0117
1.0	∞	0.5456	0.3422	0.2355	0.1693	0.1252	0.0945	0.0726	0.0567	0.0448	0.0359	0.0139
1.2	0.5235	0.4278	0.3072	0.2237	0.1666	0.1265	0.0976	0.0764	0.0605	0.0485	0.0393	0.0158
1.4	0.3293	0.3026	0.2482	0.1958	0.1535	0.1208	0.0958	0.0766	0.0619	0.0504	0.0414	0.0174
1.6	0.2338	0.2228	0.1962	0.1650	0.1358	0.1110	0.0907	0.0743	0.0611	0.0506	0.0422	0.0185
1.8	0.1767	0.1711	0.1566	0.1377	0.1180	0.0997	0.0838	0.0703	0.0590	0.0496	0.0420	0.0194
2.0	0.1390	0.1358	0.1272	0.1152	0.1018	0.0895	0.0762	0.0653	0.0559	0.0478	0.0410	0.0199
3.0	0.0580	0.0576	0.0562	0.0541	0.0514	0.0483	0.0449	0.0414	0.0380	0.0346	0.0314	0.0190

from Geertsma, 1973

2.3 CAPABILITIES AND LIMITATIONS

2.3.1 Geometric Capabilities and Limitations

The proposed method is clearly restricted to regular reservoir geometries. It is, however, valid to superimpose the effects of a number of disks. In this way it is possible to simulate fairly complex reservoir geometries. To do this well, however, more complete and extensive tabulations of the integrals in equations [2-10] and [2-11] should be developed.

The ground surface is assumed to be horizontal--an assumption that might be poor in mountainous areas.

The model computes deformations only for the ground surface and provides no values for subterranean deformations. It does not compute stress.

2.3.2 Flow Capabilities and Limitations

The model does not simulate flow.

2.3.3 Material Properties

The model assumes a linear elastic isotropic homogeneous half-space. All of these assumptions are questionable. The model can be used with nonlinear reservoir properties when computing the reservoir compaction, but this will induce some error.

2.4 USABILITY

The method is very simple to use and requires the minimum amount of input data.

2.4.1 Resume of Performance on Sample Test Problems and Case Studies

Reservoir compactions and surface subsidence profiles were determined for each sample problem and case study. Where necessary, the reservoir was made axisymmetric and the half-space material properties were made uniform so that compaction and subsidence could be approximately calculated by hand.

2.5 PERFORMANCE ON SAMPLE TEST PROBLEMS

2.5.1 Sample Problem 1: Confined Infinite Reservoir

The compaction coefficient for Sample Problem 1 (Figure 1-1) is computed as:

$$C_m = \frac{1 - K/K_s}{\lambda + 2G}$$

K_s is not specified, but for a typical value of K_s of 10^9 psf, the ratio K/K_s is almost zero. The values of ν and G are readily computed (see Miller et al. 1980 for a list of conversions) from $G = \frac{3K(1-2\nu)}{2(1+\nu)}$ and $\lambda = K - 2G/3$. The result is $C_m = 3.86 \times 10^{-7}$ psf^{-1}. The pore-pressure drop is 5.04×10^4 psf; thus for the 50-foot reservoir layer the compaction is:

$$C = 50(3.86 \times 10^{-7} \times 5.04 \times 10^4) = 0.972 \text{ ft.}$$

Since the reservoir is assumed infinite in extent, coefficient A equals 1.0 and thus the ground subsidence equals the compaction times $2(1-\nu)$ or 1.458 feet. There is no horizontal movement.

Using equations presented in Companion Report 1 (Miller et al. 1980), it is possible to compute changes in the horizontal stresses and in the pore volume as well as the quantity of fluid produced from the reservoir.

2.5.2 Sample Problem 2: Infinite Reservoir With Permeable Confining Layer

In Sample problem 2 (Figure 1-2), a permeable boundary exists between the reservoir interval and the overlying material; consequently, deformations and stress changes must also be calculated for this layer. Displacements and stresses within the reservoir interval will be the same as those obtained in sample problem 1.

The compressibility assumed for the confining shale layer was nonlinear, represented by an e-log p type expression. Displacements in the shale layer were therefore calculated using classical soil mechanics formulations. Pressures were assumed to be steady-state; therefore, the calculations represent ultimate displacement of the shale layer.

Assuming the uniform initial void ratio e_o throughout the confining layer, the total compaction of the layer is given by:

$$C = \frac{C_c}{1+e_o} \int_{z_1}^{z_2} \log_{10} \frac{\bar{\sigma}}{\bar{\sigma}_o} \, dz$$

Because the upper boundary of the clay or shale layer was assumed to remain at a constant pore pressure, the pore-pressure change varied with position in the layer from a maximum of 5.04×10^4 psf

at the reservoir top to zero at the top of the shale layer (Figure 1-2). Consequently, effective stress changes will also vary with position. The initial effective stress varied from 4.104×10^4 psf at Z = 500 feet to 2.45×10^4 psf at Z = 570 feet. In equation form:

$$\bar{\sigma}_o = 1.593 \times 10^5 - 236.6Z$$

After steady-state pressures have been reached, the effective stress varies from $4.10^4 \times 10^4$ psf at Z = 500 feet to 7.49×10^4 at Z = 570 feet. An expression for the final effective stress is thus:

$$\bar{\sigma} = -2.007 \times 10^5 + 483.4Z$$

Substituting these expressions into the above equation:

$$C = \frac{C_c}{1+e_o} \int_{500}^{570} \log_{10} \left(\frac{-2.007 \times 10^5 + 483.4\,Z}{1.593 \times 10^5 - 236.6\,Z} \right) dZ$$

Integrating and substituting $C_c = 0.15$ and $e_o = 0.3$ results in $u_z = 1.98$ feet. Similar to sample problem 1, this displacement would also be magnified by $2(1-\nu)$, giving a subsidence of 2.97 feet at the surface. Adding the deformation of the shale layer to the deformation of the reservoir layer yields a total surface displacement of 4.425 feet for sample problem 2.

2.5.3 Sample Problem 3: Confined Finite Reservoir

Problem 3 (Figure 1-3) is like problem 1 except that the reservoir has a finite lateral extent. The reservoir compaction

is the same as was computed in problem 1 (0.972 ft). If one assumes an axisymmetric reservoir, the surface subsidence can be calculated using equation [2-12] with $\eta = \frac{595}{500} = 1.19$.

$$u_z = -2(.972)(.75)A(\rho, 1.19)$$

A plot of surface subsidence as a function of distance from the reservoir centerline is presented in Figure 2-1. The maximum subsidence is 0.342 feet.

2.5.4 Sample Problem 4: Finite Reservoir With Confining Layer

Sample Problem 4 (Figure 1-4), is like problem 2 except that the reservoir has a finite lateral extent. The reservoir and shale layer compaction and the resulting surface subsidence may be approximately calculated by simplifying the system. Assuming that compaction in the shale occurs only in that portion of the layer vertically adjacent to the reservoir results in a lower bound on surface subsidence. At steady-state the compaction of the shale will be 1.98 feet, as is computed in problem 2, while the reservoir compaction is 0.972 feet. If one assumes cylindrical symmetry, the surface subsidence can be calculated using equation [2-12], modeling the two layers with disks at depths of 535 feet and 595 feet:

$$u_z = -2(.75)(0.972A(\rho, 1.19) + 1.98A(\rho, 1.07))$$

Uniform material properties in the half-space with Poisson's ratio equal to .25 have been assumed. The surface subsidence is plotted in Figure 2-2.

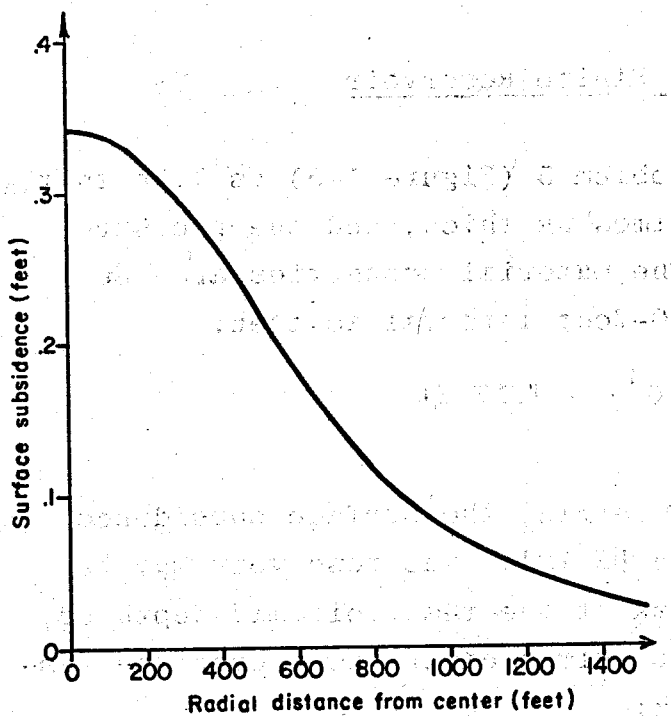

FIGURE 2-1: HAND-CALCULATION METHOD, SURFACE SUBSIDENCE, SAMPLE PROBLEM 3

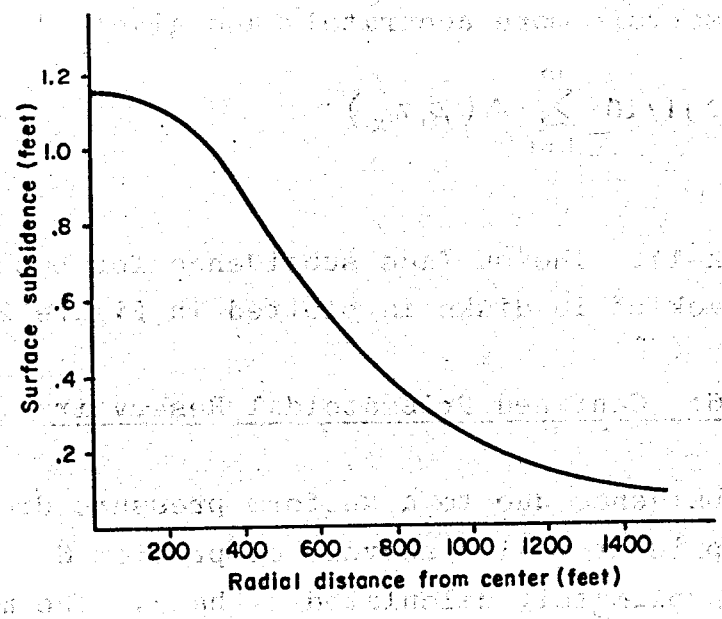

FIGURE 2-2: HAND-CALCULATION METHOD, SURFACE SUBSIDENCE, SAMPLE PROBLEM 4

2.5.5 Sample Problem 5: Thick Finite Reservoir

The reservoir in sample problem 5 (Figure 1-5) is like that in sample problem 3 but is 10 times as thick, and the pressure drop is only 2.16×10^4 psf. The material properties are the same. The compaction of the 500-foot interval is then:

$$C = 500(3.86\times10^{-7})(2.15\times10^{4}) = 4.17 \text{ ft.}$$

Assuming the reservoir is axisymmetric, the surface subsidence may be calculated using equation [2-12]. The reservoir may be modeled with either a single disk at the reservoir mid-depth or, more accurately, with a number of disks distributed over the reservoir depth. For a single disk:

$$u_z = -2(4.17)(0.75)\ A(\rho,\ 1.5)$$

Ten disks spaced 50 feet apart from D = 525 feet to D = 975 feet represent the thick reservoir more accurately and give:

$$u_z = -2(4.17)(.75)1/10 \sum_{k=1}^{10} A(\rho, \eta_k)$$

with $\eta_k = 1.05 + 0.10(k-1)$. The surface subsidence for both the single disk and the stack of 10 disks is plotted in Figure 2-3.

2.5.6 Sample Problem 6: Confined Prismatoidal Reservoir

Compaction and subsidence due to a uniform pressure drop of 2.88×10^4 psf in the prismatoidal reservoir of problem 6 (Figure 1-6) can be approximately calculated by hand. The material properties are the same as in sample problem 1. The

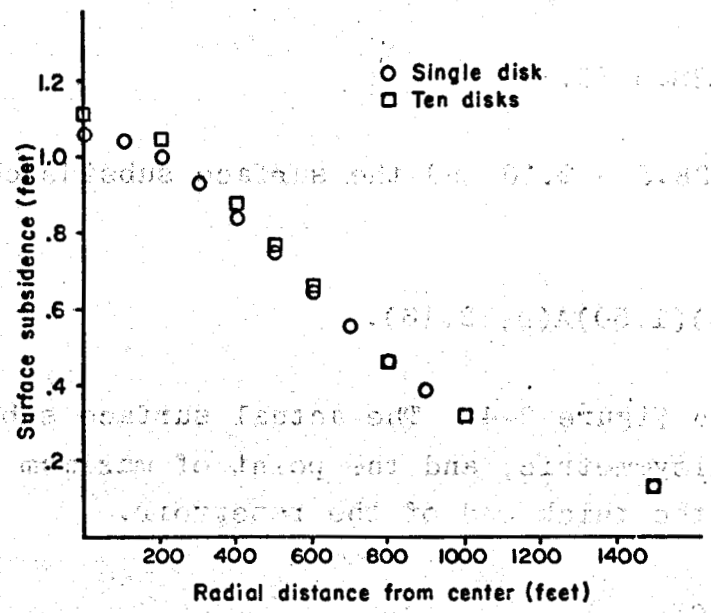

FIGURE 2-3
HAND-CALCULATION METHOD, SURFACE SUBSIDENCE, SAMPLE PROBLEM 5 (SINGLE DISK AND 10-DISK STACK)

prismatoid can be modeled as being uniformly 135 feet thick to give a one-dimensional compaction of:

$$C = (3.86\text{x}10^{-7})(2.88\text{x}10^{4})\ 135 = 1.50 \text{ ft.}$$

By molding the prismatoid into a cylinder of the same volume, the approximate surface subsidence caused by the pressure drop can be determined. The corresponding cylinder thickness is 135 feet, the depth is 732.5 feet, and the radius is:

$$R = \frac{600}{\sqrt{\pi}} = 338.5 \text{ ft.}$$

Thus, $\eta = 732.5/338.5 = 2.16$ and the surface subsidence is given by:

$$u_z = -2(.75)(1.50)A(\rho,\ 2.16).$$

This is plotted in Figure 2-4. The actual surface subsidence profile is not axisymmetric, and the point of maximum subsidence is offset toward the thick end of the reservoir.

2.5.7 Case Studies

The reservoir interval compaction and surface subsidence were calculated by hand for Wairakei, The Geysers, and Austin Bayou Prospect.

Wairakei was assumed to be a one-dimensional system, as the reservoir horizontal extent is much greater that its depth. A reservoir compaction of 2.25 feet was determined, giving a surface subsidence of 3.6 feet.

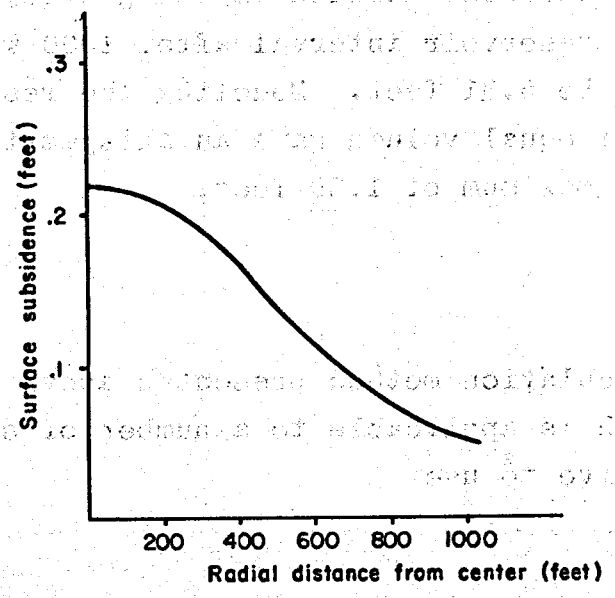

FIGURE 2-4
HAND CALCULATION OF SURFACE SUBSIDENCE, SAMPLE PROBLEM 6

The Geysers system was assumed to be axisymmetric. A reservoir compaction of 1.03 feet was calculated. Two different models were then utilized to predict surface subsidence. A single disk modeled the reservoir in one case. In the other model, 12 disks were used to better represent the vertical extent of the reservoir and the lateral distribution of pressure and temperature change. The maximum subsidence predicted by the two models was 0.344 and 0.410 feet.

Austin Bayou was also modeled as being axisymmetric. The compaction of the reservoir interval after 1000 weeks of pumping was determined to be 5.31 feet. Modeling the reservoir interval with a cylinder of equal volume gave an axisymmetric surface subsidence with a maximum of 1.29 feet.

2.6 CONCLUSIONS

The hand-calculation method presented above provides a simple model which is applicable to a number of systems. It is easy and inexpensive to use.

2.7 REFERENCES

Geertsma, J. (1973). "Land Subsidence Above Compacting Oil and Gas Reservoirs," Journal of Petroleum Technology, SPE 3730.

Miller, I., W. Dershowitz, K. Jones, L. Meyer, K. Roman, and M. Schauer (1980). "Simulation of Geothermal Subsidence," prepared for Lawrence Berkeley Laboratory, University of California, Berkeley, LBL 10571.

3.0 NUCLEUS-OF-STRAIN MODEL "SUBSID"

3.1 INTRODUCTION

A program named SUBSID that was based on a nucleus-of-strain formulation to calculate displacements and stresses due to reservoir pore pressure changes was written by Golder Associates. The nucleus-of-strain, or center of dilatation, solution was originally developed for point temperature changes in an infinite space (Goodier 1937). This solution was later used by Sen (1951) to calculate stresses and displacements due to a nucleus of strain in an infinite half-space. It was also used by Mindlin and Cheng (1971) to calculate stresses and displacements both interior and exterior to a spherical inclusion with a uniform temperature change. A point-pressure change can be treated in a similar manner. Geertsma (1973) calculated analytically the surface vertical and horizontal displacements due to a uniform pressure change over an infinitely thin disk in a half-space by integrating nuclei of strain over the disk.

In SUBSID, the Mindlin and Cheng (1971) solution for a uniform spherical temperature (or pressure) change, transformed to Cartesian coordinates, was used. Arbitrarily shaped reservoirs may be modeled by any number of spheres of arbitrary radii. The system is constrained to be a homogeneous, isotropic, linearly elastic half-space.

3.2 SOLUTION METHOD - GENERAL THEORY

3.2.1 THEORY

The displacement field interior to a spherical nucleus of strain with strength β is given by:

$$u = \frac{a^3\beta}{3}\left[\frac{x}{a^3} + \frac{3-4\nu}{R_2^3}x - \frac{6z(z+c)}{R_2^5}x\right]$$

[3-1] $$v = \frac{a^3\beta}{3}\left[\frac{y}{a^3} + \frac{3-4\nu}{R_2^3}y - \frac{6z(z+c)}{R_2^5}y\right]$$

$$w = \frac{a^3\beta}{3}\left[\frac{z-c}{a^3} - \frac{3-4\nu}{R_2^3}(z+c) + \frac{2z}{R_2^3} - \frac{6z(z+c)^2}{R_2^5}\right]$$

where: $\beta = \frac{1+\nu}{1-\nu}\frac{C_b}{3}\Delta p$ for a pressure change

$\beta = \frac{1+\nu}{1-\nu}\alpha\Delta T$ for a temperature change

a = sphere radius
ν = Poisson's ratio
$R_2 = (x^2 + y^2 + [z+c]^2)^{1/2}$
c = depth of sphere center
$C_b = 3(1-2\nu)/E$ compressibility
E = modulus of elasticity
α = coefficient of thermal expansion
x,y,z = Cartesian coordinates of observation point

Exterior to the sphere, the displacement field is given by identical formulas with $1/a^3$ within the brackets replaced by $1/R_1^3$ (with $R_1 = [x^2+y^2+(z-c)^2]^{0.5}$).

The stresses in the sphere interior are:

$$\sigma_x = \frac{E}{1+\nu}\frac{a^3\beta}{3}\left[-\frac{2}{a^3} + \frac{3-8\nu}{R_2^3} - \frac{(3-4\nu)3x^2+6z(z+c)-12\nu(z+c)^2}{R_2^5} + \frac{30x^2z(z+c)}{R_2^7}\right]$$

$$\sigma_y = \frac{E}{1+\nu}\frac{a^3\beta}{3}\left[-\frac{2}{a^3} + \frac{3-8\nu}{R_2^3} - \frac{(3-4\nu)3y^2+6z(z+c)-12\nu(z+c)^2}{R_2^5} + \frac{30y^2z(z+c)}{R_2^7}\right]$$

$$\sigma_z = \frac{E}{1+\nu}\frac{a^3\beta}{3}\left[-\frac{2}{a^3} - \frac{1}{R_2^3} + \frac{3(z+c)^2-18z(z+c)}{R_2^5} + \frac{30z(z+c)^3}{R_2^7}\right]$$

$$[3\text{-}2]\quad \tau_{xy} = -\frac{E}{1+\nu}\, a^3\beta\, \frac{xy}{R_2^5}\left[3-4\nu-\frac{10z(z+c)}{R_2^2}\right]$$

$$\tau_{yz} = \frac{-E}{1+\nu}\, a^3\beta\, \frac{y}{R_2^5}\left[3z+c-\frac{10z(z+c)^2}{R_2^2}\right]$$

$$\tau_{zx} = \frac{-E}{1+\nu}\, a^3\beta\, \frac{x}{R_2^5}\left[3z+c-\frac{10z(z+c)^2}{R_2^2}\right]$$

The exterior stress field is:

$$\sigma_x = \frac{E}{1+\nu}\,\frac{a^3\beta}{3}\left[\frac{1}{R_1^3}+\frac{3-8\nu}{R_2^3}-\frac{6z(z+c)-12\nu(z+c)}{R_2^5}-3x^2\left(\frac{1}{R_1^5}+\frac{3-4\nu}{R_2^5}-\frac{10z(z+c)}{R_2^7}\right)\right]$$

$$\sigma_y = \frac{E}{1+\nu}\,\frac{a^3\beta}{3}\left[\frac{1}{R_1^3}+\frac{3-8\nu}{R_2^3}-\frac{6z(z+c)-12\nu(z+c)}{R_2^5}-3y^2\left(\frac{1}{R_1^5}+\frac{3-4\nu}{R_2^5}-\frac{10z(z+c)}{R_2^7}\right)\right]$$

$$\sigma_z = \frac{E}{1+\nu}\,\frac{a^3\beta}{3}\left[\frac{1}{R_1^3}+\frac{1}{R_2^3}+\frac{3(z+c)^2-18z(z+c)}{R_2^5}+\frac{30z(z+c)^3}{R_2^7}-\frac{3(z-c)^2}{R_1^5}\right]$$

[3-3]

$$\tau_{xy} = -\frac{E}{1+\nu}\, a^3\beta\, \frac{xy}{R_2^5}\left[\frac{R_2^5}{R_1^5}+3-4\nu-\frac{10z(z+c)}{R_2^2}\right]$$

$$\tau_{yz} = -\frac{E}{1+\nu}\, a^3\beta\, \frac{y}{R_2^5}\left[\frac{R_2^5(z-c)}{R_1^5}+3z+c-\frac{10z(z+c)^2}{R_2^2}\right]$$

$$\tau_{zx} = \frac{-E}{1+\nu}\, a^3\beta\, \frac{x}{R_2^5}\left[\frac{R_2^5(z-c)}{R_1^5}+3z+c-\frac{10z(z+c)^2}{R_2^2}\right]$$

In the preceding equations, positive normal stresses indicate compression. The stresses are relative to the initial stress field in the half-space. The sphere center has been assumed to be at $(x,y,z) = (0,0,c)$, but it may be taken at (x_o, y_o, c) and x and y in equations [1], [2], and [3] being

replaced by $x-x_o$ and $y-y_o$. The stress and displacement fields that are caused by a number of spherical inclusions in the half-space are found by summing the contributions due to each sphere.

If a portion of the reservoir being modeled is of a different compressibility from the rest of the half-space, that effect may be included by adjusting the pressure change in that region, taking

$$(\Delta P)\text{equivalent} = \frac{(\Delta P)\ \text{actual}\ (C_b)\text{actual}}{(C_b)\text{half-space}}$$

This adjustment is only approximate, however, as the effects of "soft" and "hard" nuclei of strain cannot be linearly superposed.

3.2.2 Numerical Method

In SUBSID the contributions to the stresses and displacements at a particular point in the half-space from all spherical nuclei of strain are calculated using equations [3-1], [3-2], and [3-3] and summed.

For most reservoirs, the total volume of the spheres used to model the reservoir will not be equal to the volume of the actual reservoir. In these cases, each sphere pressure change (Δp) should be adjusted so that $\Delta p = V_o \Delta p_o / V$, where V is the sphere volume and V_o and Δp_o are the actual reservoir volume and pressure change represented by the sphere. This adjustment makes the stresses and displacements exterior to the sphere correct, as there, Δp and V appear only in the combination ΔpV. However, in the interior of the sphere, the sphere volume occurs both alone and in the pV combination in the expressions

for displacement (see equation [3-1]) and normal stress (see equation [3-2]). These quantities, therefore, will be incorrect.

The program outputs displacements, normal stresses, shear stresses, and mean stress $\sigma m = 1/3\ (\sigma x + \sigma y + \sigma z)$ at observation points chosen by the user in the semi-infinite space.

3.3 CAPABILITIES AND LIMITATIONS

3.3.1 Geometric Capabilities and Limitations

A reservoir may be modeled as a single sphere, as a linear array of spheres in the x, y, or z direction; as a rectangular array in any xy plane; or as a disk-shaped array centered at x = y = 0 in any xy plane. Any number of arrays of one of these six types may be used, but different types may not be combined. Each line or rectangle is made up of an arbitrary number of spheres with arbitrary but equal radii. The sphere center spacing is constant and specified by the user; in the rectangle the spacing of centers in the x and y directions need not be the same. A disk is made up of 1, 9, 25, 49, 81, 121, or 169 spheres. Observation points are specified similarly on lines in the x, y, or z direction or in rectangular arrays in any xy plane. Any combination of lines and rectangles may be used to form the observation array. The program is now dimensioned to allow 500 observation points and a total of 700 spheres and observation points. The array sizes may be easily changed to fit any size problem. The units of length and stress that are used need not be consistent. In a number of problems, stresses were calculated in psi and displacements in feet.

3.3.2 Flow Capabilities and Limitations

Flow is not considered in SUBSID. The material in the half-space is assumed to react instantaneously to a pressure change in the reservoir.

3.3.3 Material Properties

The reservoir and the surrounding material are assumed to be made of the same homogeneous, isotropic, linearly elastic material. The material properties specified by the user are Young's modulus E and Poisson's ratio ν.

3.4 USABILITY

3.4.1 Documentation

For further discussion of the nucleus-of-strain method see Geertsma (1973). A users' manual developed by Golder Associates is included as Appendix A. The manual includes a discussion of input parameters, a program listing, and a sample problem.

3.4.2 Input Ease

Input to SUBSID is straightforward. It is compact if the reservoir is of a regular shape with uniform pressure changes so that combinations of disks, rectangles, or lines form an appropriate model. However, if the reservoir is large and irregular in shape or if the pressure change varies within the reservoir, many single spheres are required for the model, and the input can become lengthy.

3.4.3 Output Control and Comprehensibility

The user specifies at which points in the half-space displacements and stresses are to be output. Also output are the half-space material properties, the coordinates of the sphere centers and the observation points, and the strength and radius of each source sphere. Card images of the reservoir spheres input and the observation points input are also printed.

3.4.4 Solution Efficiency

Solution cost is directly related to the product of the number of source spheres and the number of observation points. Cost in CP seconds is shown in Figure 3-1. For a three-dimensional solution, SUBSID is extremely efficient.

3.4.5 Resume of Performance on Sample Problems and Case Studies

Three sample problems, (3, 5, and 6) were solved with SUBSID. Surface displacements from problem 3 were compared with Geertsma's (1973) analytic solution for a uniform pressure drop on an infinitely thin disk. A superposition of 10 of Geertsma's disks was used to calculate surface displacements to compare with those from problem 5. The Geertsma displacements agree with the best SUBSID displacements to better than 1 percent in problem 3 and agree to better than 2 percent in problem 5. No independent solutions were available to compare with the calculated surface displacements from the prismatoid of problem 6. In all cases, the stress and displacement fields within and in the immediate neighborhood of the actual reservoir are not accurate because sphere arrays do not conform well to the actual reservoir shape.

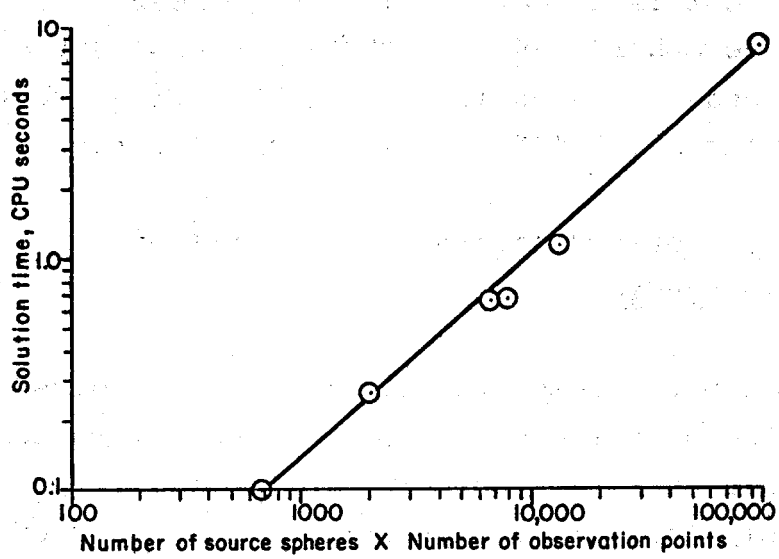

FIGURE 3-1
NUCLEUS-OF-STRAIN MODEL
SOLUTION TIME AS A FUNCTION
OF NUMBER OF SOURCE SPHERES
AND NUMBER OF OBSERVATION POINTS

Two case studies, The Geysers and Wairakei, were modeled with spherical nuclei of strain.

3.5 PERFORMANCE ON SAMPLE PROBLEMS

3.5.1 Sample Problem 3: Confined Finite Reservoir

Sample problem 3 (Figure 1-3) was run with SUBSID, using disks of 9, 25, and 169 spheres. In all cases the pressure drop in the model reservoir had to be adjusted because volume of the disk of spheres was not the actual reservoir volume. Models with 9, 25, and 169 spheres required 0.1, 1.1, and 3.2 CPU seconds, respectively. The sphere centers for the three cases were taken at z = 595 feet. The geometries and applied pressure drops were as follows.

Case 1: 9 spheres arranged in two rings

$a = 1/3\ R = 166.67$ ft

$V = 40/9\ V_o \rightarrow \Delta p = 9/40 \Delta p_o = -11340$ psf

Case 2: 25 spheres arranged in three rings

$a = 1/5\ R = 100$ ft

$V = 8/3\ V_o \rightarrow \Delta p = 3/8 \Delta p_o = -18900$ psf

Case 3: 169 spheres arranged in seven rings

$a = 1/13\ R = 38.46$ ft

$V = 40/39\ V_o \rightarrow \Delta p = 39/40 \Delta p_o = -49140$ psf

where:
- a = sphere radii
- R = reservoir radius
- V = volume of model reservoir
- V_o = volume of actual reservoir
- Δp = pressure change in spheres
- Δp_o = pressure change in the actual reservoir

Surface vertical and horizontal displacements along y = 0 are shown in figures 3-2 and 3-3. Table 3-1 gives w(0,0,0) and u(500,0,0) for the three cases and for Geertsma's analytic solution for a pressure drop of 50,400 lb/ft^2 on an infinitely thin disc at z = 595 feet. The 169-sphere disk comes closest to matching the aspect ratio (h/R) of the actual reservoir; however, the displacements from even the rough 9-sphere model are in agreement with the more precise values.

TABLE 3-1
COMPARISON OF VERTICAL AND
HORIZONTAL SURFACE DISPLACEMENT
SAMPLE PROBLEM 1

MODEL	VERTICAL DISPLACEMENT AT SURFACE w(0,0,0)(ft)	HORIZONTAL DISPLACEMENT AT SURFACE u(500,0,0)(ft)
9 spheres	-.3608	-.1493
25 spheres	-.3487	-.1430
169 spheres	-.3421	-.1398
Geertsma	-.3419	-.1398

3.5.2 Sample Problem 5: Thick Finite Reservoir

Sample problem 5 (Figure 1-5), a high-aspect ratio cylindrical reservoir at a mean depth of 750 feet subject to a 21,600 psf pressure drop, was modeled with four large spheres and with four overlapping 25-sphere disks. The surface displacements obtained were compared to those found from the superposition of 10 of Geertsma's infinitely thin discs. Solution with four large spheres required 0.1 CPU seconds; solution of the 100-sphere model required 0.7 CPU seconds.

The geometries and applied pressure drops for the two cases were as follows.

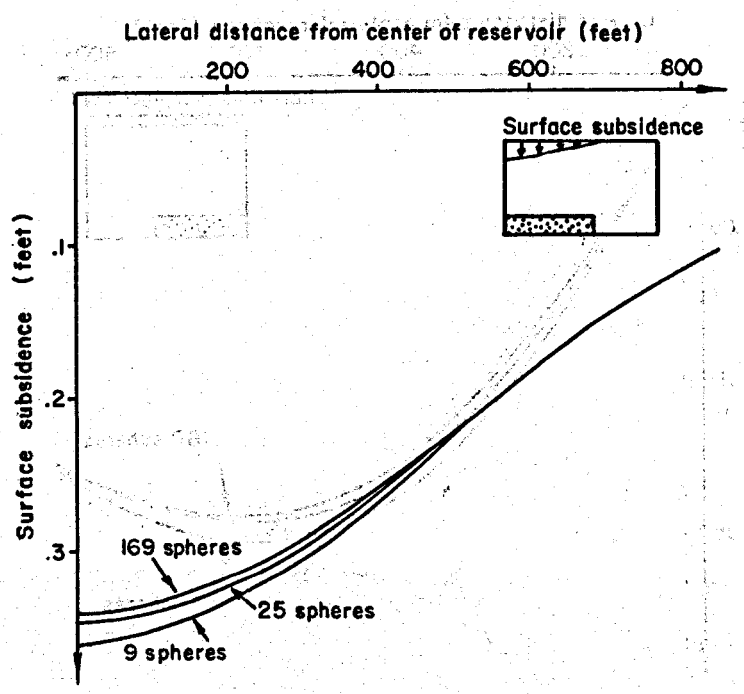

FIGURE 3-2
NUCLEUS-OF-STRAIN MODEL,
SURFACE SUBSIDENCE USING 9, 25, AND 169 SPHERES,
SAMPLE PROBLEM 3

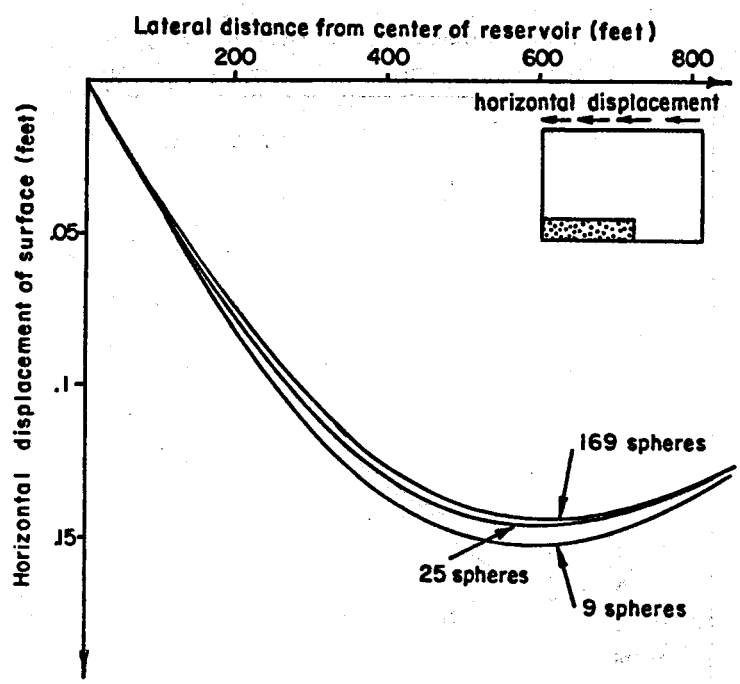

FIGURE 3-3
NUCLEUS-OF-STRAIN MODEL,
HORIZONTAL DEFORMATION OF THE SURFACE
USING 9, 25, AND 169 SPHERES,
SAMPLE PROBLEM 3

Case 1: 4 spheres with centers at z = 750 ft
a = 250 ft; sphere centers at (x,y) = (250,0), (0,250), (-250,0), (0,-250)
$V = 2/3\ V_o \rightarrow \Delta p = 3/2\ \Delta p_o = -32400$ psf

Case 2: 4 disks each made up of 25 spheres
disk centers at z = 600, 700, 800, and 900 ft
$V = 16/15\ V_o \rightarrow \Delta p = 15/16\ \Delta p_o = -20250$ psf

Surface vertical and horizontal displacements along y = 0 are shown in figures 3-4 and 3-5. Table 3-2 are gives w(0,0,0) and u(600,0,0) for the two cases and for Geertsma's analytic solution for a pressure drop of 21,600 lb/ft^2 on each of 10 infinitely thin disks spaced 50 feet apart from z = 525 ft to z = 975 feet. The latter solution and the 4-by-25-sphere disk model agree to within 2 percent.

TABLE 3-2
COMPARISON OF VERTICAL AND
HORIZONTAL SURFACE DISPLACEMENT
SAMPLE PROBLEM 5

MODEL	w(0,0,0) (FT)	u(600,0,0) (FT)
4 spheres	-1.186	-0.474
4 x 25 spheres	-1.106	-0.450
Geertsma	-1.119	-0.457

3.5.3 Sample Problem 6: Prismatoidal Confined Reservoir

Sample problem 6 (Figure 1-6), a prismatoidal reservoir subject to a pressure drop of 28,800 psf, was modeled with spherical nuclei of strain. The lower boundary of the reservoir is at z =

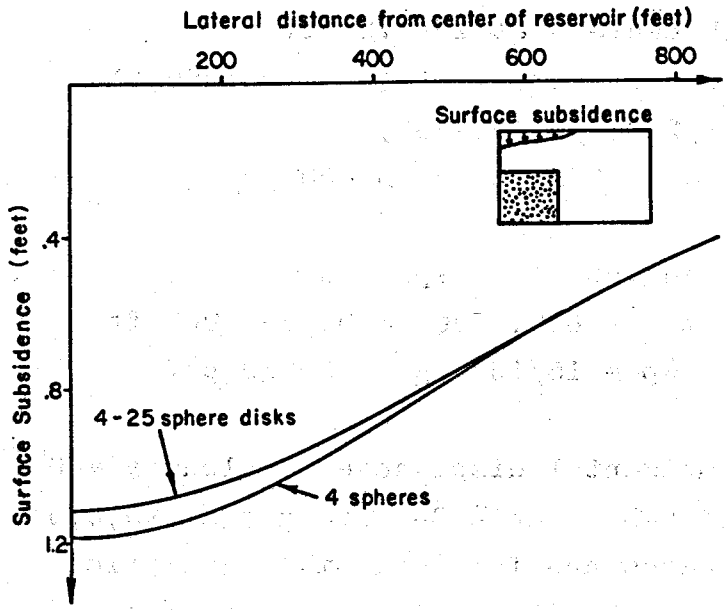

FIGURE 3-4: NUCLEUS-OF-STRAIN MODEL, SURFACE SUBSIDENCE USING 4 AND 100 SPHERES, SAMPLE PROBLEM 5

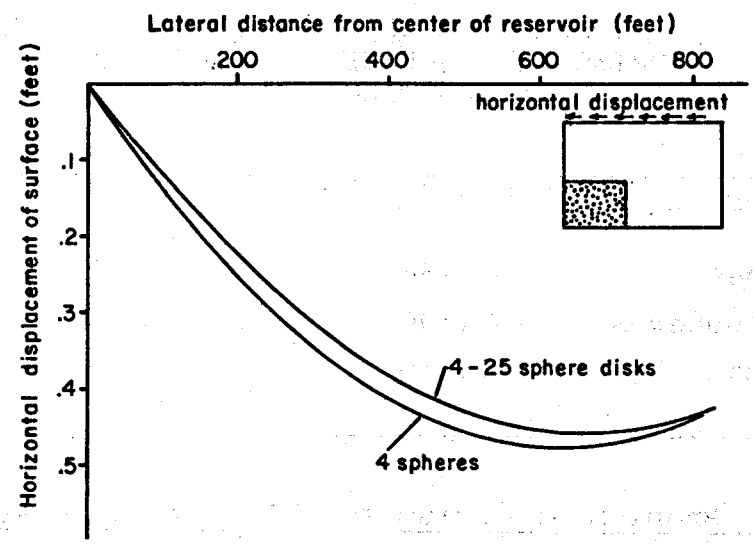

FIGURE 3-5: NUCLEUS-OF-STRAIN MODEL, HORIZONTAL DEFORMATION OF THE SURFACE USING 4 AND 100 SPHERES, SAMPLE PROBLEM 5

800 feet. The reservoir thickness ranges from 70 to 200 ft. Two models of this reservoir were tested. The simpler model (27 spheres) required 0.4 CPU seconds for solution; the more complex model (128 spheres) required 0.9 CPU seconds for solution.

3.5.3.1 Setup

The two models of this prismatoidal reservoir had very different distributions of spheres. One contained 128 spheres, the other contained 27. The geometries and the applied pressure drops are as follows.

Case 1: Case 1 uses 128 spheres arranged in three rectangles. The rectangle center planes are at z = 765,695 and 630 feet and contain 64, 48, and 16 spheres. The sphere centers are spaced at 75 feet in the x and y directions, and the sphere diameters are all 75 feet.

$$V = .582\ V_o \rightarrow \Delta p = 1.719\Delta p_o = -49504 \text{ psf}$$

Case 2: Case 2 uses 27 spheres arranged in five lines of 3, 4, 5, 6, and 9 spheres in the y direction. The centerlines of the spheres are at (x,z) = (100,700), (257,925), (382,740), (486,750), and (566.7,766.7). The corresponding sphere diameters, which are equal to the sphere center spacings in the y direction, are 200, 150, 120, 100, and 66.7 feet.

$$V = 0.591\ V_o \rightarrow \Delta p = 1.693\Delta p_o = -48758 \text{ psf}$$

3.5.3.2 Results

Both vertical and horizontal surface displacements from the two models agree to within 1 percent. A contour plot of the surface vertical displacement is presented in Figure 3-6.

3.6 CONCLUSIONS

The nucleus-of-strain formulation used in program SUBSID is unique in that it allows the solution of complex, three-dimensional geometries at relatively low cost and minimal effort. Solutions obtained by use of SUBSID suffer primarily from the simplification of material properties that is required to allow solutions.

3.7 LIST OF SYMBOLS

a	- radius of sphere
x, y, z	- Cartesian coordinates of observation point
c	- z coordinate of sphere center
$R_1 = \left(x^2+y^2+(z-c)^2\right)^{1/2}$	- distance to center of image sphere at (0,0,c) from observation point at (x,y,z)
$R_2 = \left(x^2+y^2+(z+c)^2\right)^{1/2}$	- distance to center of image sphere at (0,0,z) from observation point at (x,y,z)
Δp	- pressure change within sphere
ν	- Poisson's ratio
E	- modulus of elasticity
$C_b = 3(1-2\nu)/E$	- compressibility
α	- coefficient of thermal expansion
u, v, w	- x, y, z displacements

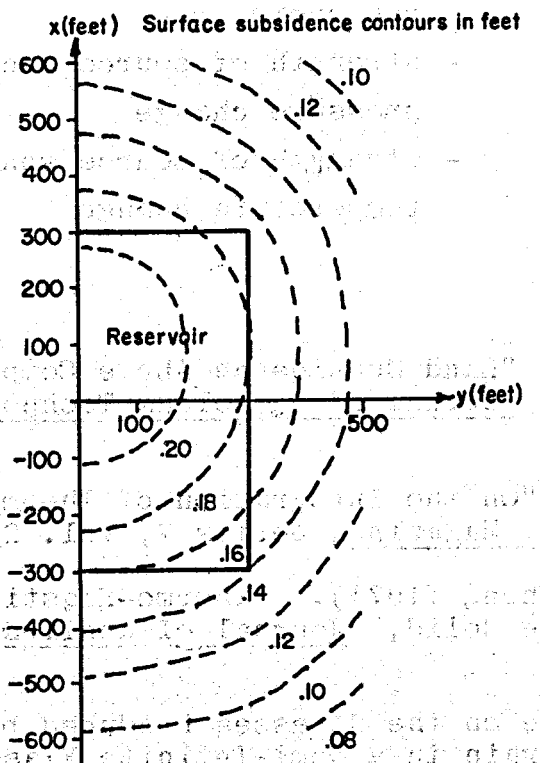

FIGURE 3-6
NUCLEUS-OF-STRAIN MODEL,
CONTOURS OF SURFACE SUBSIDENCE,
SAMPLE PROBLEM 5

σ_x, σ_y, σ_z	- normal stresses
$\sigma_m = 1/3(\sigma_x+\sigma_y+\sigma_z)$	- mean stress
τ_{xy}, τ_{yz}, τ_{zx}	- shear stress
Δp_o	- pressure change in reservoir
V_o	- volume of reservoir
V	- volume of spheres modeling reservoir
h, R	- thickness and radius of cylindrical reservoir
$\beta = \frac{1+\nu}{1-\nu}\frac{C_b}{3}\Delta P$	- strength of source sphere due to pressure change
$\beta = \frac{1+\nu}{1-\nu}\alpha\Delta T$	- strength of source sphere due to temperature change

3.8 REFERENCES

Geertsma, J. (1973). "Land Subsidence Above Compacting Oil and Gas Reservoirs," Journal of Petroleum Technology, SPE 3730, p. 734.

Goodier, J. (1937). "On the Integration of Thermo-Elastic Equations," Phil. Magazine, Series 7, Vol. 23, p. 1017.

Mindlin, R., and D. Cheng (1971). "Thermo-Elastic Stresses in the Semi-Infinite Solid," Journal of Applied Physics, p. 931.

Sen, B. (1951). "Note on the Stresses Produced by Nuclei of Thermoelastic Strain in a Semi-Infinite Elastic Solid," Quarterly of Applied Mathematics, Vol. 8, pp. 365-369.

4.0 ONE-DIMENSIONAL CONSOLIDATION MODEL "UPDOWN"

4.1 INTRODUCTION

UPDOWN is a one-dimensional consolidation program in the public domain written by Don Helm while working with the U.S. Geological Survey. Doubly draining, horizontally infinite aquitards with specified time-dependent effective stresses at the upper and lower boundaries may be modeled with this program. According to Terzaghi's theory of one-dimensional consolidation, aquitards are assumed to deform vertically. Effective stress profiles within the aquitard and the amount of aquitard consolidation are output at user-specified time intervals.

4.2 SOLUTION METHOD - GENERAL THEORY

4.2.1 Theory

The Terzaghi consolidation equation is defined in terms of effective stress p, hydraulic conductivity $K = m_v \gamma_w C_v$, and specific storage $S = m_v \gamma_w$ as:

[4-1] $$\frac{K}{S} \frac{\partial^2 p}{\partial z^2} = \frac{\partial p}{\partial t}$$

It is written as a finite difference equation in space and time and solved in UPDOWN. When p is less than the past maximum effective stress, then S is the elastic specific storage S_e; when p is greater than the past maximum effective stress, then S is the virgin specific storage S_p. Both K and S may be functions of z. If K and S are assumed to vary with effective stress, the Terzaghi equation becomes nonlinear. Helm (1976) applies a transformation to linearize the equation. The resulting

linear equation is exact only if the ratio K/S does not depend on effective stress. The linear form of the equation is approximately correct if K/S is weakly stress-dependent or if the effective stress in the aquitard does not change significantly.

4.2.2 Numerical Method

A linear finite difference formulation of [4-1] with constant coefficients is:

$$[4\text{-}2] \qquad -Ap_{j+1}^{n} + Bp_{j}^{n} - Ap_{j-1}^{n} = Ap_{j+1}^{n-1} + Ep_{j}^{n-1} + Ap_{j-1}^{n-1}$$

where: $A = \dfrac{K\Delta t}{2S\Delta Z^2}$

$B = 1 + 2A$

$E = 1 - 2A$

The superscript (n) indicates a discrete point in time and the subscript (j) a discrete point on the vertical grid. Uniform steps in space and time are denoted by z and t (see Figure 4-1). This finite-difference equation is solved deterministically by an adaptation of an efficient forward and backward substitution method developed by Thomas (see Remson et al. 1971, pp. 168-171). The nonconstant coefficient and the stress-dependent coefficient formulations of equation [4-1] are solved in a similar but more complex manner (see equation [4-2]).

4.3 CAPABILITIES AND LIMITATIONS

4.3.1 Geometric Capabilities and Limitations

The aquitard modeled may be of arbitrary vertical extent. A uniform vertical grid and uniform time steps are specified by the

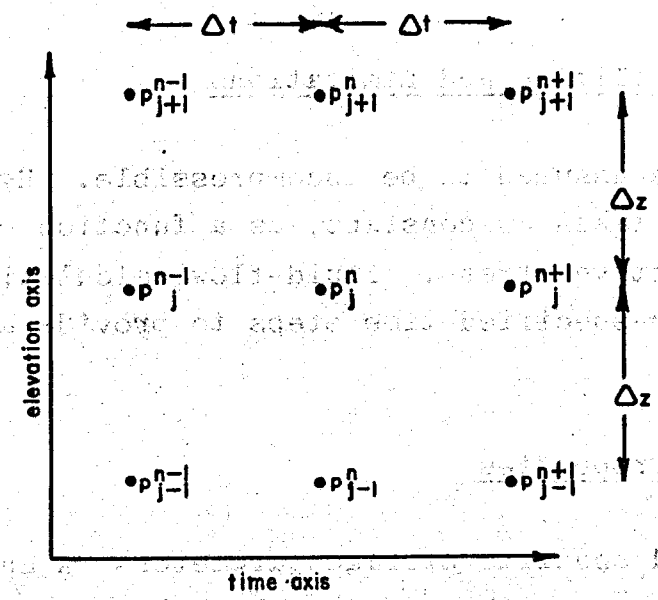

FIGURE 4-1
ONE-DIMENSIONAL CONSOLIDATION MODEL
FINITE DIFFERENCE GRID IN TIME AND SPACE

user. Helm (1976) suggests that the grid spacing be less than 1 foot. Arrays within UPDOWN are dimensioned to allow 150 grid lines, but the array sizes may be easily increased. The time step size chosen should reflect the complexity of the loading. Length is input in feet, time is input in days, effective stress is input in feet of water, hydraulic conductivity is input in feet per year, and specific storage is input in feet^{-1}. An option to the basic program allows the effective stress at the upper and lower aquitard boundaries to be specified independently. This option was not extensively used by Helm (1976) and still needs to be debugged.

4.3.2 Flow Capabilities and Limitations

The fluid is assumed to be incompressible. Hydraulic conductivity may be taken as constant, as a function of z, or as a function of effective stress. Fluid-flow calculations can be performed at user-specified time steps to provide any desired time history.

4.3.3 Material Properties

The aquitard specific storage parameters S_e and S_p may be constant, may vary with z, or may both be functions of effective stress. If S_e and S_p vary with effective stress, the hydraulic conductivity must also vary with effective stress. The user then has the choice of making K/S_e and K/S_p either constant or functions of effective stress. The program has not been tested with the heterogeneous (K = K[z] and/ or S = S[z]) and nonlinear (K = K[p] and S = S[p]) options superposed but, according to Helm (1975), should work. Neither the heterogeneous nor the nonlinear options can be used when the upper and lower boundary conditions are specified independently.

4.4 USABILITY

4.4.1 Documentation

The theory behind the program, the numerical solution method, and numerous examples using homogeneous, heterogeneous, and nonlinear aquitard parameters are presented in Helm (1975; 1976). The analytic and UPDOWN solutions to a simple consolidation problem are given in Helm (1975) and can serve as a check on the user's comprehension of the basic program.

An input manual exists in rough form. A number of additions and changes have apparently been made to the original manual. For the most part, the input parameters are clearly defined and, where necessary, are further explained.

The NDDD = 1 option, which allows the upper and lower boundary conditions to be specified independently, was added to UPDOWN in order to solve a particular problem and is not well documented.

4.4.2 Input Ease

Only eight data cards are required to specify material properties, geometry, and boundary conditions. Boundary conditions are stored on tape to be read into the program when needed.

4.4.3 Output Control and Comprehensibility

All input data are echoed in output either as card images or as labeled parameters. The user may separately specify at what time intervals aquitard compaction and effective stress profiles within the aquitard are to be output. Effective stresses are

given at every grid point. If the nonlinear option is used, profiles of hydraulic conductivity, elastic specific storage, and virgin specific storage are printed with the corresponding effective stress profiles.

4.4.4 Solution Efficiency

The solution cost for UPDOWN increases with the number of time steps and the number of grid lines in the aquitard. Some examples of solution times for aquitards with constant permeability and specific storage coefficients for different numbers of time steps and grid lines are given in Table 4-1.

TABLE 4-1
UPDOWN SOLUTION EFFICIENCY

GRID LINES	TIME STEPS	SOLUTION TIME (CPU SECONDS)
21	11	0.222
15	60	0.725
141	60	5.664

4.4.5 Resume of Performance on Sample Problems

Sample problem 2 was solved with UPDOWN. The aquitard permeability and specific storage were assumed constant. Ultimate consolidation was 1.945 feet, agreeing with the one-dimensional analytic solution. The aquitard was found to be 98 percent consolidated at 30 years.

4.5 PERFORMANCE ON SAMPLE PROBLEMS

4.5.1 Sample Problem 2: Infinite Reservoir With Permeable Confining Layer

Sample problem 2 (Figure 4-2) was solved with UPDOWN. The aquitard properties K and S were calculated from values of m_v, γ_w, and c_v and converted to the units required by UPDOWN:

$$K = m_v \gamma_w c_v = 3.78604 \times 10^{-3} \text{ ft/yr}$$

$$S_e = S_p = m_v \gamma_w = 6.9151 \times 10^{-5} \text{ ft}^{-1}.$$

The aquitard was divided into 140 6-inch intervals in accordance with Helm's suggestion that the grid spacing be less than one foot. Effective stresses at the top and bottom boundaries were specified every 180 days (1 year is taken as 360 days by UPDOWN) for 10,800 days (30 years). The effective stress on the upper boundary remained constant at 41,040 psf (658 ft of water) while the effective stress on the lower boundary was 24,480 psf (392 ft of water) at t = 0, and 74,880 psf (1200 ft of water) thereafter. The sample problem setup for UPDOWN is shown in Figure 4-2. The solution required 5.7 CPU seconds.

Effective stresses were output at 1.5-year intervals. The effective stress profiles within the aquitard at t = 0, 2, and 20 years are plotted along with the ultimate effective stress profile in Figure 4-3.

Aquitard compaction was output at 0.5-year intervals. A plot of compaction as a function of time up to 30 years is presented in Figure 4-4. The ultimate compaction is 1.945 feet.

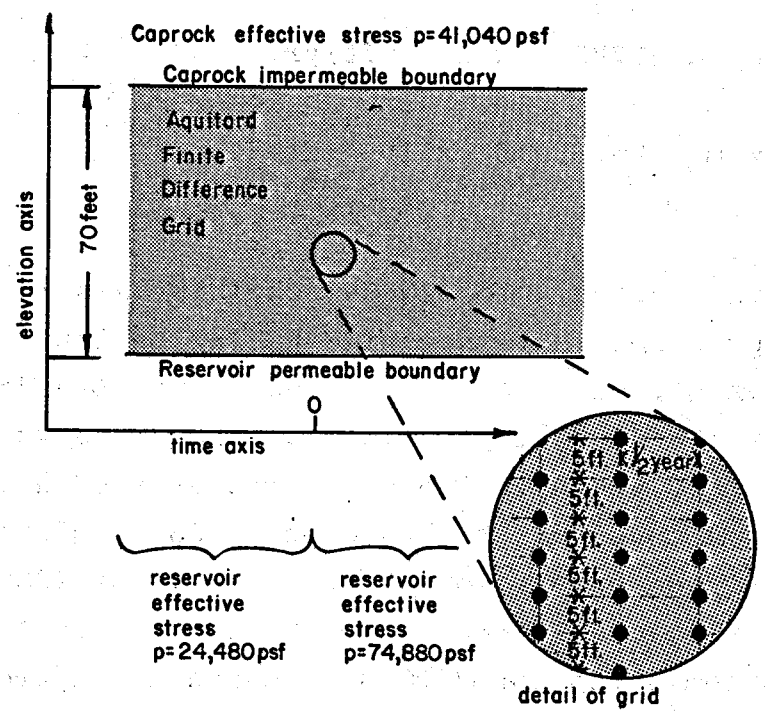

FIGURE 4-2
ONE-DIMENSIONAL CONSOLIDATION MODEL,
SET UP FOR SAMPLE PROBLEM 2

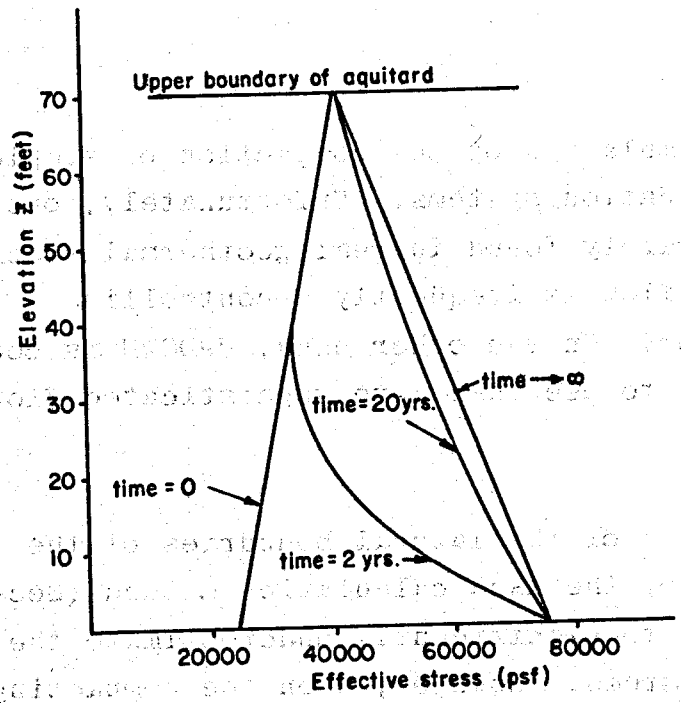

FIGURE 4-3: ONE-DIMENSIONAL CONSOLIDATION MODEL, VARIATION IN EFFECTIVE STRESS WITH TIME, SAMPLE PROBLEM 2

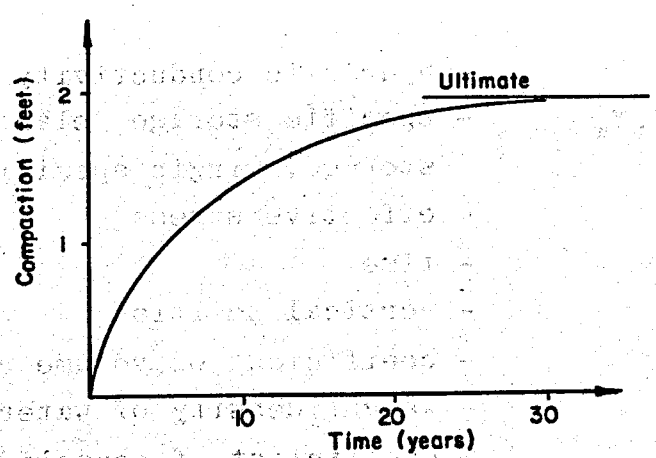

FIGURE 4-4: ONE-DIMENSIONAL CONSOLIDATION MODEL, AQUITARD COMPACTION AS A FUNCTION OF TIME, SAMPLE PROBLEM 2

4.6 CONCLUSIONS

UPDOWN is useful for simulation of the compaction of simple one-dimensional flow-consolidation systems. Unfortunately, one-dimensional conditions are rarely found in real geothermal reservoirs, and multidimensional flow is frequently a controlling factor in subsidence behavior. On the other hand, UPDOWN is considerably cheaper and easier to use than more sophisticated flow models such as CCC.

UPDOWN ignores the effect of the lateral boundries of the reservoir. As demonstrated by the hand calculation method (Section 2.0), this can cause it to significantly underestimate the subsidence of homogeneous systems. However, when the compacting layer is much more compressible than the surrounding material, UPDOWN's assumption is valid and subsidence will equal compaction.

4.7 LIST OF SYMBOLS

$K = m_v \gamma_w C_v$	- hydraulic conductivity
$S, S_e, S_p = m_v \gamma_w$	- specific storage, elastic specific storage, virgin specific storage
p	- effective stress
t	- time
z	- vertical position
m_v	- coefficient of volume change
γ_w	- weight density of water
c_v	- coefficient of consolidation

4.8 REFERENCES

Helm, D.C. (1975). "One-dimensional Simulation of Aquifer System Compaction Near Pixley, California: 1. Constant Parameters," Water Resources Research, Vol. 11, No. 3, pp. 465-478.

_____(1976). "One-dimensional Simulation of Aquifer System Compaction Near Pixley, California: 2. Stress Dependent Parameters," Water Resources Research, Vol. 12, No. 3, pp. 375-391.

Remson, I., G.M. Hornberger, and F.J. Molz (1971). "Numerical Methods in Subsurface Hydrology," John Wiley, New York.

5.0 BOUNDARY-ELEMENT MODEL "BIEM2D"

5.1 INTRODUCTION

The Boundary-Integral Equation or Boundary-Element method is similar in approach to the nucleus-of-strain method. It uses superposition of component parts of a system but with a different geometrical basis from the nucleus-of-strain method. The boundary-integral equation method is a powerful numerical technique for solving linear boundary value problems and is used in a variety of disciplines. The particular program reviewed here is designed for two-dimensional stress analysis of underground openings. Originally prepared at Imperial College, London, by John W. Bray, it was modified for the purpose of this project to incorporate thermal and pore pressure effects (see Section 2.0). A large part of the program description and code, which are presented in the following sections, are adapted from Hoek and Brown (1980) and are reprinted here with the permission of the authors.

The two-dimensional boundary-integral method uses analytic solutions for strip loads in an infinite medium to obtain the stress and strain elsewhere in the medium. Its particular advantage is that only boundaries with fixed (i.e., known) boundary conditions of stress must be discretized (as opposed to the finite-element method, where the entire body must be discretized). This means that input formulation is simpler and program solution is less expensive.

5.2 SOLUTION METHOD - GENERAL THEORY

5.2.1 Theory

In most of the literature on boundary-element or boundary-integral methods, the principles of the method, which in reality

are quite simple, are often obscured by the formal mathematical presentation. The following simplified explanation of the basis of the method is based on Hoek and Brown (1980).

The problem is to determine the stresses around a long excavation of specified cross section, given the field stresses p (vertical) and Kp (horizontal) (see Figure 5-1, a). Prior to excavation, the rock that is to be removed provides support for the surrounding rock. This support may be represented in terms of normal and tangential tractions ($\bar{\sigma}$, $\bar{\tau}$) on the potential boundary of the excavation. The magnitude of these tractions will vary from point to point, depending upon the orientation of the various parts of the potential boundary. When the hole is excavated, these tractions are reduced to zero; thus, the excavation can be regarded as being equivalent to applying a system of negative tractions to a boundary in a solid mass without an excavation. The resultant state of stress can then be considered as the superposition of two stress systems: the original uniform stress state and the stresses induced by the negative surface tractions ($-\bar{\sigma}$,$-\bar{\tau}$). The distribution of induced stresses in the medium corresponding to the negative surface tractions can be determined using the analytic solution of stress and strain due to strip loads (Brady and Bray 1978).

Figure 5-1 compares a "real" situation (a) to an imaginary situation (b) in which there is an infinite plate. In the imaginary case, there is no hole in the plate. Instead, one imagines a line inscribed on the face of the plate corresponding to the boundary of the hole in the first plate. The line is divided into a series of elemental lengths and the elements are numbered consecutively. One now imagines that each element is subjected to an external force whose line of action lies in the plane of the plate. The force is resolved into components F_n and F_t,

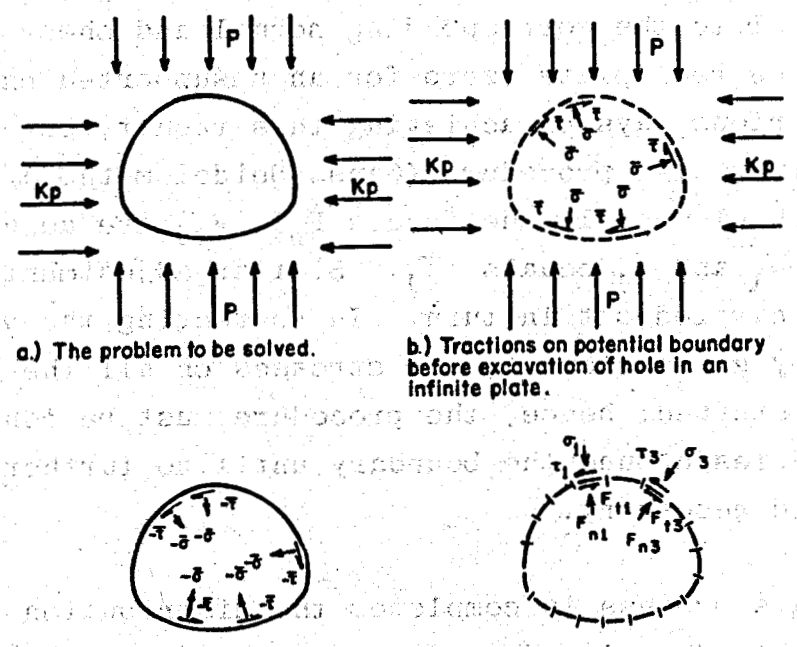

FIGURE 5-1
BOUNDARY-INTEGRAL-EQUATION METHOD
THEORETICAL DEVELOPMENT

normal and tangential to the element, and these are taken to be uniformly distributed over the length of the element. Because they do not correspond to the forces applied to the boundary of the real excavation, these forces are called fictitious. The procedure now is to adjust the forces so that the total normal and shear components of stress ($\bar{\sigma}$, $\bar{\tau}$) at the center of each element are equal to the corresponding normal and shear tractions ($-\bar{\sigma}$,$-\bar{\tau}$) of the real plate (zero for an unsupported excavation). There are various ways of achieving this result, but in this program an iterative procedure (Gauss-Seidel method) is used. Starting with element 1, the forces F_{n1}, F_{t1} are adjusted so that σ_1 equals $-\bar{\sigma}_1$ and τ_1 equals $-\bar{\tau}_1$. Similar adjustment for the elements is carried out in turn. In correcting the values of σ and τ for any given element, the stresses on all the other elements are disturbed; hence, the procedure must be continued for a series of cycles around the boundary until no further adjustment is considered necessary.

Once this process is complete, the distribution of tractions on the real boundary is identical to that on the imaginary boundary. Since these tractions determine the stress distribution in the surrounding medium, the distribution will also be the same for the two cases. To compute the stresses at any point in the imaginary plate, all that has to be done is to sum the contributions of the various fictitious forces such as F_{n1}, F_{t1}, F_{n2}, and F_{t2} (see Figure 5-1, d).

Once the stresses due to the negative surface tractions have been determined, they may be added to those of the original stress field to give the required stresses following excavation. Elastic displacements around the excavation can be calculated by using the standard solutions for displacements due to line loads in an infinite medium.

5.2.2 Modification for Incorporation of Fluid Pressure and Temperature Effects

The boundary-element program was modified to incorporate effects of fluid pressure or temperature changes. The following is a description of the theory supporting the modifications.

The basic stress-governing equation is the equilibrium equation:

[5-1] $$\sigma_{ij,i} - \rho g z_{,j} = 0$$

Note: Indicial notation is used and implicit summation over repeated indices is assumed.

In dry, isothermal elastic materials, the stress can be expressed as a function of the strain:

[5-2] $$\sigma_{ij} = \sigma_{ij}^{o} - D_{ijkl}\,\varepsilon_{kl}$$

Substituting [5-2] into [5-1] gives:

[5-3] $$\sigma_{ij,i}^{o} + (D_{ijkl}\,\varepsilon_{kl})_{,i} - \rho g z_{,j} = 0$$

Conventional numerical models for static-solid mechanics solve equation [5-3] by expanding it in terms of the displacements.

When problems involve fluid pressures or temperatures, the stress-strain equation [5-2] can be expressed as:

[5-4] $$\sigma_{ij} = \sigma_{ij}^{o} + D_{ijkl}\,(\varepsilon_{kl} - \alpha T \delta_{kl}) - P\delta_{ij}$$

Note that equation [5-4] assumes that the pore pressure interaction factor is unity, an assumption that is questionable for low porosity materials.

Substituting [5-4] into [5-1] produces the equilibrium equation used in the modified BIEM2D program:

[5-5] $$\sigma_{ij}^{o} + (D_{ijkl}\,\varepsilon_{kl})_{,i} - 2\,D_{ijkl}\,\delta_{kl}\,T_{,i} - P_{,j} - \rho g z_{,j} = 0$$

This can be compared with equation [5-3], which is formulated for the dry, isothermal case. The difference between equations [5-5] and [5-3] is in the inclusion of two pseudoforces (those of temperature and fluid pressure).

5.2.2.1 <u>Pseudo Body Forces</u>

For an isotropic material, the temperature pseudoforce is $-3K\alpha$ times the temperature gradient, where K is the bulk modulus. The pore-pressure pseudoforce is equal to minus the pore-pressure gradient.

By applying the pseudoforce as external strip loads around the edge of a temperature or pore-pressure change contour (the temperature and pore pressure changes are assumed to occur in steps at contoured lines), the computed deformation using equation [5-5] will be correct. The stresses are computed using equation [5-4] where the thermal and pore-pressure changes are applied as body forces within a pressure-change contour.

5.3 CAPABILITIES AND LIMITATIONS

5.3.1 Geometric Capabilities and Limitations

BIEM2D is limited to two-dimensional plane-strain problems within elastic whole spaces. Excavations and pressure-change surfaces must be modeled by combinations of straight-line elements.

The boundary elements can be placed in any combination or orientation within the elastic space. Boundary elements can represent conditions of stress, temperature, or pore pressure. Displacement cannot be assigned to elements as a boundary condition.

Displacements are calculated with respect to an arbitrary point included as input to the model. If a half-space is to be modeled, ground surface must be modeled by a relatively long segment of unloaded boundary elements.

5.3.2 Flow Capabilities and Limitations

No heat or mass flow calculations are performed by BIEM2D. BIEM2D computes only the influence of pressure change within the reservoirs. Pore pressure changes obtained from simulations of flow can be given as input to BIEM2D. Contours of pore pressure can be approximated by series of segments, each consisting of one element. Temperature effects are treated by conversion to the equivalent pressure change before input to the model.

5.3.3 Material Properties

The continuum is linearly elastic, homogeneous, and isotropic. Its behavior is defined by Young's modulus and Poisson's ratio.

5.4 USABILITY

5.4.1 Documentation

The original users' manual for BIEM2D is not appropriate for use with the reservoir modeling version of BIEM2D developed by Golder Associates. A new, updated users' manual incorporating recent program enhancements and an improved discussion of input parameters is included as Appendix B.

5.4.2 Input Ease

Coding of input is relatively easy in BIEM2D because of the simple geometric and material property assumptions used. In addition, automatic generation of elements along linear or curved segments simplifies the specification of boundary elements. This feature allows the user to specify whole series of elements by a single segment specification. Observation point grids can be specified with similar ease.

The program can handle symmetry about either one or two axes, which further simplifies the input.

5.4.3 Output Control and Comprehensibility

BIEM2D produces only one level of output. The output includes stresses and deformations at the midpoint of each boundary element. In addition, rock-failure information is output where relevant. Although not important in the cases studied, rock failure information may be useful in other cases.

In addition to producing output at elements, BIEM2D can produce output at any desired locations within the elastic space when a grid of observation points is specified by the user.

Output is well labeled and easy to understand.

5.4.4 Solution Efficiency

The BIEM2D program is a very efficient method for homogeneous, isotropic, linearly elastic stress-strain problems in two dimensions. Because of the small number of elements needed, the demands on computer storage and time are very low. Because solution time is also dependent on the formulation of the problem (ill-formed problems require more iterations), there is no direct relationship between solution time and the number of elements. However, Figure 5-2 gives some indication of solution time versus number of elements for the problems modeled in this study.

5.4.5 Resume of Performance on Sample Problems

One of the most critical assumptions of the boundary element method is that the subsurface geology can be modeled as a homogeneous, isotropic, linear elastic space. This assumption was considered reasonable for sample problems 1, 3, 5, and 6, and BIEM2D was used to model these problems. It was not considered reasonable for problems 2 and 4, where inhomogeneity plays an important role.

Problem 1 is one-dimensional and was modeled by use of a reservoir and ground surface much greater than the reservoir depth. Predicted settlement at the surface was 1.3 feet, which compares well with the exact result.

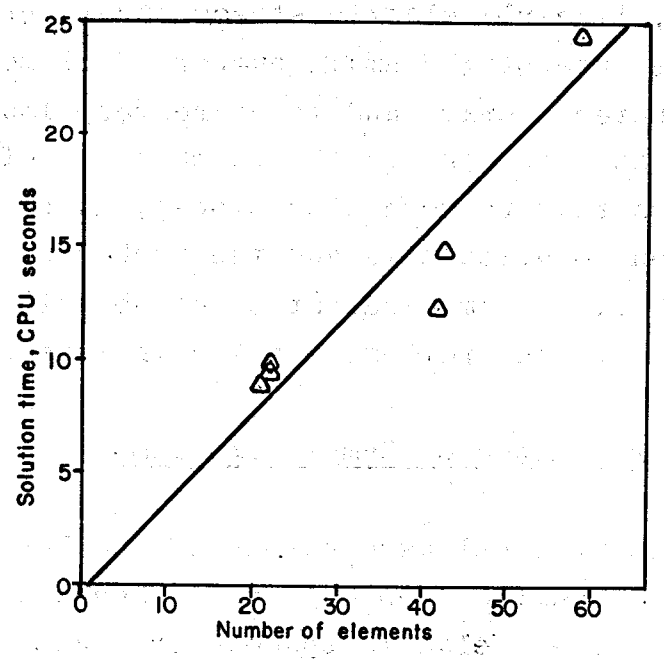

FIGURE 5-2
BOUNDARY-INTEGRAL-EQUATION METHOD
SOLUTION EFFICIENCY

Two-dimensional problems 3 and 5 had maxima of 0.6-foot and 2.5-foot surface settlement, respectively, over the center of the reservoir. Compaction of the reservoir surface exceeded surface settlement. Unexpected edge effects were observed at the sides of the reservoirs.

Three-dimensional problem 6 was modeled in two dimensions with BIEM2D. Maximum surface subsidence and maximum reservoir compaction occurred at the same horizontal location.

Results of sample problems are discussed in greater detail in Section 5.5.

5.5 PERFORMANCE ON SAMPLE PROBLEMS AND CASE STUDIES

5.5.1 Sample Problem 1: Confined Infinite Reservoir

Sample problem 1 (Figure 1-1) is a one-dimensional problem with a 50-foot-thick reservoir at a 570-foot depth. The pore pressure in the reservoir drops by 50,400 psf. Because sample problem 1 is one-dimensional, the boundary elements of the top and bottom of the pressure contour were extended to 6300 feet (about 10 times the depth to the reservoir) on the positive side of X = 0 (the axis of symmetry). This length was judged sufficient to eliminate the effects at X = 0 of the ends of the segments. The ground-surface elements were extended to X = 25,000 feet. Figure 5-3 shows the problem configuration.

The initial element lengths along the ground surface were chosen to be about one-tenth of the depth to the reservoir at X = 0 and increased as X = 6300 feet was approached. In order to model the reservoir in sample problem 1, it was necessary to have an upper-pressure drop contour of -50,400 psf where the drop

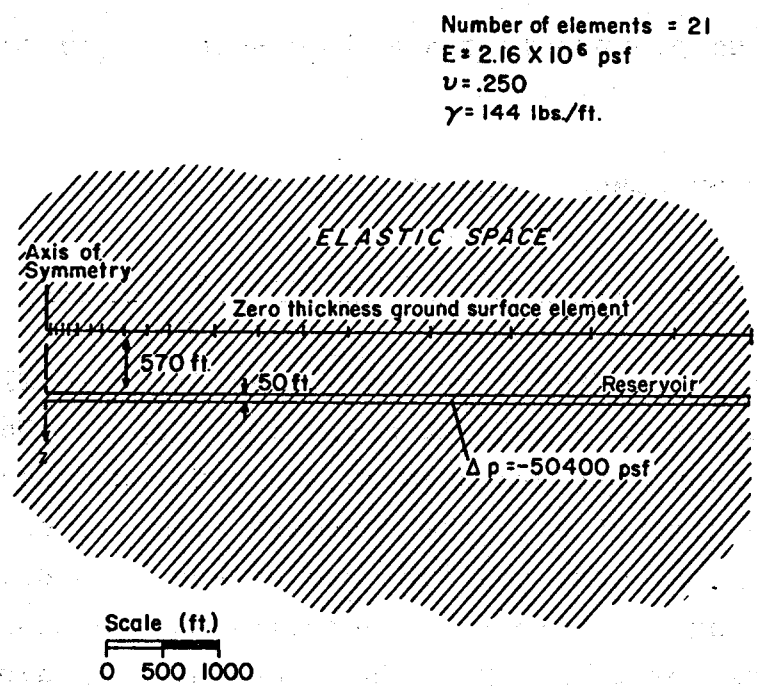

FIGURE 5-3
BOUNDARY-INTEGRAL-EQUATION METHOD
ELEMENT CONFIGURATION OF SAMPLE PROBLEM 1

applied to the material below the contour line. Then a second pressure contour of +50,400 psf was used to raise the material below the reservoir back to a condition of no pressure change. Figure 5-4 shows the variation of vertical displacement with depth. Note that these values are relative to the displacement at 1000 feet.

Sample problem 1 was rerun with the ground-surface elements half as long as in the first run (twice as many elements). There was no change in the relative deformation. Therefore it was concluded that the surface element size in the first run was adequate.

Sample problem 1 needed 13 iterations to produce a solution. Run time was 0.888 CPU seconds.

5.5.2 Sample Problem 3: Confined Finite Reservoir

Sample problem 3 (Figure 1-3) is similar to problem 1 except that the reservoir is of finite length (1000 feet) and is considered infinitely long in the Y-direction. An element configuration was used that was similar to that in sample problem 1 (see Figure 5-5).

Figure 5-6 shows the vertical displacements that occurred due to a pressure drop of 50,400 psf in the reservoir. At the center line of the reservoir, the ground surface dropped 0.62 feet. As expected, ground-surface displacement tends to zero far from the reservoir.

Closure in the reservoir at the center line was 0.93 feet. This decreased to 0.458 feet at the reservoir edge.

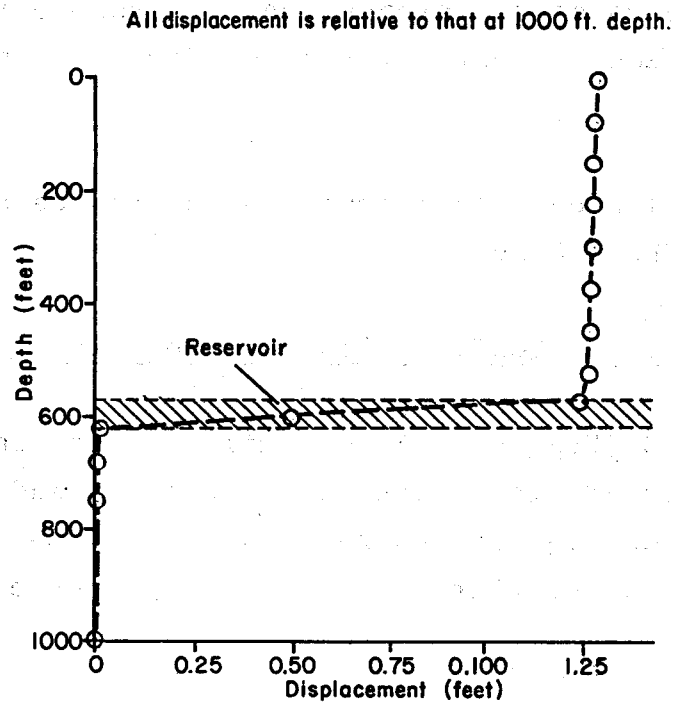

FIGURE 5-4
BOUNDARY-INTEGRAL-EQUATION METHOD
VARIATION IN VERTICAL DISPLACEMENT WITH DEPTH,
SAMPLE PROBLEM 1

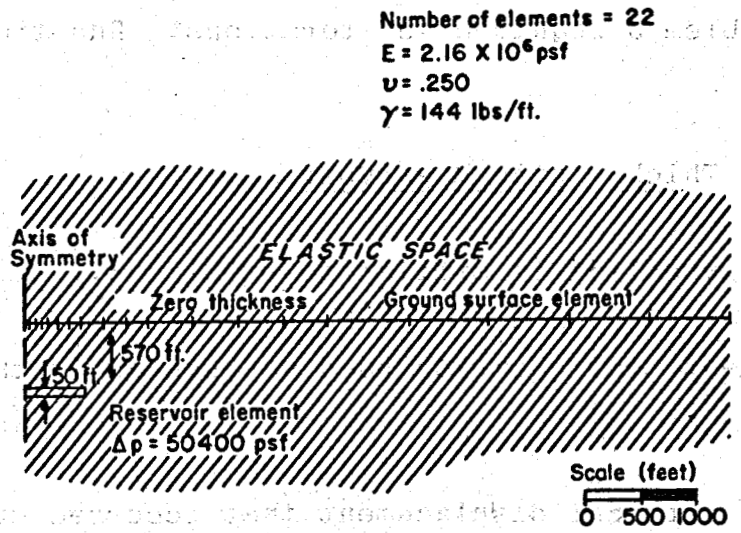

FIGURE 5-5: BOUNDARY-INTEGRAL-EQUATION METHOD ELEMENT CONFIGURATION OF SAMPLE PROBLEM 3

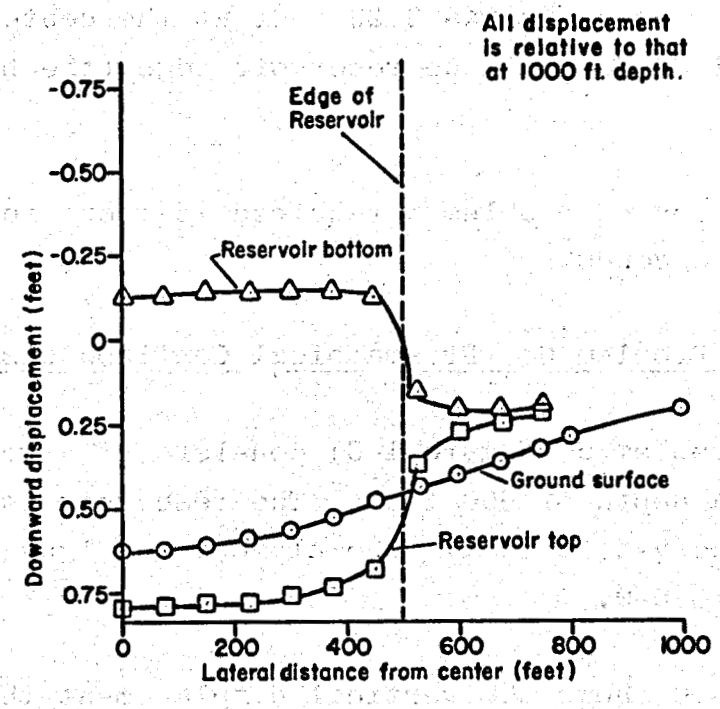

FIGURE 5-6: BOUNDARY-INTEGRAL-EQUATION METHOD VERTICAL DISPLACEMENT OF GROUND SURFACE AND RESERVOIR TOP AND BOTTOM, SAMPLE PROBLEM 3

The solution for problem 3 required 13 iterations. Run time was 0.970 CPU seconds.

5.5.3 Sample Problem 5: Thick Finite Reservoir

Sample problem 5 (Figure 1-5) is similar to problem 3. However, the reservoir in problem 5 is at a depth of 500 feet and is 500 feet thick. The element configuration used was basically the same (Figure 5-7).

Figure 5-8 shows the vertical displacement that occurred due to a pore-pressure drop of 50,400 psf in the reservoir. At the center line of the reservoir the ground surface dropped 2.54 feet. The top of the reservoir dropped 3.05 feet at the center. Closure in the reservoir was 3.23 feet at the center line. This decreased to 1.67 feet at the reservoir edge (the base moved up 0.18 feet).

The solution of problem 5 required 15 iterations. Run time was 0.956 CPU seconds.

5.5.4 Sample Problem 6: Prismatoidal Confined Reservoir

Sample problem 6 (Figure 1-6) consists of a wedge-shaped reservoir at a depth of 600 feet. The reservoir is assumed infinite in the y-direction. The element configuration used is shown in Figure 5-9.

Figure 5-10 shows the vertical displacement that occurred due to a pore-pressure drop of 21,600 psf. Maximum ground surface displacement was 0.38 feet. Maximum reservoir closure was 1.08 feet.

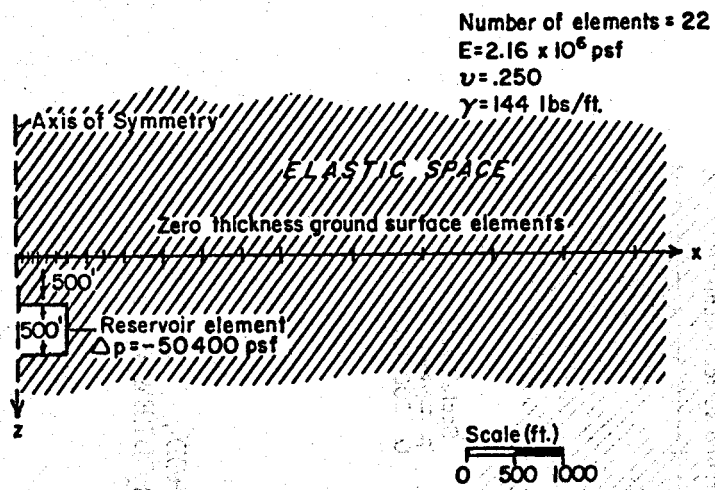

FIGURE 5-7: BOUNDARY-INTEGRAL-EQUATION METHOD ELEMENT CONFIGURATION OF SAMPLE PROBLEM 5

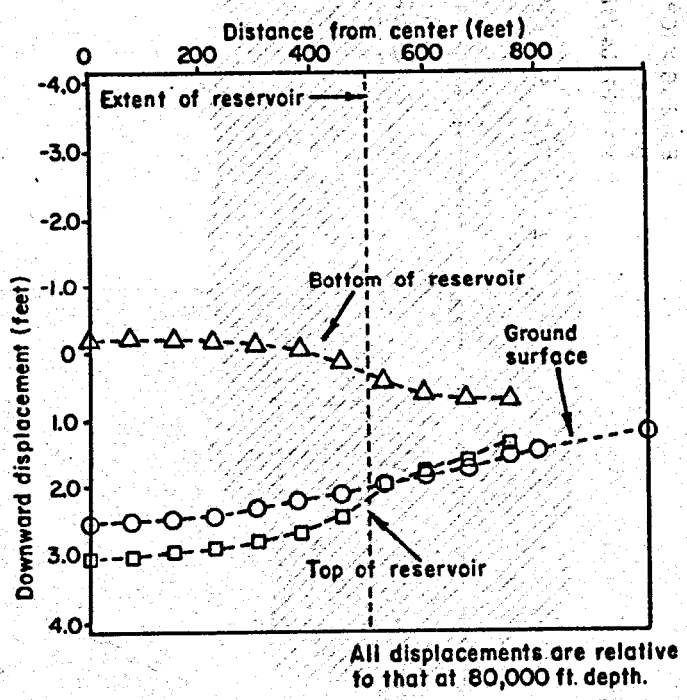

FIGURE 5-8: BOUNDARY-INTEGRAL-EQUATION METHOD VERTICAL DISPLACEMENT OF GROUND SURFACE AND RESERVOIR TOP AND BOTTOM, SAMPLE PROBLEM 5

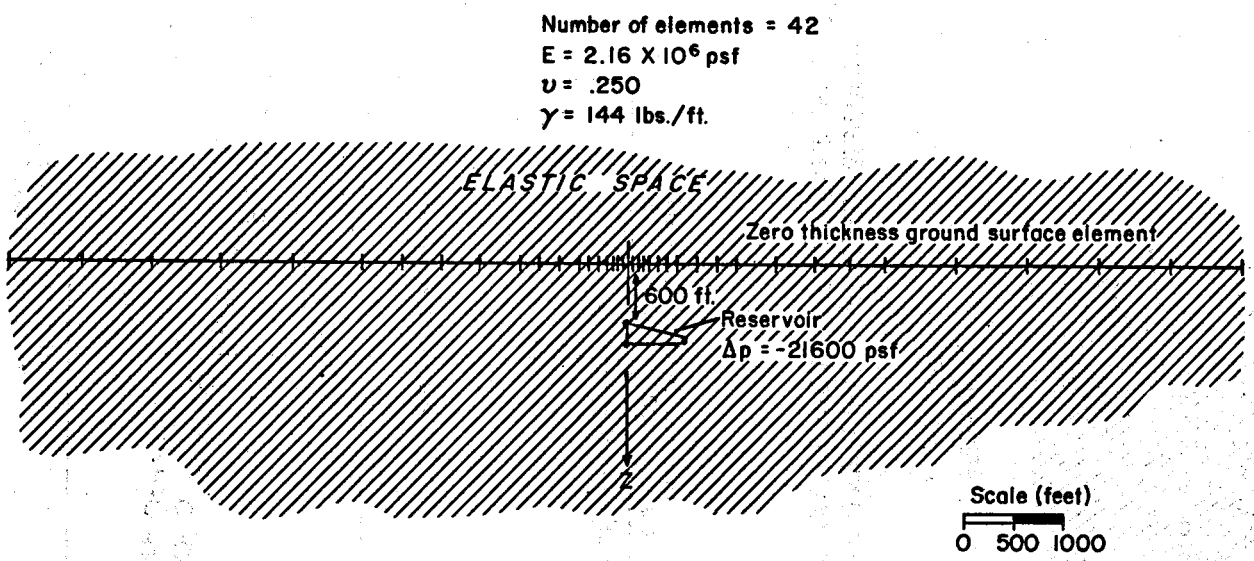

FIGURE 5-9
BOUNDARY-INTEGRAL-EQUATION METHOD,
ELEMENT CONFIGURATION OF SAMPLE PROBLEM 6

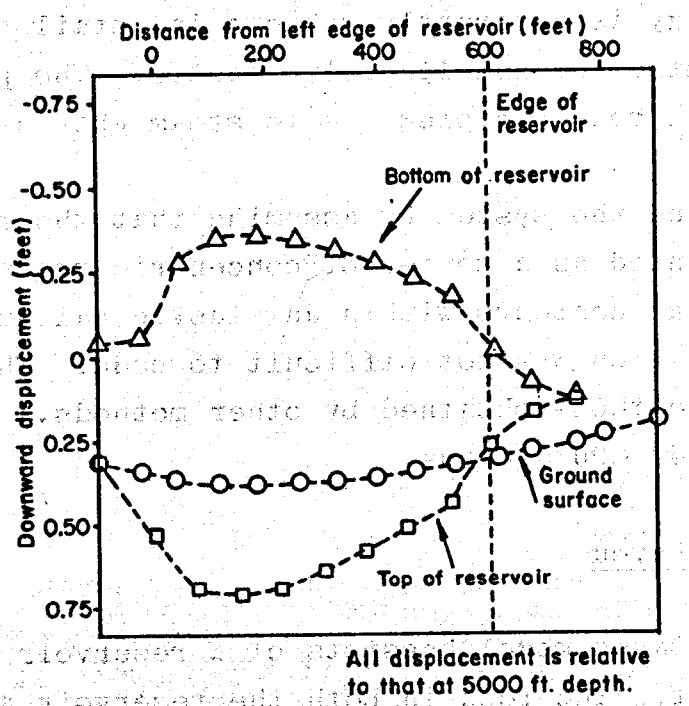

FIGURE 5-10
BOUNDARY-INTEGRAL-EQUATION METHOD
VERTICAL DISPLACEMENT OF GROUND SURFACE
AND RESERVOIR TOP AND BOTTOM,
SAMPLE PROBLEM 6

The solution of sample problem 6 required 15 iterations. Run time was 1.227 CPU seconds.

5.5.5 Case Studies

5.5.5.1 The Geysers

The Geysers area consists of a basically three-dimensional system but is simplified to two dimensions for this model reservoir. Its geology is apparently unknown in detail and is assumed homogeneous, isotropic, and linearly elastic. The pressure of the reservoir has been dropping due to steam extraction.

BIEM2D solved the system by assuming that the reservoir could be represented as a series of concentric pressure/temperature change contours within an elastic half-space. The element configuration was not difficult to code. The solution conformed well to those obtained by other methods. The solution required only 2.47 CPU seconds.

5.5.5.2 Austin Bayou

The Austin Bayou model consists of a reservoir at a depth of about 15,000 feet. The rock in both the reservoir and overburden is inhomogenous, consisting of inter-layered sands and shales. The problem was simplified to a homogeneous material for the boundary-element model. An equivalent pressure drop in the reservoir was determined to give a reservoir compaction consistent with that determined by CCC. Again, coding was relatively easy and the solution was inexpensive (1.312 CPU seconds).

5.6 CONCLUSION

The boundary-element method is applicable to modeling of geothermal subsidence if the conditions listed previously are met. It is a very easy method to use as the input is short and easily determined. Some experience is necessary for choosing the proper size of elements and in locating endpoints of "infinite" boundaries. One distinct drawback to using the method for geothermal subsidence problems is that the temperature or pressure-drop contours must be already known.

5.7 LIST OF SYMBOLS

p	vertical field stress ($ML^{-1}T^{-2}$)
Kp	horizontal field stress ($ML^{-1}T^{-2}$)
σ	normal traction ($ML^{-1}T^{-2}$)
τ	tangential traction ($ML^{-1}T^{-2}$)
F_n	normal force (MLT^{-2})
F_t	tangential force (MLT^{-2})
ρ	density (ML^{-3})
g	acceleration of gravity (LT^{-2})
Z	depth (L)
σ_{ij}	stress tensor ($ML^{-1}T^{-2}$)
σ_{ij}^{o}	initial stress tensor ($ML^{-1}T^{-2}$)
ε_{ij}	strain tensor
ε_{ij}^{o}	initial strain tensor
α	coefficient of linear thermal expansion ($°C^{-1}$)
T	change in temperature (°C)
δ_{ij}	Kronecker delta
P	pore pressure ($ML^{-1}T^{-2}$)
K	bulk modulus ($ML^{-1}T^{-2}$)
ν	Poisson's ratio
E	elastic modulus ($ML^{-1}T^{-2}$)
G	shear modulus ($ML^{-1}T^{-2}$)

5.8 REFERENCES

Brady, B.H.G., and J.W. Bray (1978). "The Boundary Element Method for Determining Stresses and Displacements Around Long Openings in a Triaxial Stress Field," Int. J. Rock Mech. Min. Sci. and Geomech. Abstr., Vol. 15, pp. 21-28.

Hoek, E. and E.T. Brown (1980). Underground Excavations in Rock (draft), to be published by the Institution of Mining and Metallurgy, London, England.

6.0 FINITE-ELEMENT STRESS-STRAIN FLOW MODEL "CONSOL3"

6.1 INTRODUCTION

The two-dimensional finite-element program CONSOL3, written by R. W. Lewis, solves a system of first-order nonlinear flow and consolidation equations. The program has been used to model the subsidence of Venice (Lewis 1978), the subsidence of the Polesine area in northeast Italy (Schrefler et al. 1977), and the progressive deformation under foundations of offshore structures due to both static and cyclic loading (Zienkiewicz et al. 1976).

6.2 SOLUTION METHOD - GENERAL THEORY

The system of first-order nonlinear flow and consolidation equations solved by CONSOL3 is written in matrix form as:

$$\begin{bmatrix} 0 & 0 \\ 0 & \underset{\sim}{H} \end{bmatrix} \begin{Bmatrix} \underset{\sim}{u} \\ \underset{\sim}{P} \end{Bmatrix} + \begin{bmatrix} \underset{\sim}{K}_T & -\underset{\sim}{L} \\ -\underset{\sim}{L}^T & -\underset{\sim}{S} \end{bmatrix} \frac{d}{dt} \begin{Bmatrix} \underset{\sim}{u} \\ \underset{\sim}{P} \end{Bmatrix} = \begin{Bmatrix} \frac{d\underset{\sim}{f}_n}{dt} + \underset{\sim}{c} \\ \underset{\sim}{f}_P \end{Bmatrix}$$

where: $\underset{\sim}{P}$ is the nodal pore pressure

$\underset{\sim}{u}$ is the nodal displacement

$\underset{\sim}{K}_T$ depends on the matrix tangential stiffness

$\underset{\sim}{L}$ is given by the matrix and solid constitutive relationships

$\underset{\sim}{H}$ depends on the material permeability

$\underset{\sim}{f}_n$ are the nodal forces due to boundary tractions and body forces

$\underset{\sim}{c}$ is due to the material creep

$\underset{\sim}{f}_p$ depends on inflow and boundary conditions

$\underset{\sim}{S}$ is due to the matrix, soil solid, and fluid compressibilities

More complete definitions of the parameters in this system can be found in Lewis and Schrefler (1978) or Zienkiewicz et al. (1976).

This system of equations is symmetric and can be solved for specified initial displacements, pore pressures, and stresses. Isoparametric finite elements are used. A complete consolidation history may be obtained using various time-stepping schemes.

6.3 CAPABILITIES AND LIMITATIONS

6.3.1 Geometric Capabilities and Limitations

CONSOL3 may be used to solve two-dimensional plane strain, plane stress, or axisymmetric systems in any consistent set of units. A unit width of material is considered in the plane-strain and plane-stress formulations and 1 radian of material is used in the axisymmetric formulation. In the latter system, no point loads or outflows may be specified at the axis of symmetry. We expected the units of outflow to be volume per time, but found that they were volume/time step. Finite elements are isoparametric quadrilaterals with either linear or quadratic shape functions. In all models but one, a rectangular mesh was used. Irregular quadrilaterals were employed for a two-dimensional Wairakei model; for undetermined reasons, however, the model was unstable. Arrays within the program are dimensioned to allow up to 200 elements and 300 nodes, of which 150 may have specified boundary conditions (displacements or pore pressures) and 100 may have specified point loads or outflows. Boundary conditions and point loads or outflows may both be functions of time. The maximum node number difference allowed is 40, and 100 time steps may be taken. The time-stepping scheme is specified by the user

and may be either forward difference, central difference, or backward difference. With some difficulty, because of the lack of documentation, we were able to increase array size limits in CONSOL3. A single Gauss point or a two-by-two or three-by-three grid of Gauss points in each element is specified by the user to integrate over elements.

6.3.2 Flow Capabilities and Limitations

CONSOL3 allows a only a single fluid phase. The ratio of hydraulic conductivity to the weight density of the fluid must be constant for a given material but need not be the same in the vertical and horizontal directions. The effects of changes in temperature and pressure on hydraulic conductivity are not modeled.

6.3.3 Material Properties

CONSOL3 is dimensioned to allow up to 200 different materials. The materials are assumed to be isotropic. Four different failure criteria (Mohr-Coulomb, Roscoe Critical State Ellipse, Displaced Critical State Model, and Combination Model of Mohr-Coulomb and Critical State Ellipse) are incorporated in the program. In most models we specified Mohr-Coulomb material failure with a very high value for cohesion so that the material behavior would always be linear. Our attempts to allow nonlinear material behavior using either the Displaced Critical State Model or the Roscoe Critical State Ellipse were unsuccessful for undetermined reasons. The displacements due to a pore-pressure decrease which were determined in those tests depended strongly on the specified value of Young's modulus and very weakly on the failure parameters P_{co} and χ.

Initial stresses are specified by supplying the material weight and the elevation of the upper boundary of each layer of different weight material. Up to 10 strata may be used. The users' manual indicates that the program also allows the user to specify initial stress values at each node by reading them from tape or disk, but this option does not work. Positive normal stresses indicate tension and positive pore-pressures compression.

6.4 USABILITY

6.4.1 Documentation

Program documentation is almost nonexistent. There is a sparse users' manual in which the input parameters are, for the most part, undefined and apparently often misnamed. A number of options described by the manual do not exist. Published papers by Lewis and his colleagues (Lewis and Schrefler 1978; Schrefler et al. 1977; Zienkiewitz et al. 1976) seemed to have only a tenuous relation to the CONSOL3 solution method. Comment cards within the program are few and far between.

Improved documentation is now being prepared and presumably will be available in the future.

6.4.2 Input Ease

Assuming that the user can come up with appropriate definitions for the input parameters, the input itself is fairly straightforward. It can, however, become lengthy and, in the case of an applied distributed load or outflow, require some simple but time-consuming calculations. If any initial displacements or pore pressures are nonzero, they must all be specified.

There is no provision for automatic generation of equal pore-pressure or displacement values for a series of nodes. If the system is subject to a uniformly distributed boundary load, the user must calculate and input the equivalent point loads that are unique to each finite-element mesh.

6.4.3 Output Control and Comprehensibility

The user may ask for (1) full output, (2) no stress output, or, (3) no input data output or stress output. In case (3), a portion of the input data is printed out along with initial stresses at Gauss points. For every time step, displacements and pore pressures at each node and reactions at nodes where displacements or pore pressures were specified are printed. In case (2), additional input data including element nodes, nodal coordinates, boundary conditions, and initial conditions are also output. If full output is specified, stresses and strains at all Gauss points are included in the time-step information. The magnitudes of reactions corresponding to specified pore pressures in all the cases we ran seemed much too large. We conjecture that a normalization factor included to make the matrices well-conditioned was not removed.

6.4.4 Solution Efficiency

The solution time depends linearly on the number of time steps used. For a given number of time steps, the cost varies with the number of elements and nodes in the model and the maximum node number difference in the elements. Some examples of costs are given in Table 6-1. Costs are plotted against the number of elements for five time steps in Figure 6-1.

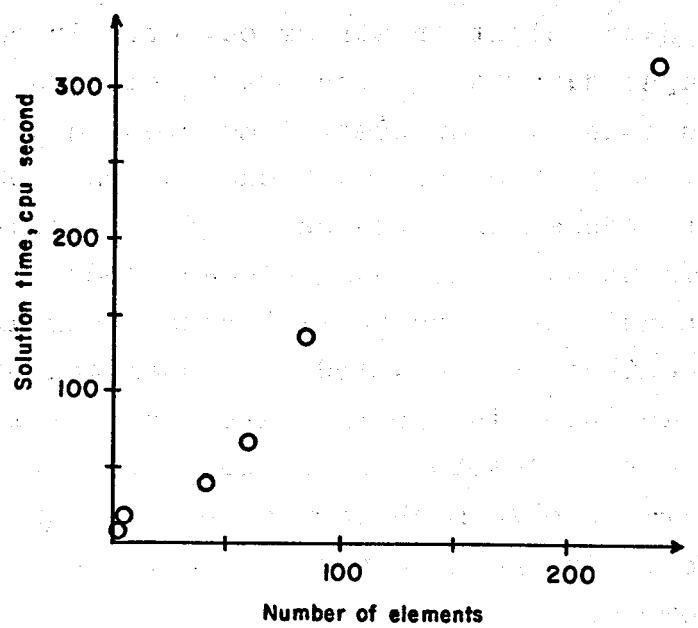

FIGURE 6-1
TWO-DIMENSIONAL FINITE-ELEMENT MODEL
SOLUTION EFFICIENCY AS A FUNCTION OF NUMBER OF ELEMENTS

TABLE 6-1
CONSOL3 SOLUTION EFFICIENCY

TIME STEPS	ELEMENTS	NODES	MAXIMUM NODE NUMBER DIFFERENCE	SOLUTION TIME (CPU SECONDS)
3	7	38	7	1.9
3	42	153	25	22.4
5	84	293	46	133.7
5	240	785	40	318.3

6.4.5 Resume of Performance on Sample Test Problems and Case Studies

Two of the sample problems, 2 and 4, were solved with CONSOL3. The reservoir and aquitard compaction at 3000 years calculated by CONSOL3 as a one-dimensional problem in sample problem 2 agreed with the analytically determined ultimate compaction. In sample problem 4, overburden was included in the finite-element model so that the surface subsidence due to the reservoir system compaction could be determined.

CONSOL3 was implemented for case studies of Wairakei and Austin Bayou. The Wairakei grid was unstable, while the Austin Bayou Model was quite useful and provided answers to a variety of questions.

In all the sample problems and case studies the following definitions were used for parameters undefined or misnamed in the input manual:

- compressibility factor:
  $S = \frac{n}{K_f}$
  where n is the porosity of the material and K_f is the fluid compressibility

- permeability per unit weight of fluid:
  $\frac{K}{\gamma_w}$ = hydraulic conductivity per unit weight of fluid

- submerged unit weight of solid:
  γ_e = saturated weight of solid minus initial pore pressure gradient

- pore pressure:
  p_e = actual pore pressure minus initial equilibrium pore pressure

- stress:
  σ_e = effective stress

- For a system with its upper boundary at a depth d below the ground surface, the uniform vertical load P at the upper boundary was calculated as:
  $P = \gamma_e d$

Using these definitions, the systems modeled were in equilibrium; that is, there were no vertical or horizontal displacements and no change in pore pressure as long as the system remained undisturbed.

6.5 PERFORMANCE ON SAMPLE PROBLEMS AND CASE STUDIES

6.5.1 Sample Problem 2: Infinite Reservoir With Permeable Confining Layer

Sample problem 2 (Figure 1-2) was modeled as a two-element, two-material, plane-strain system with an applied pore-pressure

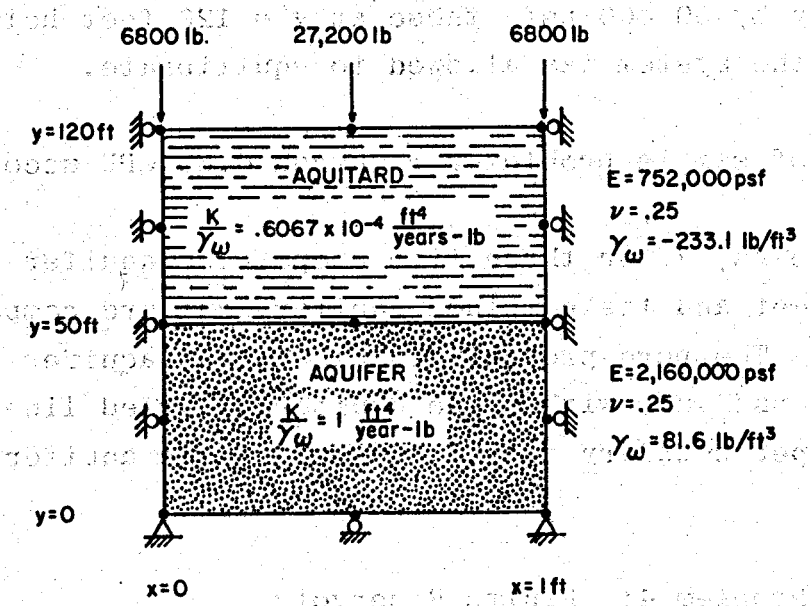

FIGURE 6-2
TWO-DIMENSIONAL FINITE-ELEMENT MODEL,
FORMULATION FOR SAMPLE PROBLEM 2

drop at the aquifer-aquitard boundary. The finite-element grid with element dimensions, overburden loads, and material properties is shown in Figure 6-2.

The nodes at x = 0 and 1 foot were constrained to have no horizontal displacement, and those at y = 0 were allowed no vertical displacement. The fluid was assumed incompressible (S = 0). Pore pressures p_e at y = 50 feet were decreased instantaneously by 50,400 psf, those at y = 120 feet held constant, and the system was allowed to equilibrate.

Solution of sample problem 2 required 0.85 CPU seconds.

At 3000 years, after three time steps, the aquifer compaction was .97 feet and the combined aquifer-aquitard compaction was 2.93 feet. The pore-pressure change in the aquifer was uniformly -50,400 psf and, within the aquitard, varied linearly from zero at the upper boundary to -50,400 psf at the aquifer-aquitard interface.

6.5.2 Sample Problem 4: Finite Reservoir With Permeable Confining Layer

Sample problem 4 (Figure 1-4) was modeled with 42 quadratic elements. Aquifer and aquitard properties are the same as in sample problem 2. Overburden with E = 2,160,000 psf was included in the model. The finite-element grid is shown in Figure 6-3. Nodes at x = 0, 5000 feet were constrained to have no horizontal displacement, and those at y = 0 were allowed no vertical displacement. However, horizontal displacement was allowed at y = 0, which is equivalent to specifying infinitely soft material below the reservoir.

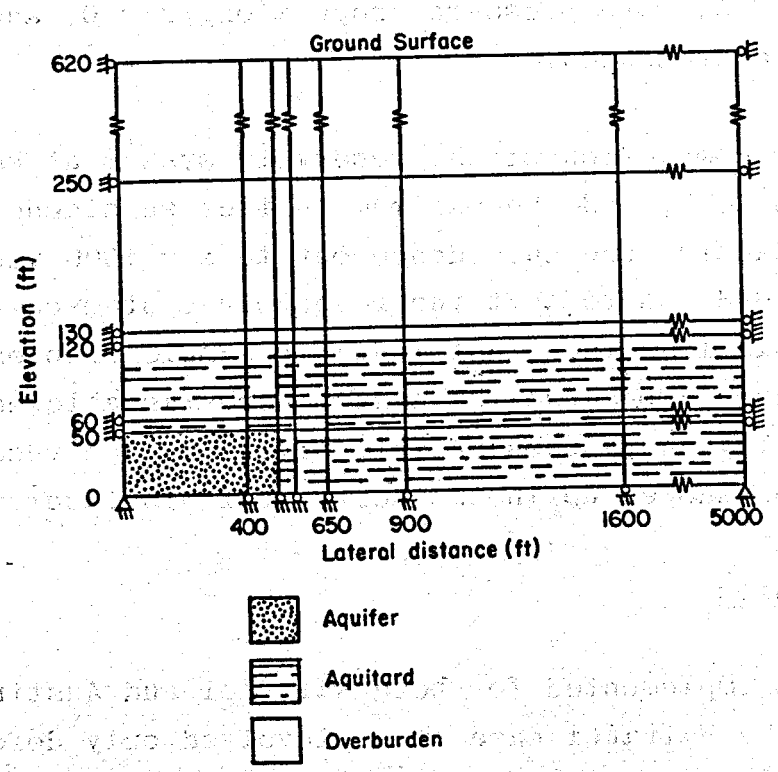

FIGURE 6-3
TWO-DIMENSIONAL FINITE-ELEMENT,
FORMULATION FOR SAMPLE PROBLEM 4

Solution of sample problem 4 required 22.14 CPU seconds.

As in sample problem 2, the equilibrium pore-pressure drop above the aquifer varied linearly from 50,400 psf at the aquifer-aquitard interface to zero at the upper aquitard boundary. In the horizontal direction, the effect of the aquifer pore- pressure drop was significant only out to x = 775 feet. In figures 6-4 and 6-5, pore pressure drops along x = 0, and y = 0, respectively, are presented.

The maximum compaction of the reservoir system at equilibrium was 2.68 feet, and the maximum surface subsidence was 2.27 feet. Compaction and subsidence out to x = 1600 feet are shown in Figure 6-6. Note that the reservoir system compaction in this problem is less than that found in sample problem 2 (2.93 feet). This occurred because the system here was allowed to deform horizontally and a substantial portion of the reservoir system compaction showed up in the horizontal displacement.

6.5.3 Case Studies

CONSOL3 was implemented for both Wairakei and Austin Bayou case studies. The Wairakei case study involved only deformation, but utilized a variety of complex trapezoidal element shapes. It was unstable. The Austin Bayou Case Study involved both flow and deformation and was used in a parametric study with considerable success.

6.6 CONCLUSIONS

With the current users' manual, CONSOL3 is an extremely difficult program to use. As a result, solutions obtained by CONSOL3 are sometimes suspect due to the possibility of errors in

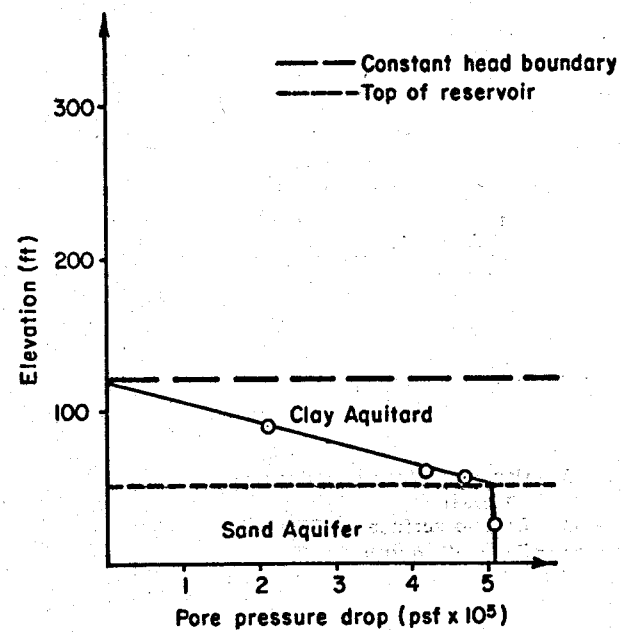

FIGURE 6-4: TWO-DIMENSIONAL FINITE-ELEMENT MODEL PORE-PRESSURE DECREASE ON VERTICAL AXIS OF SYMMETRY, SAMPLE PROBLEM 4

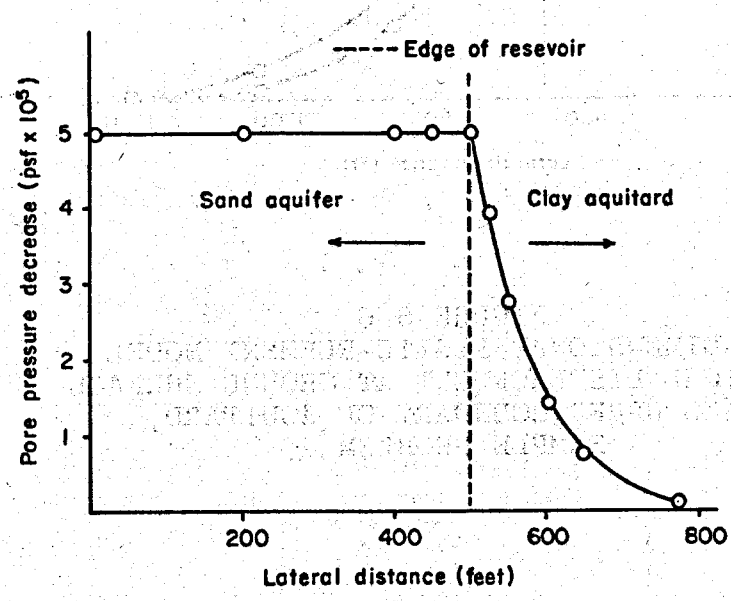

FIGURE 6-5: TWO-DIMENSIONAL FINITE-ELEMENT MODEL PORE-PRESSURE DECREASE AT LOWER BOUNDRY OF AQUIFER, SAMPLE PROBLEM 4

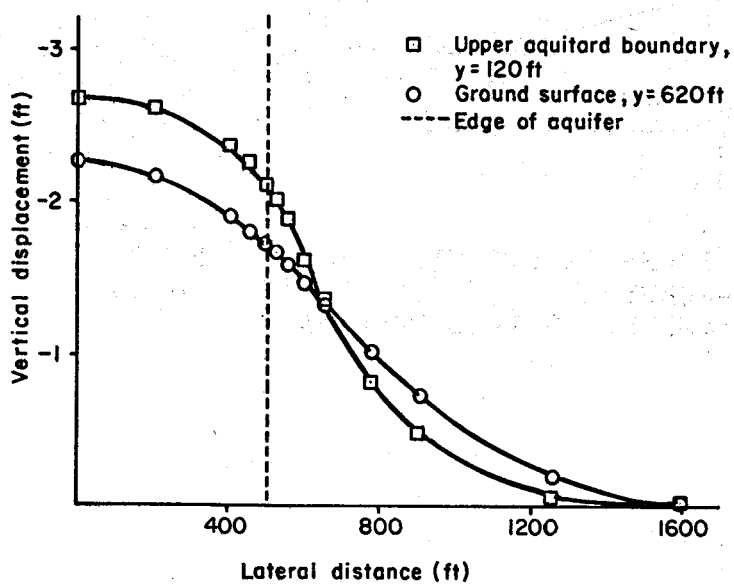

FIGURE 6-6
TWO-DIMENSIONAL FINITE-ELEMENT MODEL
VERTICAL DISPLACEMENT AT GROUND SURFACE
AND UPPER BOUNDARY OF AQUITARD,
SAMPLE PROBLEM 4

input. In addition, the complexities of CONSOL3 can lead to excessive cost in some cases.

The ability of CONSOL3 to perform coupled deformation-flow calculations and to model inhomogeneous cases, however, makes it extremely valuable for geothermal subsidence modeling.

6.7 REFERENCES

Lewis, R.W., and B. Schrefler (1978). "A Fully Coupled Consolidation Model of the Subsidence of Venice," Water Resources Research, Vol. 14, No. 2.

Schrefler, B.A., R.W. Lewis, and V.A. Norris (1977). "A Case Study of the Subsurface Subsidence of the Polesine Area," International Journal for Numerical and Analytical Methods in Geomechanics, Vol. 1, pp. 377-386.

Zienkiewicz, O.C., R.W. Lewis, V.A. Norris, and C. Humpheson (1976). "Numerical Analysis for Foundations of Offshore Structures with Special Reference to Progressive Deformation," Society of Petroleum Engineers, Spring Meeting, 1976, SPE 5760.

7.0 MASS AND HEAT FLOW MODEL "CCC"

7.1 INTRODUCTION

Single-phase, water-dominated geothermal systems are characterized by a circulating liquid that transfers most of the heat and largely controls subsurface pressures. Fluid production from the reservoir of such a system results in a reduction of pressures and vertical consolidation in the whole system (reservoir and surrounding rocks) and may lead to land surface subsidence. CCC (for Conduction Convection Consolidation) is a numerical model developed at the Lawrence Berkeley Laboratory that simulates both the transport of water and heat through saturated, porous, single phase, water-dominated geothermal systems and the vertical deformation of the flow region.

7.2 SOLUTION METHOD - GENERAL THEORY

7.2.1 Theory

Based on the principles of conservation of mass, momentum, and energy, several authors have developed the equations governing the transport of fluid and heat through porous media (e.g., Faust and Mercer 1977; Mercer et al. 1974). For a slightly compressible fluid (e.g., water), the fluid-flow equation may be expressed as (Lippmann et al. 1977c)

[7-1]
$$\frac{\partial}{\partial t}\int_V \frac{\rho}{1+e}\left(ek+\frac{de}{d\sigma'}\right)P\,dV=\int_S \frac{k\rho}{\mu}\left(\nabla P-\rho\bar{g}\right)\cdot\bar{n}\,dS+\int_V Q\,dV$$

and the heat flow equation may be expressed as

[7-2]
$$\frac{\partial}{\partial t}\int_V (\rho c)_M T\,dV=\int_S K_M \nabla T\cdot\bar{n}\,dS-\int_S \rho c_F \delta T\bar{v}_d\cdot\bar{n}\,dS+\int_V q\,dV$$

A list of symbols and their definitions is given at the end of this chapter.

The left-hand side of the fluid-flow equation [7-1] is the capacity term, which incorporates the one-dimensional consolidation theory of Terzaghi (1925). According to this theory, the void ratio of a material is a function of its present (vertical) effective stress and, for nonelastic (nonlinear) materials, its previous stress history. From the effective-stress law, vertical effective stress is the vertical total stress due to the weight of the overlying rock minus the fluid (pore) pressure.

Linear, elastic, consolidation behavior is described by a linear void ratio versus effective stress curve. As the effective stress increases, the void ratio of the material decreases. The absolute value of the slope of this curve is the coefficient of compressibility of the material (a_v).

Nonlinear, inelastic consolidation behavior is described by void ratio versus logarithm of effective-stress curves. As the effective stress increases, the void ratio of the material decreases. There is a virgin curve with a slope whose absolute value is the compression index (C_c) and a series of parallel swelling-recompression curves (CCC neglects the hysteresis between swelling and recompression curves) with slopes whose absolute values are the swelling index (C_s). If the effective stress is greater than or equal to the previous maximum effective stress, the virgin curve is followed and the rock is said to be normally consolidated. If the effective stress is less than the previous maximum effective stress, the swelling curve is followed and the rock is said to be overconsolidated.

Thus, deformation is dependent on stress history for nonelastic materials.

Since pore pressure and effective stress are related by the effective stress law, pore pressure changes are reflected by effective stress changes, which in turn are related to void ratio changes. Void ratio changes give pore volume changes if the solid volume is defined to remain constant. Because of the one-dimensional nature of Terzaghi's consolidation theory, vertical strains and displacement result in, and are restricted to, the saturated formations which release water from storage during fluid production. These vertical displacements may or may not be directly expressed at the ground surface as land subsidence. The external loading of the overburden, caused by the vertical deformation of the deeper saturated formations, may result in displacements at the ground surface that are different in magnitude and direction than those at the top of the saturated flow region.

In hydrogeology, it is more customary to express the capacity term in the fluid flow equation [7-1] (Lippmann et al. 1977b) as:

[7-3] $$\frac{\partial}{\partial t}\int_V \frac{S_s}{\bar{g}} P dV$$

The coefficient of specific storage (S_s) combines the compressibilities of the fluid and the rock/soil skeleton. The coefficient of specific storage is usually taken to be constant. This form of the capacity term can be used when consolidation is not being considered.

The equations governing fluid and heat flow (equations 7-1 and 7-2) are interconnected or coupled by the following:

- The second-order equation of state for the fluid (Lippmann et al. 1977c):

[7-4] $$\rho = \rho_0 \left[1 - \beta (T - T_0) - \gamma (T - T_0)^2 \right]$$

- The Darcy fluid velocity ($\overline{V}_d$) used in the convection term of the heat equation.

- The temperature and/or pressure dependence of certain parameters used in the equations (Lippmann et al. 1977c).

7.2.2 Numerical Method

The numerical model CCC, developed at the Lawrence Berkeley Laboratory, is based on computer programs SCHAFF (Sorey 1975) for fluid and heat transport through saturated porous media and TRUST (Narasimhan 1975) for one-dimensional consolidation. CCC numerically solves the fluid- and heat-flow equations by an Integrated Finite-Difference Method (Narasimhan and Witherspoon 1976) by using a mixed explicit-implicit iterative scheme and variable time steps chosen by the program to advance in time. CCC also computes the vertical consolidation of simulated systems using Terzaghi's one-dimensional consolidation theory. Details of the various applicable algorithms are given by Edwards (1972), Narasimhan (1975) and Sorey (1975). In finite difference form, the fluid- and heat-flow equations (equations 7-1 and 7-2) are given by Lippmann et al. (1977a):

[7-5]

$$\left[\frac{\rho}{1+e}\left(ek+\frac{\Delta e}{\Delta\sigma'}\right)V\right]_n \frac{\Delta P_n}{\Delta t} = \sum_m \left[\left(\frac{k\rho A}{\mu}\right)_{n,m}\left(\frac{P_m-P_n}{d_{n,m}+d_{m,n}}\right)-\left(\frac{k\rho^2\eta A}{\mu}\right)\bar{g}\right]+(QV)_n$$

[7-6]

$$\left[(\rho c)_M V\right]_n \frac{\Delta T_n}{\Delta t} = \sum_m \left[\left(K_M A\right)_{n,m}\left(\frac{T_m-T_n}{d_{n,m}-d_{m,n}}\right)+\left(\rho c_F \bar{V}_d A\right)_{n,m}\left(T_{m,n}-T_n\right)\right]+(qV)_n$$

CCC solves the fluid and heat flow equations (equations 7-5 and 7-6) coupled by equation 7-4 by alternatively interlacing them in time. For temperatures below the reference temperature, CCC uses the following coupling equation with a different coefficient of volume fluid thermal expansion (β_v):

[7-7] $\rho = \rho_o(1-\beta_v \Delta T)$

The flow equation (equation 7-5) solves for P, $\bar{V}_d$, and e assuming that the temperature-dependent properties of the fluid and rock remain constant. Then the heat equation (equation 7-6) is solved for T assuming that $\bar{V}_d$ and the pressure-dependent properties of the fluid and rock remain constant. Since pressure varies much faster than temperature, smaller time steps have to be taken in the fluid-flow cycles than in the heat cycles in order to compute pressure variations accurately (Lippmann et al. 1977c).

A further explanation of the mixed explicit-implicit iterative scheme used by CCC is as follows. For heat calculations, all nodes are considered initially to be regular (explicit) nodes unless otherwise specified as special (implicit) nodes. Regular nodes are reclassified as special nodes only when necessary to

maintain the stability limit of a node above the time step. All heat calculations are first done explicitly; corrections are then applied to any special nodes and to any nodes connected to a special node. Therefore, the interpolation factor for a regular node is 0.0 and the forward-difference method is used. For the special node corrections, the interpolation factor is varied from 0.5 (central difference method) to 1.0 (backward difference method) by the program. Stability is then unconditional, and the iteration acceleration factor is set at 0.2.

For fluid calculations, all nodes are considered to be special nodes. All fluid calculations are done explicitly and then corrections are applied to all nodes. The interpolation factor is 1.0 (backward difference method), the iterative scheme is unconditionally stable, and the iteration acceleration factor is set at 0.2.

It is also possible to use either an explicit or an implicit scheme for the heat calculations. With an explicit scheme, all nodes are always regular nodes with an interpolation factor of 0.0 (forward difference method). With an implicit scheme, all nodes are special nodes with an iteration acceleration factor set at 0.2 and a choice of differencing methods. If the interpolation factor is 1.0, the backward difference method is used; if the interpolation factor is 0.5, the central difference method is used. For both of these it is apparent that stability is unconditional.

A maximum of 80 iterations is allowed for convergence in heat or fluid calculations. If convergence is not accomplished by then, the time step is reduced by half, if possible, and the iterations are repeated. A similar thing is done when the maximum pressure or temperature change in a cycle exceeds twice the value of the maximum desired change.

7.3 CAPABILITIES AND LIMITATIONS

7.3.1 Geometric Capabilities and Limitations

CCC can model one-, two-, and three-dimensional problems (rectangular coordinates) as well as axisymmetric (cylindrical coordinates) and centrisymmetric (spherical coordinates) problems. Since an integrated finite difference (IFD) method is used, the nodal points of the modeled system may be arranged randomly and do not have to be parallel to the coordinate axes. CCC can have a maximum of 200 nodal points and 350 connections between nodes. Boundary conditions that can be handled include impermeable and/or adiabatic (no heat flow) boundaries, constant-pressure and/or temperature boundaries, and constant fluid-flow and/or heat-flow boundaries (including fluid and heat sources [injection] and sinks [production]). Because it considers only saturated fluid flow, CCC cannnot handle free-surface or seepage-face boundaries.

7.3.2 Flow Capabilities and Limitations

7.3.2.1 Fluid Flow Capabilities and Limitations

CCC uses a single-phase fluid in its fluid-flow calculations, specifically water, whic is a slightly compressible fluid. Hydraulic and thermal properties of the fluid (fluid viscosity, first coefficient of fluid thermal expansion β and fluid-specific heat capacity may be constant or tabulated as linear or nonlinear functions of temperature or pressure. Twelve points are allowed on each table. Initial conditions for fluid-flow calculations are assigned through initial fluid pressures and preconsolidation stresses.

If both fluid- and heat-flow calculations are desired, fluid density cannot be constant and will instead be calculated by equations 7-4 or 7-7. So a reference fluid density, reference temperature, and the first coefficient of fluid thermal expansion (β) must be assigned. In the code for CCC, the second coefficient of fluid thermal expansion (α) and the coefficient of volume fluid expansion used in equation 7-7 (β_V) are given in inverse degrees Celsius. Thus the system of units chosen for input must give temperatures and thermal properties of the fluid and rock in degrees Celsius. If both fluid- and heat-flow calculations are desired until the fluid flow reaches steady-state and then only heat-flow calculations are desired, fluid density must be constant. For the case of constant fluid density, any consistent set of units can be chosen for input. A limitation of calculating fluid density by equations 7-4 or 7-7 is that only the variation with temperature is considered. Variation with pressure, which is smaller in magnitude, is ignored.

7.3.2.2 Heat Flow Capabilities and Limitations

CCC handles nonisothermal problems. Initial conditions for heat-flow calculations are assigned through initial temperatures. CCC can also handle isothermal (constant temperature) problems if the initial conditions of the entire system are assigned to be isothermal, and boundary conditions and sources/sinks are set up so that no temperature changes occur. However, heat-flow calculations are always done, so CCC may not be the best (fastest) program to use for isothermal problems. It should be noted that Lippmann et al. (1977c) concluded that the use of isothermal models to simulate nonisothermal systems may result in predicting somewhat larger and more conservative consolidation values than nonisothermal models. They attributed this to using a constant average fluid viscosity and, to a lesser extent, a constant-average fluid density.

Connections between nodes are assigned heat-transfer coefficients for heat conduction and convection across the connected interface. A heat-transfer coefficient of 10^{12} corresponds to a perfect thermal connection, while a coefficient less than this, to a minimum of 10^{-24}, includes the effects of a surface film, gas gap, contact resistances, or an open space and signifies a less-than-perfect thermal connection.

CCC uses an upstream weighting factor of 0.7 in calculating heat convection.

CCC cannot model chemical reactions or salt precipitation that might occur when waters of a different temperature and salinity than those in a reservoir are injected into the reservoir.

7.3.3 Material Properties

CCC can handle heterogeneous isotropic systems with a maximum of 10 materials. Material and thermal properties of the rock (intrinsic permeability, specific heat, and thermal conductivity) may be constant or tabulated as linear or nonlinear functions of temperature or pressure. Twelve points are allowed on each table. Permeability may be a function of the void ratio if the void ratio is a function of the logarithm of effective stress (nonelastic material). The relationship assumed between k (permeability) and e (void ratio) is: $e = e_o + C_k \log (k/k_o)$ where e_o, k_o are initial conditions and C_k is the slope of the curve (Lambe and Whitman 1969; Narasimhan and Witherspoon 1977). When this relationship is used, intrinsic permeability cannot be tabulated as a function of temperature or pressure.

If consolidation calculations are desired, they must be done for the entire system, with each material designated as independently elastic or nonelastic. In calculating effective stress,

pendently elastic or nonelastic. In calculating effective stress, CCC assumes that the total stress is constant and due to the weight of the overlying rock. When consolidation calculations are not desired, all the materials of the entire system are assigned individual coefficients of specific storage.

7.3.4 Other Capabilities and Limitations

CCC is capable of producing output on punched cards (or, with minor modifications, on a magnetic disk or tape) when a problem ends normally and giving the final conditions at the end of a simulation. These conditions include temperature, fluid pressure, fluid source/sink flow rate, specific heat content of a fluid source or heat source/sink, preconsolidation stress, and nodal volume change. This output, which can be used to continue the problem, ensures that the initial and maximum allowable problem times are updated.

7.4 USABILITY

7.4.1 Documentation

A fairly comprehensive users' manual by Lippmann and Mangold (1977) is available. Golder Associates' experience with the program has been incorporated into a revised input manual. All input parameters are clearly explained in the input manual, although explanations of protocols for the preparation of grids and the use of run parameters DELTO, SMALL, TVARY, DELTOF, SMALLF, and RVARY are weak.

Edwards (1972) provides a reasonably thorough layman's explanation of the way the integrated-finite-difference method works.

7.4.2 Input East

Coding for CCC is fairly complicated; not only the location and size of each element but also all connections must be specified.

The degree of sophistication of heat and mass flow analysis with CCC requires a comparable level of sophistication in input. Where functional relationships are required between material properties and temperature, the relationship must be input point by point on input cards.

Program efficiency is highly dependent upon the selection of parameters DELTOF, SMALLF, and RVARY. These parameters control selection of time steps, iteration tolerances, and convergence tolerance. It is difficult to determine the proper values for these parameters; their selection in one of the most significant limitations on the ease of input.

Grid coding is aided somewhat by provisions for automatic generation of repetitive identical elements. Unfortunately, this facility is limited to identical elements. This greatly limits the number of elements which can be generated automatically, especially in geothermal reservoir problems.

7.4.3 Output Control and Comprehensibility

Output is available at three levels: normal, minimum, and maximum. Generally, the maximum level available is desirable. Output includes node stresses, volumes, temperatures and densities at each time step, total change since initial conditions, change during time step, and conditions at the end of time step. Output is generally fairly well labeled and organized. One weakness in program output is that only node and total volume changes

are output. This makes calculation of compaction tedious. Summation of column volume changes would be desirable.

Output can, theoretically, be taken at any desired time interval within the time period being simulated. However, CCC chooses time steps according to internal criteria of gradients and times and can only adjust time step calculations by a maximum of 33 percent. This results in intermediate output at quite irregular intervals.

7.4.4 Solution Efficiency

Figure 7-1 shows the relationship between problem complexity, as represented by the number of nodal points, and computation time in CPU seconds of Boeing Computer Service's EKS-CDC system. Costs increase roughly linearly with the number of nodes for a constant time period. Due to the time-step algorithm used by CCC, time period and cost are not clearly correlated. A time period of 10 years costs less than 10 times what a time period of 1 year costs.

7.4.5 Resume of Performance on Sample Problems and Case Studies

CCC was used to predict mass and heat flow in the aquifer and aquitard for sample problems 2 and 4. CCC was unable to analyse sample problems 1, 3, 5, and 6 because no pore-pressure gradient exists which can cause flow.

Sample problem 2, a simple one-dimensional problem, produced a steady-state pore-pressure gradient after about 30 years. Compaction predicted at the reservoir surface was 1.08 feet or

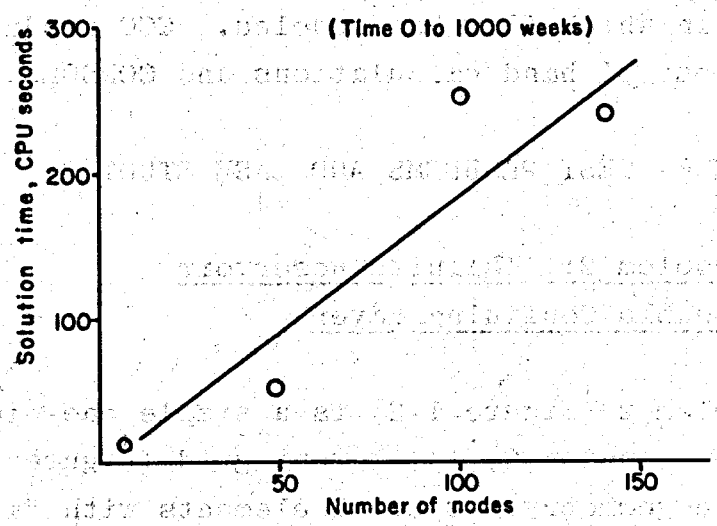

FIGURE 7-1
HEAT-AND-MASS FLOW MODEL
SOLUTION EFFICIENCY AS A FUNCTION
OF NUMBER OF NODES

0.76 feet after 5 years, depending on the use of either constant or void-ratio dependent permeabilities.

Sample problem 4 can be viewed as either plane-strain or axisymmetric. In both cases a pore-pressure gradient similar to that of sample problem 2 occurs over the reservoir, and the aquifer's effect dissipates rapidly past the edge of the aquifer in the lateral direction. Compaction follows a similar pattern and is identical in the plane-strain and axisymetric cases.

CCC was implemented for the Austin Bayou case study, the only case study in which flow was modeled. CCC produced results comparable to those of hand calculations and CONSOL3.

7.5 PERFORMANCE ON TEST PROBLEMS AND CASE STUDIES

7.5.1 Sample Problem 2: Infinite Reservoir With Permeable Confining Layer

Sample problem 2 (Figure 1-2) is a simple one-dimensional problem. A one-dimensional, 14-element grid (Figure 7-2) was used to model the geometry. Special elements with "infinite" (10^{12}) volume were used to maintain constant pressure boundaries. Since there was no temperature gradient, only mass flow calculations were necessary. One of the advanced features of CCC is its ability to model variable permeability materials. Therefore, in addition to modeling sample problem 2 with constant k, it was also modeled with a e-log k relationship with a slope of $C_k = 0.15$.

With constant permeability, solution to 5 years required 1.7 CPU seconds and solution to 30 years required 3.5 CPU seconds. With e-log k, solution to 5 years required 1.8 CPU seconds.

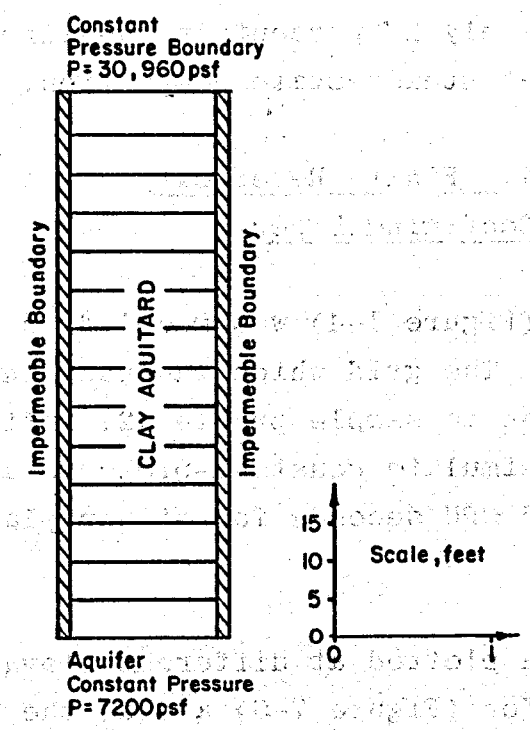

FIGURE 7-2
HEAT-AND-MASS FLOW MODEL,
ELEMENT LAYOUT FOR SAMPLE PROBLEM 2

Figure 7-3 shows the change in pore pressure with time in the clay aquitard. Steady-state is reached in about 30 years, as predicted by Terzaghi calculations. A linear gradient between two constant head boundaries results, as expected.

Compaction of the clay aquitards is shown in Figure 7-4. Both constant permeability and e-log k results are shown. A compaction of approximately 2 feet occurs after 30 years. The use of a void ratio dependent permeability decreases the rate of compaction by approximately 25 percent in the first 5 years, but probably will not affect steady-state compaction.

7.5.2 Sample Problem 4: Finite Reservoir With Permeable Confining Layer

Sample problem 4 (Figure 1-4) was modeled as both planar-flow and axisymmetric. The grid which was used in both cases is shown in Figure 7-5. As in sample problem 2, infinite-volume elements were used to simulate constant-pressure aquifers. Solution required 18.75 CPU seconds for either planar or axi-symmetric cases.

Pore pressures are plotted at different elevations above the constant-pressure aquifer (Figure 7-6) and at the surface of the aquifer as a function of lateral distance (Figure 7-7). Variation of pressures with elevation are identical to those of sample problem 2 at the center. This is not surprising since one-dimensional conditions are approximated at the center. There is also little variation of pore pressure horizontally above the sand. Edge effects are noticeable only to a small degree in the node nearest the edge. Pore-pressure changes fall rapidly to zero past the edge of the aquifer.

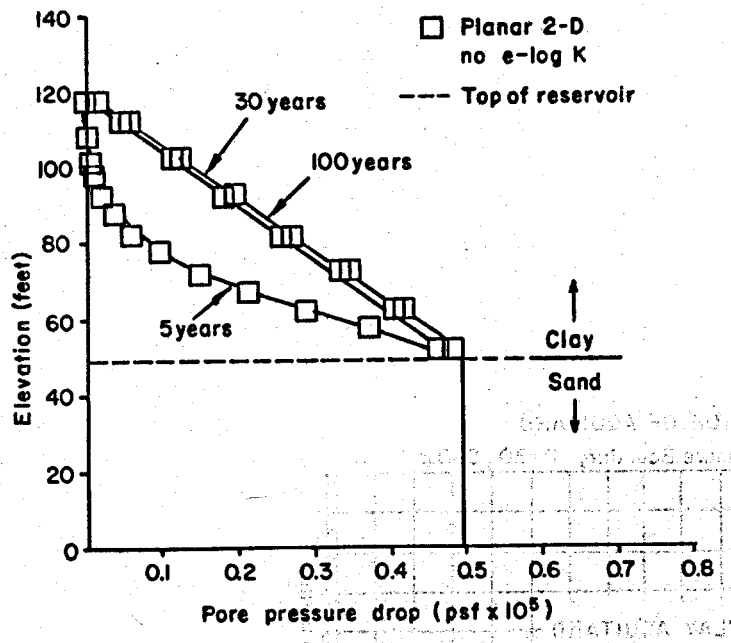

FIGURE 7-3: HEAT-AND-MASS FLOW MODEL PORE-PRESSURE DROP WITH TIME, SAMPLE PROBLEM 2

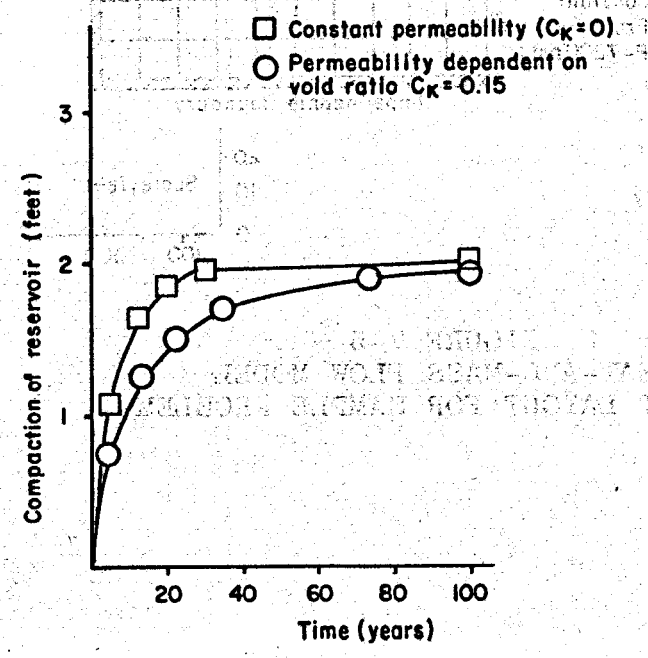

FIGURE 7-4: HEAT-AND-MASS FLOW MODEL RESERVOIR COMPACTION WITH CONSTANT AND VOID RATIO DEPENDENT PERMEABILITY, SAMPLE PROBLEM 2

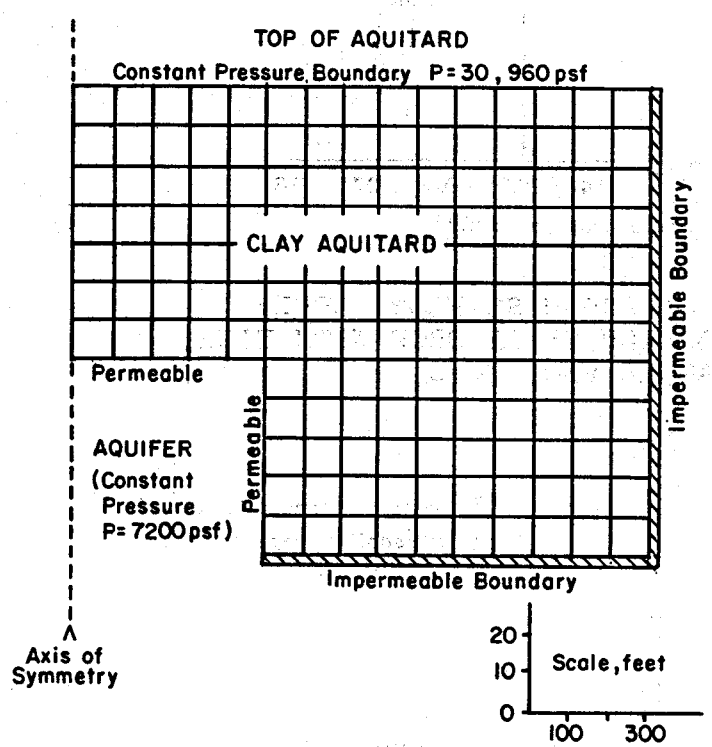

FIGURE 7-5
HEAT-AND-MASS FLOW MODEL
ELEMENT LAYOUT FOR SAMPLE PROBLEM 4

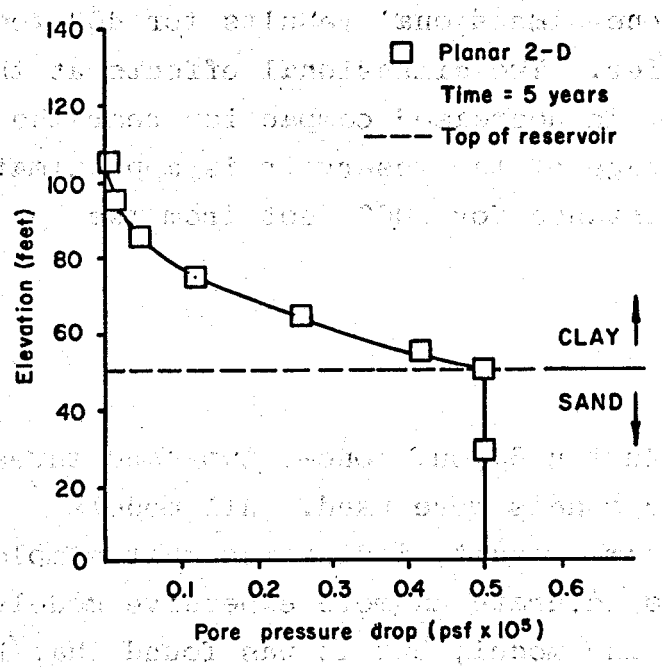

FIGURE 7-6: HEAT-AND-MASS FLOW MODEL PORE-PRESSURE PROFILE AT 5 YEARS, SAMPLE PROBLEM 4

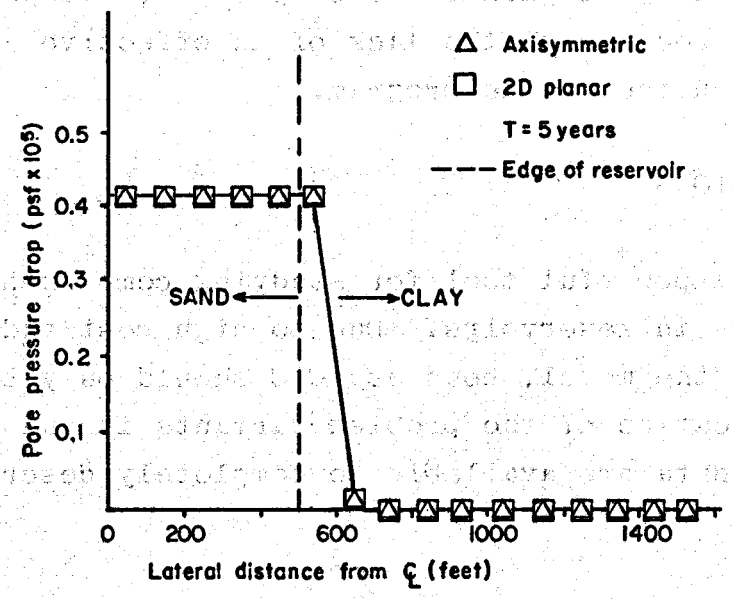

FIGURE 7-7: HEAT-AND-MASS FLOW MODEL PORE-PRESSURE DROP IN AXISYMMETRIC AND 2-D PLANAR FLOW MODELS AFTER 5 YEARS, SAMPLE PROBLEM 4

Compaction at the reservoir surface is shown in Figure 7-8. Compaction is identical to one-dimensional results for 400 feet near the center of the aquifer. Two-dimensional effects at the edge of the reservoir result in decreased compaction near the edge. Compaction past the edge of the reservoir is approximately constant, with horizontal distance for 1000 feet from the aquifer.

7.5.3 Case Studies

CCC was used to study Austin Bayou. One-, two- and three-dimensional and axisymmetric models were used. All models produced approximately the same result, indicating that simple CCC models are frequently as accurate as more expensive models. Heat gradients were used in the model, but it was found that heat flow played an insignificant role.

CCC models for Austin Bayou were difficult to code because of the complexity of parameters coupled with temperature and pressure and because of the lack of an effective automatic node generation routine in the program.

7.6 CONCLUSIONS

CCC is a powerful tool for studying complex heat- and mass-flow problems in reservoirs. Due to high cost and the complexity of input for the model, however, CCC should only be used where the sophistication of the problem warrants it and where sufficient field data are available to completely describe the geology.

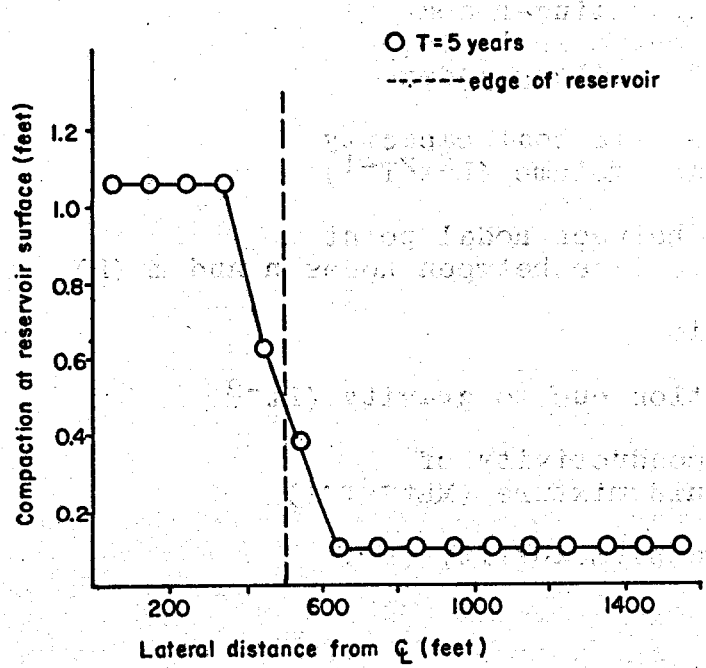

FIGURE 7-8
HEAT-AND-MASS FLOW MODEL
RESERVOIR COMPACTION AFTER 5 YEARS
PLANAR FLOW MODEL OF SAMPLE PROBLEM 4

7.7 LIST OF SYMBOLS

A	area (L^2)
a_v	slope of curve in "e-σ' plot," coefficient of compressibility ($M^{-1}Lt^2$)
C_c	slope of virgin curve in "e-log σ' plot," compression index
C_k	slope of straight line in "e-log k plot"
C_s	slope of swelling-recompression curve in "e-log σ' plot," swelling index
c_F	fluid specific heat capacity at constant volume ($L^2t^2T^{-1}$)
$d_{n,m}$	distance between nodal point n and interface between nodes n and m (L)
e	void ratio
$\bar{g}$	acceleration due to gravity (Lt^{-2})
K_M	thermal conductivity of solid-fluid mixture ($MLt^{-3}T^{-1}$)
k	intrinsic permeability (L^2)
$\bar{n}$	outward unit normal on surface S
P	fluid (pore) pressure ($ML^{-1}t^{-2}$)
Q	mass injection rate per unit volume ($ML^{-3}t^{-1}$)
q	energy injection rate per unit volume ($ML^{-1}t^{-3}$)
S	surface (L^2)

dS	surface element (L^2)
S_s	coefficient of specific storage(L^{-1})
T	temperature (T)
t	time (t)
V	volume (L^3)
dV	volume element (L^3)
$\bar{v}_d$	Darcy fluid velocity (Lt^{-1})
β	first coefficient of fluid thermal expansion (T^{-1})
β_v	coefficient of volume fluid expansion (T^{-1})
γ	second coefficient of fluid expansion (T^{-2})
τ	difference between the mean temperature within volume element dV and that on surface dS (T)
$\eta_{n,m}$	direction cosine of the angle between the outward normal of node n and $\bar{g}$
κ	fluid compressiblity ($M^{-1}Lt^2$)
μ	fluid viscosity ($ML^{-1}t^{-1}$)
ρ	fluid density (ML^{-3})
$(\rho c)_m$	heat capacity per unit volume of the solid-fluid mixture ($ML^{-1}t^{-2}T^{-1}$)
σ'	effective stress ($ML^{-1}t^{-2}$)

<u>Superscripts</u>

-	average

Subscripts

m	at node m
n	at node n
n,m	at interface between nodes n and m
o	reference quantity

7.8 REFERENCES

American Society of Mechanical Engineers (1967). 1967 ASME Steam Tables, New York.

Edwards, A.L. (1972). "TRUMP: A Computer Program for Transient and Steady State Temperature Distribution in Multidimensional Systems," prepared for Lawrence Livermore Laboratory; UCRL-14754, Rev. 3, 259 p.

Faust, C.R., and J.W. Mercer (1977). "Theoretical Analysis of Fluid Flow and Energy Transport in Hydrothermal Systems," U.S. Geological Survey Open-File Report 77-60.

Garg, S.K., J.W. Pritchett, M.H. Rice, and T.D. Riney (1977). U.S. Gulf Coast Geopressured Geothermal Reservoir Simulation, Systems, Science, and Software Final Report (Year 1), SSS-R-77-3147, La Jolla, California.

Lambe, T.W., and R.V. Whitman (1969). Soil Mechanics, J. Wiley and Sons, New York, 553 p.

Lippmann, M.J., T.N. Narasimhan, and P.A. Witherspoon (1977a). "Numerical Simulation of Reservoir Compaction in Liquid Dominated Geothermal Systems," Proceedings of the Second International Symposium on Land Subsidence, Anaheim, California, December 10-17 1976, Lawrence Berkeley Laboratory, University of California, Berkeley, reprint LBL-4462, 11 p.

Lippmann, M.J., C.F. Tsang, and P.A. Witherspoon (1977b). "Analysis of the Response of Geothermal Reservoirs Under Injection and Production Procedures," presented at the April 13-15 1977 47th Annual California Regional Meeting of the Society of Petroleum Engineers of AIME, Bakersfield, California (preprint SPE 6537).

Lippmann, M.J., T.N. Narasimhan, and P.A. Witherspoon (1977c). "Modeling Subsidence Due to Geothermal Fluid Production," presented at the American Society of Civil Engineers Fall Convention and Exhibit, San Francisco, California, October 17-21 1977, 25 p. (preprint 3107).

Lippmann, M.J., and D. Mangold (1977). Preparation of Input Data for Program CCC (April 1977 version), preliminary notes (subject to revision), prepared for Lawrence Berkeley Laboratory, University of California, Berkeley.

Mercer, J.W., C. Faust, and G.F. Pinder (1974). "Geothermal Reservoir Simulation," Proceedings of the Conference for Resource Development of Geothermal Energy Resources, Pasadena, California, September 23-25, 1974, pp. 256-267.

Narasimhan, T.N. (1975). A Unified Numerical Model for Saturated-Unsaturated Groundwater Flow, Ph.D. thesis, University of California, Berkeley, 244 p.

Narasimhan, T.N., and P.A. Witherspoon (1976). "An Integrated Finite Difference Method for Analyzing Fluid Flow in Porous Media," Water Resources Research, Vol. 12, No. 1, pp. 57-64.

Narsimhan, T.N., and P.A. Witherspoon (1977). "Numerical Model for Saturated-Unsaturated Flow in Deformable Porous Media I. Theory," Water Resources Research, Vol. 13, No. 3, pp. 657-664.

Pritchett, J.W., S.K. Garg, D.H. Russell, D.H. Brownell, Jr., and H.B. Levine (1975). Geohydrological Environmental Effects of Geothermal Power Production, Phase I, Systems, Science and Software Report SSS-R-75-2733, La Jolla, California, 90 p.

Sorey, M.L. (1975a). Numerical Modeling of Liquid Geothermal Systems, Ph.D. thesis, University of California, Berkeley, 65 p.

_____(1975b). SCHAFF, U.S. Geological Survey Open-File Report 75-613.

Terzaghi, K. (1925). "Principles of Soil Mechanics, A Summary of Experimental Results of Clay and Sand," Engineering News Record, Vol. 98, No. 3.

Tsang, C.F., M.J. Lippmann, C.B. Goranson, and P.A. Witherspoon (1976). "Numerical Modeling of Cyclic Storage of Hot Water in Aquifers," presented at the Symposium on Cyclic Storage of Aquifers, Fall Annual Meeting, American Geophysical Union, San Francisco, California, December 6-10, 1976, Lawrence Berekeley Laboratory, LBL 5929.

Witherspoon, P.A., S.P. Neuman, M.L. Sorey, and M.J. Lippmann (1975). "Modeling Geothermal Systems," Lawrence Berkeley Laboratory, University of California, Berkeley, reprint LBL 3263, 68 p.

8.0 THREE-DIMENSIONAL DISPLACEMENT-DISCONTINUITY MODEL "NFOLD"

8.1 INTRODUCTION

NFOLD is a three-dimensional displacement-discontinuity model developed by Sinha and Crouch at the University of Minnesota in 1976 and enhanced and adapted by Golder Associates in 1978 and 1979. The displacement-discontinuity technique allows the modeling of thin seams with complex, nonelastic properties within an isotropic, homogeneous elastic space. The advantage of NFOLD over other displacement-discontinuity models is that it handles three-dimensional geometries and incorporates several efficiency-enhancement features. NFOLD is not suited for one- or two-dimensional problems because all problems must be modeled in three dimensions.

NFOLD was designed as a model for the mechanics of underground mining. As a result, NFOLD deals exclusively with stress-deformation mechanics and cannot handle flow, thermal effects, effective stress, or coupling of properties.

Golder's adaptation of NFOLD for geothermal problems allows it to be used to compute the effect of reservoir deformations at depth on surface deformations and on deformation of adjacent geologic features such as faults. NFOLD, which models the propogation of deformation and stress outside a reservoir, complements a model such as CCC, which models only behavior within a reservoir.

8.2 SOLUTION METHOD - GENERAL THEORY

8.2.1 Theory

Within an elastic body, a displacement at one point produces a change in stress at every other point in the body. The displacement discontinuity method is based on this fact. It replaces a thin seam by a number of rectangular elements and then solves equations for the closure and shear displacements at each element.

The theory of elasticity is used in NFOLD to determine the coupling coefficients which relate the stress at one element to the displacements at the others.

[8-1] $$\sigma_i = \sigma_{io} + \sum_j C_{ij} d_j$$

σ_i is the stress at element i
σ_{io} is the initial stress before any displacements occurred
C_{ij} is a coupling coefficient
d_j is the displacement at element j

Coupling coefficients are computed for each of three stress components at element i and for each of three displacements at element j. The three directions used are closure, shear parallel to strike, and shear downdip. NFOLD solves the above equations by temporarily fixing all the values of displacement at elements other than i. This produces an equation with two unknowns: σ_i and δ_i.

[8-2] $$\sigma_i = \left(\sigma_{io} + \sum_{j \neq i} c_{ij} d_j\right) + c_{ii} d_i$$

This equation is now solved simultaneously with the equation describing the seam's stress-deformation relation. The result is an estimate of the stress and displacements at element i. NFOLD solves the equations for each element in turn and iteratively repeats the solution until the computed displacements stabilize.

The nature of the seam's stress-deformation relation is quite general. In the case studies, seam elements were used to model the geothermal reservoir, those faults that would slip if overly stressed, and the surface of the earth. NFOLD has five different types of seam behavior models (see Section 3.3).

NFOLD was modified by Golder Associates to incorporate the effects of pore pressure or temperature changes. Assuming a thin reservoir, the initial strain due to pressure and temperature is integrated over the depth of the reservoir and then lumped as a fixed-amplitude normal displacement at an otherwise-rigid seam element. It is also possible to account for a reservoir having different elastic properties from the rest of the continuum; this feature, however, was not incorporated into NFOLD.

8.2.2 Numerical Methods

The displacement discontinuity method requires solution of equilibrium between the seam stresses and the continuum stresses at each element, where the continuum stresses of each element are dependent on the displacements of all the elements. Therefore, the number of simultaneous equations to be solved is equal to three times the number of elements. To simplify the equations, the effects due to distant elements are approximated by lumping

five-by-five sets of elements into an equivalent larger element and using the average displacements of the 25 subelements. This simplification can reduce computations by an order of magnitude without compromising accuracy (Figure 8-1). NFOLD carries out all calculations in three dimensions, so use of NFOLD for one- or two-dimensional problems is inefficient. Two-dimensional plane-strain versions of the displacement-discontinuity method are available.

8.3 CAPABILITIES AND LIMITATIONS

8.3.1 Geometric Capabilities and Limitations

NFOLD is designed for three-dimensional analysis and can therefore be used for three-dimensional or any simpler geometry. It is extremely inefficient for simple geometries, however, because three-dimensional calculations must still be performed. NFOLD has no capability for handling symmetry and must therefore be used to model the entire problem, even where axes of symmetry exist. NFOLD is dimensioned for an array of "large" elements (each consisting of 25 true elements) that is up to 10 "large" elements along strike. Any number of seam planes can be used, but all must have the same strike direction and the combined number of downdip "large" elements can be no more than 25. All elements must have the same dimensions. Different material properties may be specified for each true element. All seam planes must have the same number of elements in the strike direction.

8.3.2 Flow Capabilities and Limitations

NFOLD handles only stress-displacement calculations and therefore has no facilities for modeling flow. In addition,

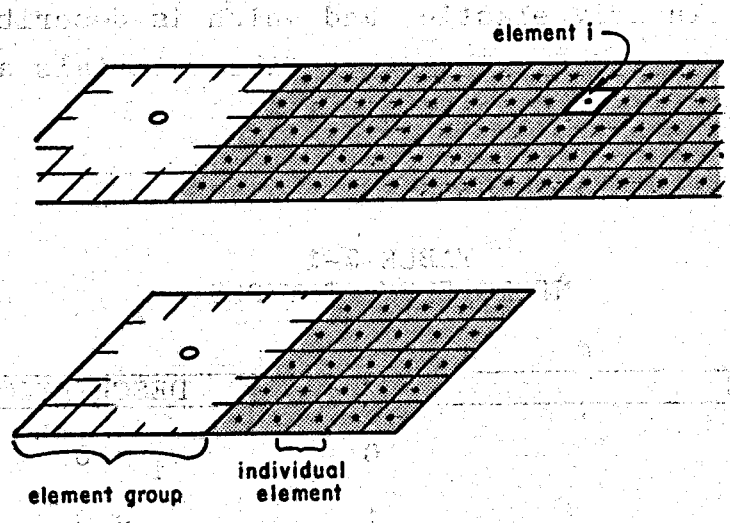

NFOLD COUPLING OF DEFORMATIONS

element i is coupled with :

Individual element of neighboring groups

Group average for distant groups

FIGURE 8-1
THREE-DIMENSIONAL DISPLACEMENT-DISCONTINUITY MODEL
COUPLING OF ELEMENTS AND ELEMENT GROUPS

NFOLD ignores all time-dependent phenomena. NFOLD takes as input the reservoir compaction based on assuming a constant total vertical stress, which must be determined by a reservoir-flow program such as CCC.

8.3.3 Material Properties

NFOLD handles six different types of materials. One material represents the elastic space, which must be isotropic, homogeneous, and linearly elastic, and which is described with the two parameters, ν and E. The other five materials are discontinuity materials (see Table 8-1).

TABLE 8-1
NFOLD ELEMENT TYPES

ELEMENT NAME	NUMBER	DESCRIPTION
Mined	0	$\sigma_i = 0$
Rigid	1	$\delta_i = 0$
Linear	2-6, 8-10	$\delta_i = \frac{\sigma_i t}{E_s}$
Nonlinear (See Figure 8-2)	11-51	$\delta_i = f(\sigma_i)$
Aquifer	7	δ_i = constant

σ_i = stress within element
δ_i = deformation within element
t = element thickness

$$f(\sigma_i) = \begin{cases} \sigma_i t/E_s & \sigma_i < \sigma_{max} \\ \sigma_{max}\, t/E_s + \sigma_i t/E_r & \sigma_{max} < \sigma_i < \sigma_{rup} \\ t & \sigma > \sigma_{rup} \end{cases}$$

1. Mined. Mined elements have zero internal stress; therefore, deformations must occur that cause the induced stresses to exactly cancel initial stresses. Mined elements are used in reservoir modeling to represent the ground surface.

2. Rigid. Rigid elements have zero deformation. No coupling coefficients are computed for rigid elements.

3. Linear Elastic. NFOLD allows specification of linear elastic properties for eight discontinuity materials. These may be used to model aquitards or compressible layers. E and ν must be the same for all elastic materials, but thicknesses may be different.

4. Nonlinear. As many as 39 materials can be specified with nonlinear properties (see Figure 8-2). Nonlinear elements are ideal for modeling faults. The elastic position of the nonlinear stress-strain curve must be the same as that for the linear-elastic discontinuity material.

5. "Aquifer." NFOLD is adapted to the reservoir modeling problem with the "aquifer" element. "Aquifer" elements are rigid elements with fixed displacements. As predicted by computer program CCC, the fixed displacements can be taken as reservoir compaction. NFOLD adjusts displacement throughout the elastic space to reflect disdisplacements in the reservoir.

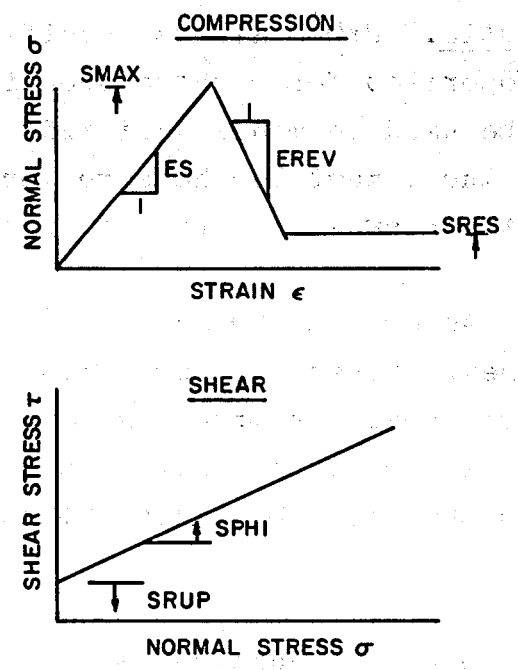

FIGURE 8-2
THREE-DIMENSIONAL DISPLACEMENT-DISCONTINUITY MODEL
NONLINEAR STRESS-STRAIN PROPERTIES

NFOLD allows specification of different discontinuity materials for each of 25 small elements within each "large" element.

8.4 USABILITY

8.4.1 Documentation

NFOLD has a users' manual that provides a thorough explanation of all input parameters. The manual lacks sample problems that would facilitate coding considerably. NFOLD's source code is fairly well commented and therefore relatively easy to follow.

Few case histories of NFOLD's use are publicly available, although Golder Associates does have access to some. An analog computer model utilizing the same principles as NFOLD is described in Crouch and Fairhurst (1973). The theory of two-dimensional displacement discontinuities is developed in Crouch (1976). Sinha (1979) discusses the development of NFOLD in three dimensions.

8.4.2 Input Ease

Coding for NFOLD is quite simple and logical. Complex three-dimensional geometries can be described on a few cards by use of element grouping and automatic generation.

NFOLD ignores flow, thermal, dynamic, and coupled material property effects and therefore requires only stress-strain constitutive relations as input.

The displacement discontinuity method's accuracy is highly dependent upon proper selection of element sizes and interrelationships. An understanding of these dependencies is essential to accurate modeling and represents the only significant constraint on ease of input.

8.4.3 Output Control and Comprehensibility

NFOLD has two levels of output, standard and complete. Standard output includes an echo of all input data and lineprinter contour plots of stresses and displacements at every grid square of every element. Complete output includes summary statistics as each iteration is completed and printout of all stresses and displacements at every grid square.

Unfortunately, in its present form, NFOLD lineprinter plots require specification of a scaling factor with input and can only output scaled values from -9 to 99. For problems with significant results outside of that range, lineprinter contour plots cannot be used, and output values available only with complete output must be used.

NFOLD only outputs results at elements, so elements must be included wherever output is desired, including the surface.

8.4.4 Solution Efficiency

NFOLD is designed for three-dimensional problems and is thereore most efficient in that mode. One-dimensional and two-dimensional problems can be implemented on NFOLD, but only by modeling the simple geometry in three dimensions. This results in extreme inefficiency for simple geometries.

NFOLD's solution time depends upon two factors: the total number of "large" elements and the number of elements between which complete coupling exists. Costs increase linearly with the number of elements (see Figure 8-3).

NFOLD is considerably more efficient for three-dimensional problems than it is for three-dimensional finite elements or for finite-difference models.

8.4.5 Resume of Performance on Sample Problems and Case Studies

The Sample Problems for which reservoir compactions are known are all either one- or two-dimensional and are therefore not really appropriate for use with NFOLD. NFOLD was used only with sample problem 3, which is two-dimensional. NFOLD was given reservoir compaction and was used to predict surface subsidence. However, the cost to obtain accurate subsidence profiles was prohibitive.

Due to its assumption of "thin" seams, NFOLD was used only for the Austin Bayou case study. In this case study, NFOLD produced reasonable, three-dimensional results at a relatively high cost.

8.5 PERFORMANCE ON SAMPLE PROBLEMS AND CASE STUDIES

8.5.1 Sample Problem 3

NFOLD is a three-dimensional model and is therefore inappropriate for all Sample Problems except Problem 6. Reservoir

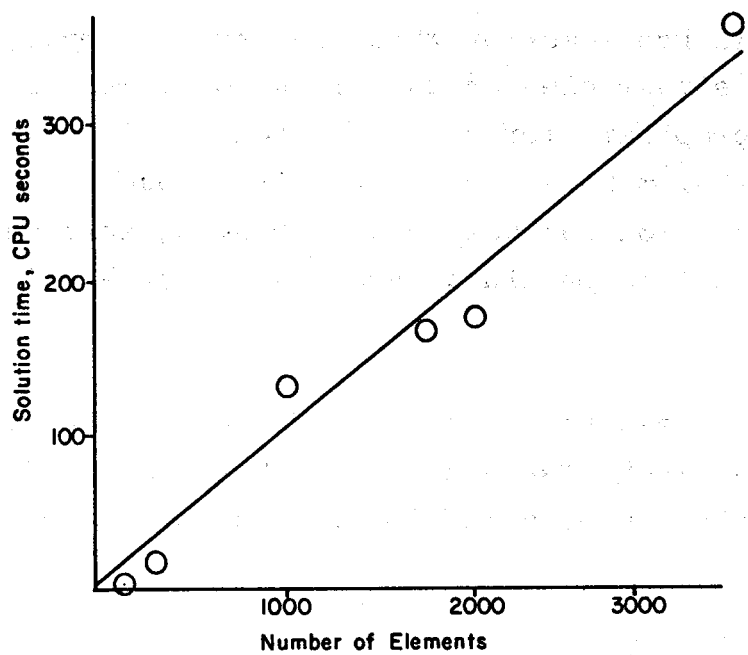

FIGURE 8-3
THREE-DIMENSIONAL DISPLACEMENT-DISCONTINUITY MODEL
SOLUTION EFFICIENCY

deformation values from sample problem 6 are, however, unavailable, so NFOLD could not be used for that problem. NFOLD was used to model sample problem 3, a two-dimensional problem. Reservoir compaction from the hand calculations was used. Solution of the two-dimensional problem in three dimensions was very inefficient and required 130 CPU seconds.

To model the two-dimensional geometry of sample problem 3, the ground surface and the aquifer were modeled as close to infinite planes as possible, with attention to the avoidance of edge effects and interference between adjacent discontinuity planes. The model used is illustrated in Figure 8-4. "Mined" elements at elevation zero were used to create the zero-stress condition at the ground surface.

"Aquifer" elements with compaction equal to that predicted for the reservoir by the hand calculations (0.972 feet) were used to model the reservoir.

The model for sample problem 3 shown in Figure 8-4 resulted in a maximum displacement at the surface of 2.35 feet--over twice as large as the reservoir compaction. This is the result of the use of elements of dimension 100 feet by 100 feet, while the distance between the surface and the reservoir is only 500 feet. Reducing elements to 10 feet by 10 feet produces a maximum settlement of 0.69 feet. The number of elements, however, is increased 25 times, and so are the costs.

8.5.2 Case Studies

NFOLD was only used on the Austin Bayou case study. Model CCC was used to determine the compaction of the reservoir. NFOLD

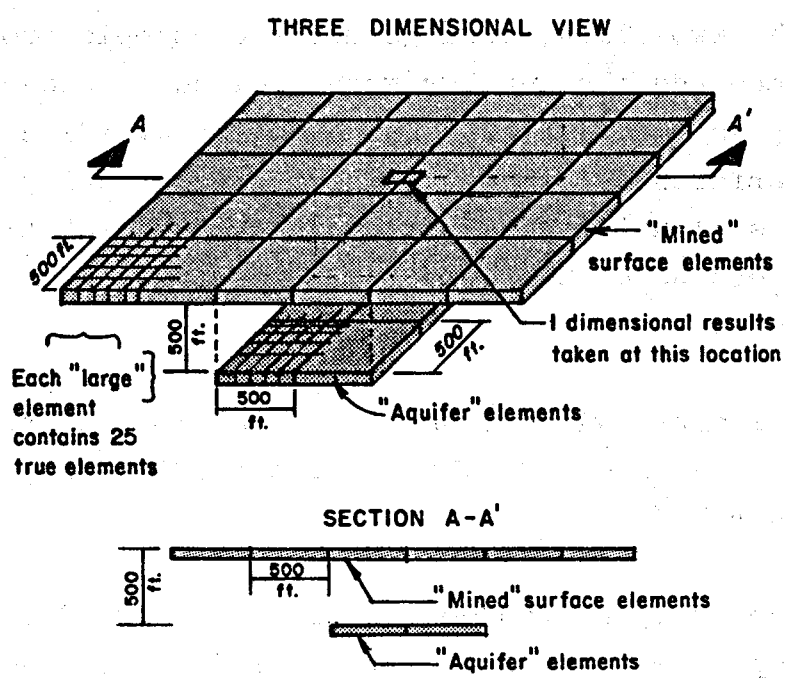

FIGURE 8-4
THREE-DIMENSIONAL DISPLACEMENT-DISCONTINUITY MODEL
FOR SAMPLE PROBLEM 3

was then used to model the propogation of stresses and strains to the surface and to nearby faults. Figure 8-5 is a sketch of the element layout.

The use of NFOLD allowed determination of three-dimensional settlement at the surface at a cost of approximately 300 CPU seconds--considerably less than the cost of a comparable finite element or finite difference model, but still a very significant cost. In addition, stresses on the faults were computed, and it was predicted that no slip would occur. However, this result is apparently due to the large fault and reservoir elements that had to be used to obtain a solution at a reasonable cost. A much-improved determination of stresses on the faults was achieved with the two-dimensional displacement-discontinuity program DDJ2D.

8.6 CONCLUSIONS

NFOLD is a very useful program for analyzing three-dimensional propogation of reservoir deformation effects and is therefore an excellent companion to a reservoir-flow modeling program such as CCC. Simpler displacement-discontinuity programs such as DDJ2D and MINAP (Crouch 1976) are useful for one- and two-dimensional geometries. The major limitations are (1) the assumed homogeneous linear-elastic continuum in which the "seams" are embedded and (2) the requirement that the "seams" be thin.

8.7 REFERENCES

Crouch, S.L. (1976). Analysis of Stresses and Displacements Around Underground Excavations: An Application of the Displacement Discontinuity Method, Dept. of Civil and Mineral Engineering, University of Minnesota.

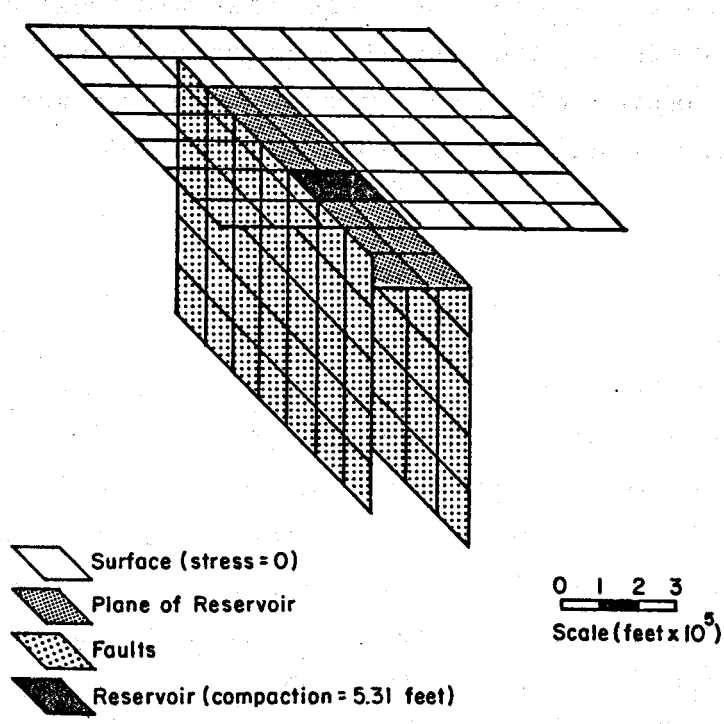

FIGURE 8-5
THREE-DIMENSIONAL DISPLACEMENT-DISCONTINUITY MODEL
ELEMENT LAYOUT FOR AUSTIN BAYOU CASE STUDY

Crouch, S.L., and C. Fairhurst (1973). "The Mechanics of Coal Mine Bumps and the Interaction Between Coal Pillars, Mine Roof, and Floor," Final Report, USBM Research Contract H0101778.

Sinha, K.P. (1979). Displacement Discontinuity Technique for Analysing Stresses and Displacements Due to Mining in Seam Deposits, Ph.D. thesis, University of Minnesota.

APPENDIX A

USERS' MANUAL
PROGRAM "SUBSID"

A.1 INTRODUCTION

The program SUBSID models geothermal reservoirs subject to pore-pressure changes using spherical nuclei of strain. This users' manual describes the use of SUBSID but does not present the theory of the method employed. The detailed report on SUBSID provides that background and should be read in conjunction with this users' manual.

Although this manual does not refer to temperature changes, they can be specified by applying a pressure change equal to $3K\alpha\delta T$, where K is the bulk modulus ($K = \frac{E}{3(1-2\nu)}$), α is the coefficient of linear thermal expansion, and δT is the temperature change.

Pressure increases and compressive stresses are positive, while pressure decreases and tensile stresses are negative. The pressure change Δp and volume V of a particular sphere should be chosen so that $\Delta pV = \Delta p_o V_o$, where Δp_o and V_o are the pressure change and volume of the corresponding portion of the reservoir. If this is done, then displacements and stresses at points away from the reservoir will be calculated correctly. Points within either the model or the actual reservoir will show incorrect values for displacements and stresses, since a model made of spheres does not conform well to an actual nonspherical reservoir.

The program allows 500 observation points at which displacements and stresses are to be calculated and a total of 700 observation points plus spherical nuclei of strain.

The reservoir pressure change and the modulus of elasticity must be specified in the same units. The units of length used in

describing the reservoir geometry need not be consistent with this. Displacement will be output in the units of length used and stresses will be output in the units of pressure used.

The subroutine CYLIN in SUBSID combines spheres with centers in the same XY plane to form a cylinder. The user specifies the depth of the centerplane of the cylinder, the number of spheres in the cylinder and the radius of these spheres. The center of the cylinder, is assumed to be at (X, Y) = (0, 0). Table A-1 presents the number of spheres that may be specified, their arrangement in rings from the center out, the radius of the spheres as a function of cylinder radius, and the aspect ratio (h/R = height/radius) of the cylinder whose volume exactly equals the volume of the spheres in the model.

TABLE A-1
CYLINDERS MODELED WITH SPHERES

NUMBER OF RINGS N	NUMBER OF SPHERES	ARRANGEMENT IN RINGS	RADIUS OF SPHERES	EFFECTIVE ASPECT RATIO H/R
1	1	1	R	4/3 = 1.333
2	9	1,8	R/3	4/9 = 0.444
3	25	1,8,16	R/5	4/15 = 0.267
4	49	1,8,16,24	R/7	4/21 = 0.190
5	81	1,8,16,24,32	R/9	4/27 = 0.148
6	121	1,8,16,24,32,40	R/11	4/33 = 0.121
7	169	1,8,16,24,32,40,48	R/13	4/39 = 0.103

A.2 INPUT

There are five types of input cards. Only one card of each of types 1, 2, and 4 is used. The number of cards of type 3.SOR (where SOR varies from 0 to 5) is equal to LAYER, as specified on card type 2. The number of cards of type 5 is equal to NOB, which is specified on card type 4.

Card 1: FORMAT (2F8.2) NU, E

COLUMN		
1-8	NU	value of ν for the half-space
9-16	E	value of Young's modulus in units of $ML^{-1}\ t^{-2}$ for the half-space

Card 2: FORMAT (2I8, F8.0) LAYER, IR, SOR

COLUMN		
1-8	LAYER	number of reservoir arrays (integer)
9-16	IR	total number of reservoir spheres (integer)
17-24	SOR	type of reservoir arrays:

- Ø. single spheres
- 1. horizontal rectangles (in X-Y plane)
- 2. lines in the X direction
- 3. lines the Y direction
- 4. lines in the Z direction (depth)
- 5. cylinders (in X-Y plane)

<u>LAYER cards of type 3.SOR</u>

Card 3.Ø: (used if SOR = Ø.) FORMAT (I8,5F8.2) I, X(I), Y(I), Z(I), A(I), BETA(I)

COLUMN		
1-8	I	number of reservoir sphere (integer)
9-16	X(I)	X coordinate of center of ith sphere
17-24	Y(I)	Y coordinate of center of ith sphere
25-32	Z(I)	Z coordinate of center of ith sphere
33-40	A(I)	radius of ith sphere
41-48	BETA(I)	pressure change in ith sphere ($ML^{-1}\ t^{-2}$)

(note that LAYER = IR for SOR = Ø.)

Card 3.1: (used if SOR = 1.) FORMAT (6F8.2, 3I8, F8.0) RØ, XØ, YØ, ZØ, OX, OY, I, NX, NY, BET

COLUMN		
1-8	RØ	radius of spheres
9-16	XØ	spacing of sphere centers in X direction
17-24	YØ	spacing of sphere centers in Y direction
25-32	ZØ	Z coordinate of sphere centers
33-40	OX	X coordinate of rectangle midpoint
41-48	OY	Y coordinate of rectangle midpoint
49-56	I	number of first sphere in rectangle (integer)
57-64	NX	number of spheres in X direction (integer)
65-72	NY	number of spheres in Y direction (integer)
73-80	BET	pressure change in spheres ($ML^{-1}\ t^{-2}$)

Card 3.2: (used if SOR = 2.) FORMAT (5F8.2, 8X, 2I8, 8X, F8.0) RØ, XØ, YØ, ZØ, O, I, N, BET

COLUMN		
1-8	RØ	radius of spheres
9-16	XØ	spacing of sphere centers in X direction
17-24	YØ	Y coordinate of sphere centers
25-32	ZØ	Z coordinate of sphere centers

33-40	O	X coordinate of first sphere center
49-50	I	number of first sphere in line (integer)
57-64	N	number of spheres in line (integer)
73-80	BET	pressure change in spheres (ML^{-1} t^{-2})

Card 3.3: (used if SOR = 3.) FORMAT (5F8.2, 8X, 2I8, 8X, F8.0)
RØ, XØ, YØ, ZØ, O, I, N, BET

COLUMN		
1-8	RØ	radius of spheres
9-16	XØ	X coordinate of sphere centers
17-24	YØ	spacing of sphere centers in Y direction
25-32	ZØ	Z coordinate of sphere centers
33-40	O	Y coordinate of first sphere center
49-56	I	number of first sphere in line (integer)
57-64	N	number of spheres in line (integer)
73-80	BET	pressure change in spheres (ML^{-1} t^{-2})

Card 3.4: (used if SOR = 4.) FORMAT (5F8.2, 8X, 2I8, 8X, F8.0)
RØ, XØ, YØ, ZØ, O, I, N, BET

COLUMN		
1-8	RØ	radius of spheres
9-16	XØ	X coordinate of sphere centers
17-24	YØ	Y coordinate of sphere centers
25-32	ZØ	spacing of sphere centers in Z direction
33-40	O	Z coordinate of first sphere center
49-50	I	number of first sphere in line (integer)
57-64	N	number of spheres in line (integer)
73-80	BET	pressure change in spheres (ML^{-1} t^{-2})

Card 3.5: (used if SOR = 5.) FORMAT (5F8.2, 2I8, F8.0) RØ, ZØ,
I, N, BET

COLUMN		
1-8	RØ	radius of spheres in array
9-16	ZØ	Z coordinate of sphere centers
17-24	I	number of first sphere in cylinder (integer)
25-32	N	number of spheres in cylinder (integer = 1, 9, 25, 49, 81, 121, or 169)
33-40	BET	pressure change in spheres ($ML^{-1}\ t^{-2}$)

Card 4: FORMAT (2I8) NOB, IO

COLUMN		
1-8	NOB	number of observation arrays (integer)
9-16	IO	total number of observation points (integer)

<u>NOB Cards of Type 5.OBS</u>:

Card 5.1: (used if OBS = 1.) FORMAT (6F8.2, 3I8) OBS, XØ, YØ, ZØ, OX, OY, I, NX, NY

COLUMN		
1-8	OBS	1. (indicates rectangular observation array)
9-16	XØ	X spacing of observation points
17-24	YØ	Y spacing of observation points
25-32	ZØ	Z coordinate of observation points
33-40	OX	X coordinate of rectangle midpoint
41-48	OY	Y coordinate of rectangle midpoint
49-56	I	number of first point in rectangle (integer)
57-64	NX	number of points in X direction (integer)
65-72	NY	number of points in Y direction (integer)

Card 5.2: (used if OBS = 2.) FORMAT (5F8.2, 8X, 2I8) OBS, XØ, YØ, ZØ, O, I, N

COLUMN		
1-8	OBS	2. (line of observation points in X direction)
9-16	XØ	X spacing of observation points
17-24	YØ	Y coordinate of observation points
25-32	ZØ	Z coordinate of observation points
33-40	O	X coordinate of first point in line
49-56	I	number of first point in line (integer)
57-64	N	number of points in line (integer)

Card 5.3: (used of OBS = 3.) FORMAT (5F8.2, 8X, 2I8) OBS, XØ, YØ, ZØ, O, I, N

COLUMN		
1-8	OBS	3. (line of observation points in Y direction)
9-16	XØ	X coordinate of observation points
17-24	YØ	Y spacing of observation points
25-32	ZØ	Z coordinate of observation points
33-40	O	Y coordinate of first point in line
49-56	I	number of first point in line (integer)
57-64	N	number of points in line (integer)

Card 5.4: (used if OBS = 4.) FORMAT (5F8.2, 8X, 2I8) OBS, XØ, YØ, ZØ, O, I, N

COLUMN		
1-8	OBS	4. (line of observation points in Z direction)
9-16	XØ	X coordinate of observation points
17-24	YØ	Y coordinate of observation points
25-32	ZØ	Z spacing of observation points
33-40	O	Z coordinate of first point in line
49-56	I	number of first point in line (integer)
57-64	N	number of points in line (integer)

A.3 OUTPUT

Most output from SUBSID is automatic; however, the user must specify a grid of points at which displacements and stresses are to be determined.

The following parameters are automatically output:

1. Poisson's ratio and Young's modulus
2. Echo of reservoir spheres input
3. Echo of observation points input
4. Positions of sphere centers and observation points
5. Strength and radius of reservoir spheres.

Displacements and stresses are output at observation points specified by the user. Quantities output are displacements U, V, and W in the X, Y, and Z directions; normal stresses σ_x, σ_y, and σ_z, shear stresses τ_{xy}, τ_{xz}, and τ_{yz}, and the mean stress σ_m. The observation points are ordered as follows:

1. Arrays (rectangles or lines) are output in the order of input
2. Within a line array, the points are ordered from the lowest to the highest coordinate
3. Within a rectangle, the points are ordered from the lowest value of Y, with X varying from its lowest to highest value, up to the highest value of Y, with X varying from its lowest to highest value (Figure A-1).

A.4 SAMPLE PROBLEM

A reservoir is to be modeled by seven spheres whose geometry is shown in Figure A-2. Five spheres have their centers on a

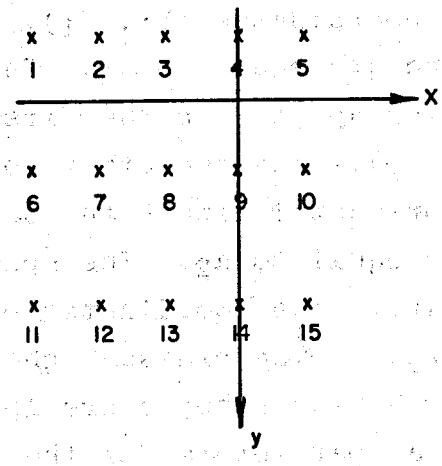

FIGURE A-1
SUBSID USERS' MANUAL
ORDERING OF NODAL POINTS
WITHIN RECTANGULAR GRIDS

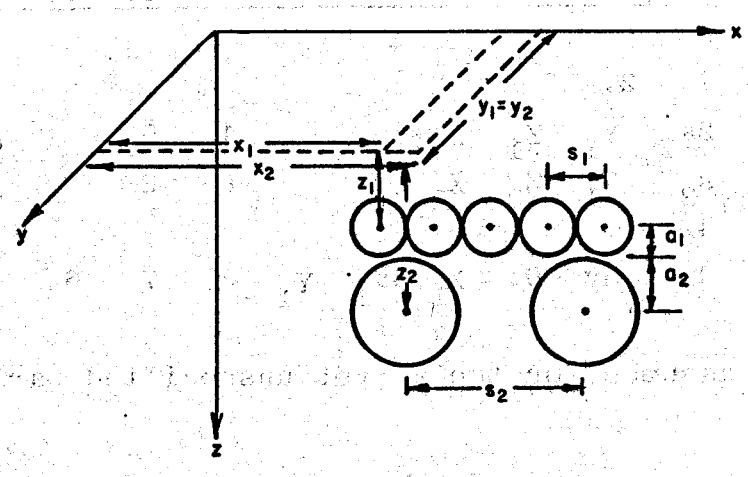

FIGURE A-2
SUBSID USERS' MANUAL
GEOMETRY OF SPHERES
REPRESENTING SAMPLE PROBLEM RESERVOIR

horizontal line with coordinates (Y_1, Z_1). The sphere radii are the same and are equal to a_1. The sphere centers are spaced one diameter apart with the first sphere center at coordinates (X_1, Y_1, Z_1). The two other spheres have their centers on a horizontal line with coordinates (Y_1, Z_2). Their radii are equal to a_2. The sphere centers are a distance s_2 apart. The coordinates of the first sphere center are (X_2, Y_1, Z_2). The pressure changes of the five spheres and the two spheres are Δp_1 and Δp_2, respectively. Material parameters for the half-space are E and ν.

Observation points are chosen to form a 7 by 6 rectangle at the surface Z = 0. The points are spaced at d_x in the X direction and d_y in the Y direction. The center of the rectangle has coordinates ($X_1 + 4a_1$, Y_1, 0).

Input values for this problem would be:

Card	1	9	17	25	33	41	49	57	65	73
1	ν	E								
2	2	7	2.							
3.2	a_1	$2a_1$	Y_1	Z_1	X_1		1	5		Δp_1
	a_2	s_2	Y_1	Z_2	X_2		6	2		Δp_2
4	1	42								
5.1	1.	dx	dy	0.	X_1+4a_1	Y_1	8	7	6	

Values will be assumed for the as yet unspecified parameters as follows:

$\nu = 0.25$, $E = 10^5$ lb/in^2

$a_1 = 50$ ft, $Y_1 = 0$, $Z_1 = 400$ ft, $X_1 = 100$ ft

$\Delta p_1 = -300\ lb/in^2$

$a_2 = 100$ ft, $s_2 = 300$ ft, $Z_2 = 550$ ft, $X_2 = 200$ ft

$\Delta p_2 = -300\ lb/in^2$

$d_x = 50$ ft, $d_y = 30$ ft.

A.4.1 Input Data for Sample Problem

```
.25      100000.
         2        72.
50.      100.     0.       400.     100.                    1        5        -300.
100.     300.     0.       550.     200.                    6        2        -300.
         1        42
1.       50.      30.      0.       300.     0.             8        7        6
```

A.4.2 Output for Sample Problem

```
.10      E
.250 100000.

RESERVOIR SPHERES INPUT
  50.00  100.00    0.00  400.00  100.00    0.00      1      5      0  -300.
 100.00  300.00    0.00  550.00  200.00    0.00      6      2      0  -300.

OBSERVATION POINTS INPUT
   1.00   50.00   30.00    0.00  300.00    0.00      8      7      6

POSITIONS OF SPHERE CENTERS AND OBSERVATION POINTS
  100.  200.  300.  400.  500.  200.  500.  150.  200.  250.  300.  350.  400.  450.  150.  200.  250.  300.  350.  400.
  450.  150.  200.  250.  300.  350.  400.  450.  150.  200.  250.  300.  350.  400.  450.  150.  200.  250.  300.  350.
  400.  450.  150.  200.  250.  300.  350.  400.  450.
    0.    0.    0.    0.    0.    0.    0.  -75.  -75.  -75.  -75.  -75.  -75.  -75.  -45.  -45.  -45.  -45.  -45.  -45.
  -45.  -15.  -15.  -15.  -15.  -15.  -15.  -15.   15.   15.   15.   15.   15.   15.   15.   45.   45.   45.   45.   45.
   45.   45.   75.   75.   75.   75.   75.   75.   75.
  400.  400.  400.  400.  400.  550.  550.    0.    0.    0.    0.    0.    0.    0.    0.    0.    0.    0.    0.    0.
    0.    0.    0.    0.    0.    0.    0.    0.    0.    0.    0.    0.    0.    0.    0.    0.    0.    0.    0.    0.
    0.    0.    0.    0.    0.    0.    0.    0.    0.

STRENGTH AND RADIUS OF RESERVOIR SPHERES
-.00250  50.0 -.00250  50.0 -.00250  50.0 -.00250  50.0 -.00250  50.0 -.00250 100.0 -.00250 100.0 0.00000   0.0 0.00000   0.0
0.00000   0.0 0.00000   0.0 0.00000   0.0 0.00000   0.0 0.00000   0.0 0.00000   0.0 0.00000   0.0 0.00000   0.0 0.00000   0.0
0.00000   0.0 0.00000   0.0 0.00000   0.0 0.00000   0.0 0.00000   0.0 0.00000   0.0 0.00000   0.0 0.00000   0.0 0.00000   0.0
0.00000   0.0 0.00000   0.0 0.00000   0.0 0.00000   0.0 0.00000   0.0 0.00000   0.0 0.00000   0.0 0.00000   0.0 0.00000   0.0
0.00000   0.0 0.00000   0.0 0.00000   0.0 0.00000   0.0 0.00000   0.0 0.00000   0.0 0.00000   0.0 0.00000   0.0 0.00000   0.0
0.00000   0.0 0.00000   0.0 0.00000   0.0 0.00000   0.0
```

U	V	W	SIGX	SIGY	SIGZ	TXY	TXZ	TYZ	SIGM
.00582	.00308	.01992	-3.845	-4.797	.000	.327	0.000	0.000	-2.881
.00438	.00326	.02107	-4.361	-5.142	.000	.245	0.000	0.000	-3.168
.00276	.00338	.02187	-4.710	-5.379	.000	.149	0.000	0.000	-3.363
.00104	.00345	.02229	-4.881	-5.497	-.000	.047	0.000	0.000	-3.459
-.00072	.00344	.02230	-4.875	-5.493	.000	-.057	0.000	0.000	-3.456
-.00244	.00338	.02192	-4.695	-5.369	.000	-.157	0.000	0.000	-3.355
-.00405	.00325	.02115	-4.346	-5.130	.000	-.248	0.000	0.000	-3.159
.00592	.00189	.02033	-3.962	-5.085	.000	.202	0.000	0.000	-3.016
.00446	.00200	.02152	-4.495	-5.456	.000	.151	0.000	0.000	-3.317
.00281	.00208	.02234	-4.853	-5.710	0.000	.092	0.000	0.000	-3.521
.00106	.00211	.02277	-5.028	-5.835	-.000	.029	0.000	0.000	-3.621
-.00073	.00211	.02278	-5.022	-5.830	-.000	-.035	0.000	0.000	-3.617
-.00248	.00207	.02238	-4.836	-5.694	-.000	-.097	0.000	0.000	-3.510
-.00412	.00199	.02159	-4.475	-5.435	-.000	-.154	0.000	0.000	-3.303
.00597	.00064	.02054	-4.023	-5.236	-.000	.069	0.000	0.000	-3.086
.00449	.00067	.02174	-4.564	-5.621	.000	.051	0.000	0.000	-3.395
.00283	.00070	.02258	-4.928	-5.884	.000	.031	0.000	0.000	-3.604
.00106	.00071	.02301	-5.105	-6.013	-.000	.010	0.000	0.000	-3.706
-.00074	.00071	.02303	-5.098	-6.006	.000	-.012	0.000	0.000	-3.701
-.00251	.00070	.02262	-4.909	-5.865	.000	-.033	0.000	0.000	-3.591
-.00416	.00067	.02181	-4.541	-5.596	.000	-.052	0.000	0.000	-3.379
.00597	-.00064	.02054	-4.023	-5.236	-.000	-.069	0.000	0.000	-3.086
.00449	-.00067	.02174	-4.564	-5.621	.000	-.051	0.000	0.000	-3.395
.00283	-.00070	.02258	-4.928	-5.884	.000	-.031	0.000	0.000	-3.604
.00106	-.00071	.02301	-5.105	-6.013	-.000	-.010	0.000	0.000	-3.706
-.00074	-.00071	.02303	-5.098	-6.006	.000	.012	0.000	0.000	-3.701
-.00251	-.00070	.02262	-4.909	-5.865	.000	.033	0.000	0.000	-3.591
-.00416	-.00067	.02181	-4.541	-5.596	.000	.052	0.000	0.000	-3.379
.00592	-.00189	.02033	-3.962	-5.085	.000	-.202	0.000	0.000	-3.016
.00446	-.00200	.02152	-4.495	-5.456	.000	-.151	0.000	0.000	-3.317
.00281	-.00208	.02234	-4.853	-5.710	0.000	-.092	0.000	0.000	-3.521
.00106	-.00211	.02277	-5.028	-5.835	-.000	-.029	0.000	0.000	-3.621
-.00073	-.00211	.02278	-5.022	-5.830	-.000	.035	0.000	0.000	-3.617
-.00248	-.00207	.02238	-4.836	-5.694	-.000	.097	0.000	0.000	-3.510
-.00412	-.00199	.02159	-4.475	-5.435	-.000	.154	0.000	0.000	-3.303
.00582	-.00308	.01992	-3.845	-4.797	.000	-.327	0.000	0.000	-2.881
.00438	-.00326	.02107	-4.361	-5.142	.000	-.245	0.000	0.000	-3.168
.00276	-.00338	.02187	-4.710	-5.379	.000	-.149	0.000	0.000	-3.363
.00104	-.00345	.02229	-4.881	-5.497	-.000	-.047	0.000	0.000	-3.459
-.00072	-.00344	.02230	-4.875	-5.493	.000	.057	0.000	0.000	-3.456
-.00244	-.00338	.02192	-4.695	-5.369	.000	.157	0.000	0.000	-3.355
-.00405	-.00325	.02115	-4.346	-5.130	.000	.248	0.000	0.000	-3.159

A.5 MODELING A CYLINDER WITH SPHERES

The arrangement of spheres to form a cylinder that was used in SUBSID is derived as follows. The cylinder radius is divided into 2n-1 equal segments. Ring boundaries are drawn at the division point closest to the center and at every two division points thereafter to form n rings (the middle ring is a cylinder) Figure A-3 illustrates this with n = 4. Ring volumes V_r are:

$$V_r = \pi h (a_o^2 - a_i^2)$$

where a_o and a_i are the outer and inner ring radii, respectively, and h is the cylinder height. This may be written as:

$$V_r = \frac{\pi R^2 h}{(2n-1)^2} \left[(2k-1)^2 - (2k-3)^2 \right]$$

$$= \frac{\pi R^2 h}{(2n-1)^2} \, 8(k-1) \qquad k = 2, \ldots, n$$

for the actual rings and

$$V_c = \frac{\pi R^2 h}{(2n-1)^2}$$

for the center cylinder.

The ring volumes relative to the center cylinder are then

$$\frac{V_r}{V_c} = 8(k-1) \qquad k = 2, \ldots, n$$

Therefore, if the central cylinder is modeled with one sphere, the surrounding rings must have in order 8, 16, 24, 32, ..., 8(n-1) rings. The aspect ratio of the cylinder whose volume

V_o is exactly equal to the total volume of spheres is found by comparing V and V_o for each n. For n = 4 there are 49 spheres. Since their radii equals one-seventh of the cylinder radius:

$$V = 49\left(\frac{4}{3}\pi\left(\frac{R}{7}\right)^3\right)$$

and $V_o = \pi R^2 h$.

Thus, for $V = V_o$ we must have

$$\frac{h}{R} = \frac{4(49)}{3(7^3)} = \frac{4}{21}$$

This means that the generated cylinder for n = 4 (49 spheres) has an effective aspect ratio of h/R = 4/21. Table A-1 gives the aspect ratios for the other generated cylinder types.

A.6 CHANGING THE PROGRAM

The limits on the number of observation points and spherical nuclei of strain may be increased by making the following changes:

<u>Main Program SUBSID</u>

- Increase dimension of arrays B, C, XX, YY, D, W1, S1, S2, S3, T1, and T2 in the DIMENSION list to the number of observation points desired.

- Increase dimension of arrays U, V, W, S1GX, SIGY, SIGZ, TXY, TXZ, TYZ, BETA, and A in the DIMENSION list and X, Y, Z in the COMMON list to the number of spheres plus observation points desired.

- Increase the upper limit of the DO loop in line 15 to the number of spheres plus observation points desired.

Subroutines XLINE, YLINE, ZLINE, RECT, CYLIN

- Increase dimension of arrays X, Y, Z in the COMMON list to the number of spheres plus observation point desired.

The subroutine CYLIN could be easily changed so that a smaller aspect ratio cylinder could be generated. For example, a cylinder with aspect ratio 4/45 = 0.089 would be modeled by 196 spheres of radius R/15 arranged in eight rings, with the outermost containing 56 spheres.

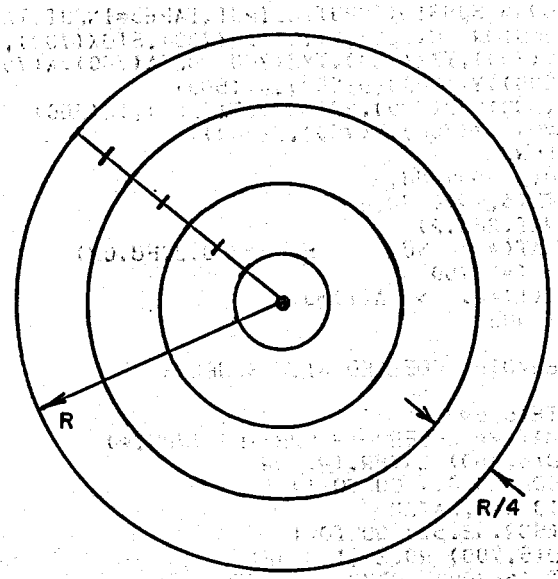

FIGURE A-3
SUBSID USERS' MANUAL
FORMING MODEL CYLINDER WITH SPHERES (N=4)

A.7 SOURCE LISTING OF SUBSID

```
C
C     CALCULATION OF DISPLACEMENTS AND STRESSES DUE TO SUBSIDENCE
C
      PROGRAM SUBSID(INPUT,OUTPUT,TAPE5=INPUT,TAPE6=OUTPUT)
      DIMENSION  U(700),V(700),W(700),SIGX(700),SIGY(700),SIGZ(700)
     $,TXY(700),TXZ(700),TYZ(700),BETA(700),A(700),B(500),C(500),
     $XX(500),YY(500),D(500),WI(500)
     $,S1(500),S2(500),S3(500),T1(500),T2(500)
      COMMON  X(700),Y(700),Z(700)
      REAL NU
      READ(5,200) NU,E
      WRITE(6,199) NU,E
  200 FORMAT(2F8.2)
  199 FORMAT(*    NU       E    */F8.3,F8.0/)
      DO 5 I=1,700
      BETA(I)=0.  $  A(I)=0.
    5 CONTINUE
C
C     RESERVOIR MODELLED WITH SPHERES
C
      WRITE(6,699)
  699 FORMAT(/* RESERVOIR SPHERES INPUT*)
      READ(5,400) LAYER,IR,SOR
      IF(SOR.EQ.0.) GO TO 14
      DO 13 K=1,LAYER
      IF (SOR.NE.5.) GO TO 1
      READ(5,700) R0,Z0,I,N,BET
      WRITE(6,700) R0,Z0,I,N,BET
  700 FORMAT(2F8.2,2I8,F8.0)
      CALL CYLIN(R0,Z0,I,N)
      GO TO 140
    1 READ(5,500) R0,X0,Y0,Z0,OX,OY,I,NX,NY,BET
      WRITE(6,500) R0,X0,Y0,Z0,OX,OY,I,NX,NY,BET
      IF (SOR.NE.1.) GO TO 130
      CALL RECT(X0,Y0,Z0,OX,OY,I,NX,NY)
      N=NX*NY
      GO TO 140
  130 O=OX  $  N=NX
      IF (SOR-3.) 131,132,133
  131 CALL XLINE(X0,Y0,Z0,O,I,N)
      GO TO 140
  132 CALL YLINE(X0,Y0,Z0,O,I,N)
      GO TO 140
  133 CALL ZLINE(X0,Y0,Z0,O,I,N)
  140 JF=I+N-1
      DO 13 J=I,JF
      BETA(J)=BET*(1.+NU)*(1.-2.*NU)/((1.-NU)*E)  $  A(J)=R0
      B(J)=BETA(J)*A(J)**3/3.  $  C(J)=B(J)*E/(1.+NU)
   13 CONTINUE
      GO TO 3
C
C     SINGLE SPHERE INPUT
C
   14 DO 15 J=1,IR
```

```
      READ(5,300)I,X(I),Y(I),Z(I),A(I),BETA(I)
  300 FORMAT(I8,5F8.2)
      BETA(I)=BETA(I)*(1.+NU)*(1.-2.*NU)/((1.-NU)*E)
      B(I)=BETA(I)*A(I)**3/3.  $  C(I)=B(I)*E/(1.+NU)
   15 CONTINUE
      WRITE(6,701)IR
  701 FORMAT(1X,I5,* SINGLE SPHERES*)
C
C     OBSERVATION POINTS
C
    3 READ(5,400) NOB,IO
  400 FORMAT(2I8,F8.0)
      IT=IR+IO
      WRITE(6,499)
  499 FORMAT(/* OBSERVATION POINTS INPUT*)
      DO 110 II=1,NOB
      READ(5,500) OBS,X0,Y0,Z0,OX,OY,I,NX,NY
      WRITE(6,500) OBS,X0,Y0,Z0,OX,OY,I,NX,NY
  500 FORMAT(6F8.2,3I8,F8.0)
      IF(OBS.NE.1.) GO TO 120
      CALL RECT(X0,Y0,Z0,OX,OY,I,NX,NY)
      GO TO 110
  120 O=OX  $  N=NX
      IF(OBS-3.) 121,122,123
  121 CALL XLINE(X0,Y0,Z0,O,I,N)
      GO TO 110
  122 CALL YLINE(X0,Y0,Z0,O,I,N)
      GO TO 110
  123 CALL ZLINE(X0,Y0,Z0,O,I,N)
  110 CONTINUE
      WRITE(6,599)
  599 FORMAT(/* POSITIONS OF SPHERE CENTERS AND OBSERVATION POINTS*)
      WRITE(6,600) (X(J),J=1,IT)
      WRITE(6,600) (Y(J),J=1,IT)
      WRITE(6,600) (Z(J),J=1,IT)
  600 FORMAT(1X,20F6.0)
      WRITE(6,799)
  799 FORMAT(/* STRENGTH AND RADIUS OF RESERVOIR SPHERES*)
      WRITE(6,800)(BETA(J),A(J),J=1,IT)
  800 FORMAT(9(F8.5,F6.1))
      WRITE(6,99)
   99 FORMAT(///9X,*U            V            W            SIGX*,8X,
     $*SIGY        SIGZ        TXY         TXZ         TYZ*,9X,*SIGM*/)
      IRR=IR+1
      DO 20 I=IRR,IT
      U(I)=V(I)=W(I)=0.
      SIGX(I)=SIGY(I)=SIGZ(I)=0.
      TXY(I)=TXZ(I)=TYZ(I)=0.
      CHECK=1.
      DO 25 J=1,IR
      IF(BETA(J).EQ.0.) GO TO 25
      XX(J)=X(I)-X(J)  $  YY(J)=Y(I)-Y(J)
      ZZ=Z(I)-Z(J)  $  ZI=Z(I)+Z(J)
      RI=SQRT(XX(J)**2+YY(J)**2+ZZ**2)
```

```
      R2=SQRT(XX(J)**2+YY(J)**2+ZI**2)
      IF(R1.GT.A(J)) GO TO 30
      IF((A(J)-R1).LE..001.AND.CHECK.LE..001) GO TO 30
      IF((A(J)-R1).LE..001) CHECK=.001
C
C     PARTIAL DISPLACEMENTS AND STRESSES AT OBSERVATION POINT INTERIOR TO
C     A RESERVOIR SPHERE
C
      D(J)=1./A(J)**3+(3.-4.*NU)/R2**3-6.*Z(I)*ZI/R2**5
      W1(J)=ZZ/A(J)**3-(3.-4.*NU)*ZI/R2**3+2.*Z(I)/R2**3
     $-6.*Z(I)*ZI**2/R2**5
      S1(J)=-2./A(J)**3+(3.-8.*NU)/R2**3-6.*ZI*(Z(I)-2.*NU*ZI)/R2**5
      S2(J)=3.*(-3.+4.*NU+10.*Z(I)*ZI/R2**2)/R2**5
      S3(J)=-2./A(J)**3-1./R2**3+3.*ZI*(ZI-6.*Z(I)+10*Z(I)*ZI**2/R2**2
     $)/R2**5
      T1(J)=(3.-4.*NU-10.*Z(I)*ZI/R2**2)/R2**5
      T2(J)=(3.*Z(I)+Z(J)-10.*Z(I)*ZI**2/R2**2)/R2**5
      GO TO 40
C
C     PARTIAL DISPLACEMENTS AND STRESSES AT OBSERVATION POINT EXTERIOR
C     TO A RESERVOIR SPHERE
C
   30 D(J)= 1./R1**3+(3.-4.*NU)/R2**3-6.*Z(I)*ZI/R2**5
      W1(J)= ZZ/R1**3-(3.-4.*NU)*ZI/R2**3
     $+2.*Z(I)/R2**3-6.*Z(I)*ZI**2/R2**5
      S1(J)=1./R1**3+(3.-8.*NU)/R2**3-6.*ZI*
     $(Z(I)-2.*NU*ZI)/R2**5
      S2(J)=3.*(10.*Z(I)*ZI/R2**2-3.+4.*NU)/
     $R2**5-3./R1**5
      S3(J)=-1./R2**3+3.*ZI*(ZI-6*Z(I))/R2**5
     $+30.*Z(I)*ZI**3/R2**7+(1.-3.*(ZZ/R1)**2)
     $/R1**3
      T1(J)=(3.-4.*NU-10.*Z(I)*ZI/R2**2)/R2**5
     $+1./R1**5
      T2(J)=(3.*Z(I)+Z(J)-10.*Z(I)*ZI**2/R2**2)
     $/R2**5+ZZ/R1**5
C
C     TOTAL DISPLACEMENTS AND STRESSES AT AN OBSERVATION POINT
C
   40 U(I)=U(I)+XX(J)*B(J)*D(J)
      V(I)=V(I)+YY(J)*B(J)*D(J)
      W(I)=W(I)+B(J)*W1(J)
      SIGX(I)=SIGX(I)+C(J)*(S1(J)+XX(J)**2*S2(J))
      SIGY(I)=SIGY(I)+C(J)*(S1(J)+YY(J)**2*S2(J))
      SIGZ(I)=SIGZ(I)+C(J)*S3(J)
      TXY(I)=TXY(I)-3.*C(J)*XX(J)*YY(J)*T1(J)
      TYZ(I)=TYZ(I)-3.*C(J)*YY(J)*T2(J)
      TXZ(I)=TXZ(I)-3.*C(J)*XX(J)*T2(J)
   25 CONTINUE
C
C     MEAN STRESS
C
      SIGM=(SIGX(I)+SIGY(I)+SIGZ(I))/3.
C
```

```
C     OUTPUT DISPLACEMENT IN UNITS OF LENGTH AND STRESS IN UNITS OF E
C
      WRITE(6,100)U(I),V(I),W(I),SIGX(I),SIGY(I),SIGZ(I),
     $TXY(I),TXZ(I),TYZ(I),SIGM
  100 FORMAT(1X,3F12.5,7F12.3)
   20 CONTINUE
    2 STOP
      END
      SUBROUTINE XLINE(X0,Y0,Z0,O,I,N)
      COMMON  X(700),Y(700),Z(700)
      X(I)=O  $  Y(I)=Y0  $  Z(I)=Z0
      IN=I+N-2
      DO 1 J=I,IN
      X(J+1)=X(J)+X0  $  Y(J+1)=Y0  $  Z(J+1)=Z0
    1 CONTINUE
      END
      SUBROUTINE YLINE(X0,Y0,Z0,O,I,N)
      COMMON  X(700),Y(700),Z(700)
      X(I)=X0  $  Y(I)=O  $  Z(I)=Z0
      IN=I+N-2
      DO 1 J=I,IN
      X(J+1)=X0  $  Y(J+1)=Y(J)+Y0  $  Z(J+1)=Z0
    1 CONTINUE
      END
      SUBROUTINE ZLINE(X0,Y0,Z0,O,I,N)
      COMMON  X(700),Y(700),Z(700)
      X(I)=X0  $  Y(I)=Y0  $  Z(I)=O
      IN=I+N-2
      DO 1 J=I,IN
      X(J+1)=X0  $  Y(J+1)=Y0  $  Z(J+1)=Z(J)+Z0
    1 CONTINUE
      END
      SUBROUTINE RECT(X0,Y0,Z0,OX,OY,I,NX,NY)
      COMMON  X(700),Y(700),Z(700)
      REAL LX,LY,LL
      LX=(NX-1)/2.  $  LY=(NY-1)/2.  $  LL=(NX+1)/2.
      X(I)=OX-LX*X0  $  Y(I)=OY-LY*Y0  $  Z(I)=Z0
      KI=I  $  KF=KI+NX-2
      DO 2 J=1,NY
      DO 1 K=KI,KF
      X(K+1)=X(K)+X0  $  Y(K+1)=Y(I)+(J-1)*Y0  $  Z(K+1)=Z0
      IF(X(K+1).EQ.OX+LL*X0) X(K+1)=OX-LX*X0
    1 CONTINUE
      KI=I+J*NX-1  $  KF=KI+NX-1
    2 CONTINUE
      END
      SUBROUTINE CYLIN(R0,Z0,I,N)
      COMMON  X(700),Y(700),Z(700)
      IF(N.LE.49) GO TO 8
      IF(N-121) 3,2,1
    8 IF(N.EQ.1) GO TO 7
      IF(N-25) 6,5,4
    1 JI=I+121
      DO 60 JJ=1,48
```

```
      J=JJ-1
      X(JI+J)=12.*COS(J*.1308997)  $  Y(JI+J)=12.*SIN(J*.1308997)
      Z(JI+J)=Z0
60    CONTINUE
2     JI=I+81
      DO 50 JJ=1,40
      J=JJ-1
      X(JI+J)=10.*COS(J*.1570796)  $  Y(JI+J)=10.*SIN(J*.1570796)
      Z(JI+J)=Z0
50    CONTINUE
3     JI=I+49
      DO 40 JJ=1,32
      J=JJ-1
      X(JI+J)=8.*COS(J*.1963495)  $  Y(JI+J)=8.*SIN(J*.1963495)
      Z(JI+J)=Z0
40    CONTINUE
4     JI=I+25
      DO 30 JJ=1,24
      J=JJ-1
      X(JI+J)=6.*COS(J*.2617994)  $  Y(JI+J)=6.*SIN(J*.2617994)
      Z(JI+J)=Z0
30    CONTINUE
5     JI=I+9
      DO 10 JJ=1,16
      J=JJ-1
      X(JI+J)=4.*COS(J*.3926991)  $  Y(JI+J)=4.*SIN(J*.3926991)
      Z(JI+J)=Z0
10    CONTINUE
6     JI=I+1
      DO 20 JJ=1,8
      J=JJ-1
      X(JI+J)=2.*COS(J*.7853982)  $  Y(JI+J)=2.*SIN(J*.7853982)
      Z(JI+J)=Z0
20    CONTINUE
7     X(I)=Y(I)=0.  $  Z(I)=Z0
      JF=I+N-1
      DO 70 J=I,JF
      X(J)=R0*X(J)  $  Y(J)=R0*Y(J)
70    CONTINUE
      END
```

APPENDIX B

USERS' MANUAL
PROGRAM "BIEM2D"

B.1 INTRODUCTION

The boundary integral equation or "boundary element" method does not represent the continuum by discrete elements as do most numerical methods (e.g., finite elements). In the boundary-element method, the problem configuration is described through the use of boundary elements, linear elements that represent the boundaries of excavations, contours of temperature changes, or contours of pressure changes. The supporting load on boundary elements representing excavations can be described. Ground surface must be described by elements with the supporting load set to zero.

Regions of temperature or pressure change are prescribed by contours. Each of these contours is additive, i.e., if contours are circumscribed, the pressure change in the outer contour also applies to the material within the inner contour.

The number of elements used to describe each boundary surface can affect the accuracy of the results. Smaller elements are needed where the stress field is changing rapidly. The user must experiment with element size until he is satisfied with the accuracy of the results for each particular problem. The exception to this is the temperature- and pressure-change contours. These need only one element for every change in the direction of the boundary surface (e.g., a square contour would need just four elements).

A general discussion of the theory and application of BIEM2D cn be found in the detailed report on BIEM2D, which should be read in conjunction with this users' manual.

B.2 DISCUSSION OF INPUT PARAMETERS

B.2.1 Boundary Segments

In representing a boundary or pressure/temperature change contour of arbitrary shape, the boundary is divided into a number of segments. These segments may be of three types: (a) straight lines, (b) circular arcs, and (c) elliptical arcs. In the following specifications, reference is made to the end points of a segment, which are described as the initial and final points. In deciding which is which, the rule is that when the boundary or contour is traced from the initial to the final point and one faces the direction of travel, the solid material (the outside of the contour) lies on the right-hand side.

Straight-Line Segments (Figure B-1)

XO, ZO = coordinates of initial point
XL, ZL = coordinates of final point

Circular-Arc Segments (Figure B-2)

XC, ZC = coordinates of center of circle
RAD = radius of circle
THET1 = polar angle of initial point
THET2 = polar angle of final point

Line CB is drawn from the center C in the direction of the +Z axis.

The polar angles are measured in a counter-clockwise direction from CB.

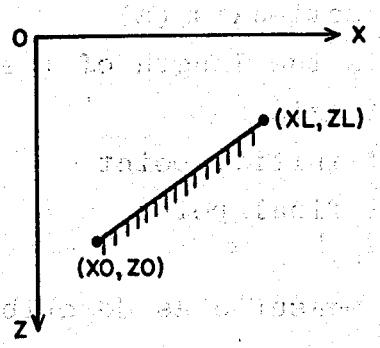

FIGURE B-1
BIEM2D USERS' MANUAL
ILLUSTRATION OF STRAIGHT-LINE ELEMENT

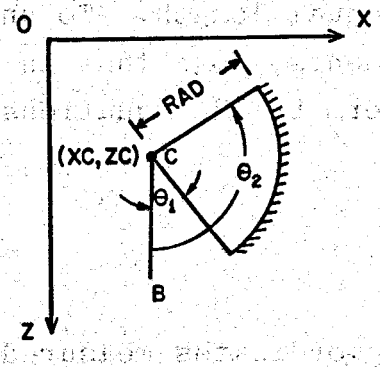

FIGURE B-2
BIEM2D USERS' MANUAL
ILLUSTRATION OF
CIRCULAR-ARC BOUNDARY ELEMENTS

Elliptical Arc Segments (Figure B-3)

XC, ZC = coordinates of center C
SEMIAX = length of one semi-axis (a)
RATIO = b/a, where b is the length of the other semi-axis
PSI = polar angle of axis a
THET1 = polar angle of initial point
THET2 = polar angle of final point

These polar angles are measured as described above.

These segments may be combined to form a boundary of virtually any shape (see Figure B-4).

NSEG = the total number of segments used in defining all the boundary surfaces of the problem.

B.2.2 Elements

Each segment is divided into a number (NELR) of elements. In the case of straight-line and circular segments, the elements are all straight and of equal length. To understand the formation of elliptical segments, note that an ellipse may be represented in parametric form by the equations:

$$m = a \cos \phi$$
$$n = b \sin \phi$$

where m and n represent coordinates measured parallel to the a and b axes of the ellipse. Each element corresponds to the same increment of the angle ϕ. It follows that the length of the

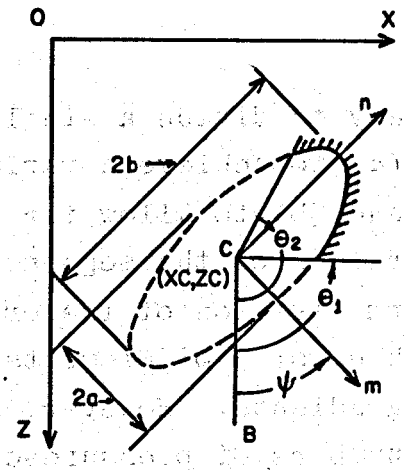

FIGURE B-3
BIEM2D USERS' MANUAL
ILLUSTRATION OF
ELLIPITICAL-ARC BOUNDARY ELEMENT

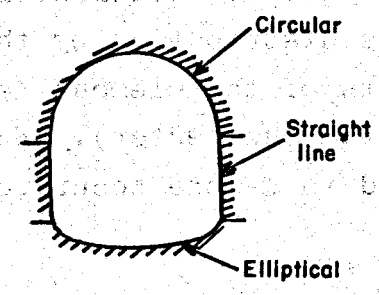

FIGURE B-4
BIEM2D USERS' MANUAL, EXAMPLE OF USE OF
STRAIGHT-LINE, CIRCULAR-ARC,
AND ELLIPITICAL-ARC BOUNDARY ELEMENTS

element varies, since it is small where the radius of curvature is small.

It may be necessary to divide a single segment into a number of separate segments (a) to achieve a variation in length along the original segment and (b) to allow for the application of loads to specified portions of the segment which would not be possible with a uniform division of the original segment. Note that a relatively high density of elements is desirable in regions of high-stress gradients. However, accuracy does not improve with increased numbers of pressure-change elements. Therefore, a pressure change segment need not be subdivided. The elements are numbered progressively from I = 1 to I = MAXJ over all segments. There is currently an upper MAXJ limit of 60 elements.

B.2.3 Gaussian Averaging

Usually, the stress along an element due to a load on another element is approximated by the stress at the center of the element. This can lead to error if the stress distribution along the element is not linear. Gaussian averaging allows the user to approximate the stress distribution by the average of the stress at the two Gauss points of the element (each approximately one-sixth of the length from the center). While this uses more solution time, it may lead to a more accurate solution.

B.2.4 Symmetry

In order to minimize the storage requirements for doubly subscripted variables, advantage should be taken of any symmetry exhibited by the system under investigation. This can be done only if the symmetry refers to both the geometry of all

boundaries and the disposition of all loads. The presence or absence of symmetry is indicated in the program by the values accorded to the codes KXS, KZS. The following rules apply:

- KXS = 0, KZS = 0 indicates that there is no symmetry

- KXS = 1, KZS = 0 indicates symmetry about the X-axis, in which case only the boundaries or parts of the boundaries which lie on the positive side (or, alternatively, the negative side) of the Z-axis are to be specified (see Figure B-5)

- KXS = 0, KZS = 1 indicates symmetry about the Z-axis; only half the system is to be specified

- KXS = 1, KZS = 1 indicates symmetry about both axes; only one quadrant of the system must be specified.

B.2.5 Loading

FPX and FPZ denote the principal field stresses, parallel to the X and Z axes. These can be uniform stresses or can vary with depth, depending on the type of input.

BPX (BPZ) denotes the X (Z) components of load applied to given boundary elements per unit of area projected on to the Z (X) plane. The range of elements over which this load is applied is specified by giving the numbers (LP1, LP2) of the first and last elements of the loaded section.

B.2.6 Pressure Contours

PRESS denotes the normal traction applied at given elements due to changing fluid pressure or material temperature. For

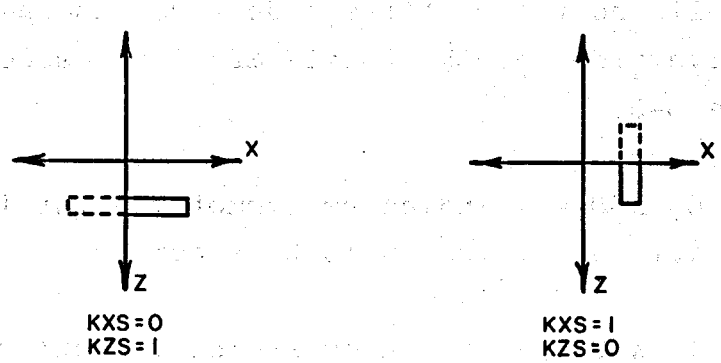

FIGURE B-5
BIEM2D USERS' MANUAL
EXAMPLES OF SYMMETRY CONDITIONS

purposes of calculating stress at interior points, a material number is assigned to the interior region of a temperature or pore-pressure change surface. If pressure-change surfaces are not closed (e.g., hydrostatic fluid pressure), variable NCODE on the segment card should be set to 1. Using NCODE, the pressure change is applied to all materials below the element surface where Z increases with depth. However, the pressure tractions that are applied to the pressure-change surface must still follow the rule that, as you traverse the element from start to finish, the pressure change should occur in the material to the left. Care <u>must</u> be taken when using unclosed pressure change surfaces.

For contours of pore-pressure change, PRESS should equal the pore-pressure drop multiplied by $(1-\frac{K}{K_S})$, where K is the bulk modulus $(K = \frac{E}{3(1-2\nu)})$ and K_S is the bulk modulus of the solid matrix material (note that for soils and soft rocks, $K/Ks \ll 1$, so that PRESS would equal the pore pressure drop). For contours of temperature change, PRESS should equal the temperature drop multiplied by $3K\alpha$ where α is the coefficient of linear thermal expansion.

B.2.7 Cycles

Part of the analytic procedure involves the solution of the matrix equations. This is carried out by a simple iteration and the maximum number of cycles of iteration has to be decided. For most problems, 25 cycles is sufficient, but a greater number may be required where the boundaries are close together. The program will iterate until the maximum error is less than TOL or the maximum number of iterations is reached.

B.2.8 Grid Points

Internal stresses and displacements are determined at the nodes of horizontal and vertical grid lines as specified in the input.

B.3 INPUT

Card 1: Title card (80 characters)

Card 2: ICODE, NSEG, KXS, KZS, NCYC, I, TOL, E, RNU (6I5, 3F10.0)

ICODE = 1 for infinite isotropic medium
= 2 homogeneous gravitational medium where Z = 0 at the ground surface.

NSEG = number of segments

KXS = 1 for symmetry about the X (horizontal) axis (see Symmetry, above)

KZS = 1 for symmetry about the Z (downward) axis (see Symmetry, above)

NCYC = maximum number of iterations (see Cycles above)

I = if $I \neq 0$, Gaussian averaging will be performed

TOL = Tolerance of error (default value = 1×10^{-5})

E = Young's modulus

RNU = Poisson's ratio

Card 3: SIGC, SIGT, M, S (4F10.0)

SIGC = σ_c, uniaxial compressive strength

SIGT = σ_t, uniaxial tensile strength

M, S = empirical constants describing failure criterion (see Hoek and Brown, p. 141)

The stresses are tested against the strength at each observation point and an informative message is printed if the strength is exceeded.

Card 4:

Option 1: ICODE = 1
FPX, FPZ (2F10.0)

FPX = uniform horizontal field stress
FPZ = uniform vertical field stress

Option 2: ICODE = 2
GAMMA, FSR (2F10.0)

GAMMA = unit weight of the material
FSR = field stress ratio, $K = \sigma_x/\sigma_z$

Card 5: (NSEG cards) (see previous note)

Option 1: straight-line segments
PRESS, NELR, XO, ZO, XL, ZL, NCODE, MAT
(F8.0, I2, 4F10.0, 20X, 2I5)

PRESS = fluid (or equivalent temperature) pressure drop on left-hand side of element (= 0 if not on pressure contour) representing discretized fluid or temperature force.

NELR = number of elements into which the segment is divided.

XO, ZO = coordinates of the first point in the segment (so that the "inside" of the element is on the left hand side as you move along the segment). Note: X is positive to the right, Z is positive downward.

XL, ZL = coordinates of last point of segment.

NCODE = code indicating whether boundary material is a closed or open surface (used for pressure change surfaces). NCODE = 0 for closed contours, 1 for open contours.

MAT = material type on "inside" of contour when segment represents a pressure contour. For normal boundary elements, leave MAT = 0. Material types must be consecutively numbered, i.e., materials 1 and 3 cannot be used without defining a material 2.

Option 2: Circular Segments

PRESS, NELR, XC, ZC, THET1, THET2, RADIUS, NCODE, MAT (F8.0, I2, F10.0, 10X, 2I5)

PRESS = as above.
NELR = as above.

XC, ZC = coordinates of circle center.

THET1, THET2 = angles in degrees of initial and final point of segment (measured counter-clockwise from the Z-direction).

RADIUS = circle radius.

NCODE = as above.
MAT = as above.

Option 3: Elliptical Segments

PRESS, NELR, XC, ZC, THET1, THET2, SEMIAX, RATIO, PSI, NCODE, MAT (F8.0, I2, 5F10.0, 2F5.0, 2I5)

PRESS = as above.
NELR = as above.

XC, ZC = coordinates of ellipse center.

THET1, THET2 = as above.

SEMIAX = length of one semi-axis "a."

RATIO = ratio of semi-axes "a/b."
PSI = angle in degrees of semi-axis "a."
NCODE } = as above.
MAT } = as above.

Card 6: LP1, LP2, BPX, BPZ (2I10, 2F10.3)

Note: These cards may not be used when the problem does not contain normal boundary elements.

LP1, LP2 = initial and final element numbers to which loads are applied

BPX, BPZ = components of load per unit of projected area in the X and Z directions. Note that BPX and BPZ are positive when acting into the material.

The last card of the applied loads should be zero. If there are no applied loads but there are normal boundary elements, a blank card is needed.

Card 7: NXP, NZP, XMIN, ZMIN, XMAX, ZMAX (2I5, 4F10.0)

NXP, NZP = number of rows and columns of grid of interior points to have stress and displacement calculated.

XMIN, ZMIN = minimum X and Z coordinates.

XMAX, ZMAX = maximum X and Z coordinates.

The last grid-card should be blank.

RATIO	= ratio of semi-axes "a/b."
PSI	= angle in degrees of semi-axis "a."
NCODE	= as above.
MAT	= as above.

Card 6: LP1, LP2, BPX, BPZ (2I10, 2F10.3)

Note: These cards may not be used when the problem does not contain normal boundary elements.

LP1, LP2	= initial and final element numbers to which loads are applied
BPX, BPZ	= components of load per unit of projected area in the X and Z directions. Note that BPX and BPZ are positive when acting into the material.

The last card of the applied loads should be zero. If there are no applied loads but there are normal boundary elements, a blank card is needed.

Card 7: NXP, NZP, XMIN, ZMIN, XMAX, ZMAX (2I5, 4F10.0)

NXP, NZP	= number of rows and columns of grid of interior points to have stress and displacement calculated.
XMIN, ZMIN	= minimum X and Z coordinates.
XMAX, ZMAX	= maximum X and Z coordinates.

The last grid-card should be blank.

B.4 OUTPUT

1. Echo of input data
2. Boundary stress distribution for "normal" boundary elements, tabulated as follows:

I	CX	CZ	SIG1	SIG3	ALPHA	UX	UZ	FOS	BETA	failure type

where:

I	= element number
CX, CZ	= coordinates of center of element
SIG1, SIG3	= principal stresses at center of element
ALPHA	= angle that SIG1 makes with the normal to the boundary
UX, UZ	= displacements
FOS	= factor of safety against failure

3. Internal stresses, tabulated under the same headings as in (2), but now I, CX, CZ, and ALPHA have different meanings:

I	= grid point number
CX, CZ	= coordinates of grid point
ALPHA	= angle that SIG1 makes with the Z axis
UX, UZ	= displacments
FOS	= factor of safety against failure

B.5 SAMPLE PROBLEM

BIEM2D was used on a sample problem of an infinite reservoir (Figure 1-1). In practice, the model used symmetry about the Z axis and extended the reservoir only to X = 6300 feet. The

elements representing the ground surface were extended to X = 25,000 feet. The following pages present the input and output to this problem.

B.5.1 Input Data for Sample Problem

```
PROBLEM 1 -- 1-D, INFINITE RESERVOIR.  UNITS- FEET,POUNDS
    2    9    0    1   50                    2.16E06       .25
     1000.     -100.       10.        1.
      144.        1.
        4         0.        0.      200.        0.
        3       200.        0.      500.        0.
        3       500.        0.     1100.        0.
        4      1100.        0.     2700.        0.
        5      2700.        0.     6300.        0.
       10      6300.        0.    25000.        0.
 5.04E04 1        0.      620.     6300.      620.                    1    1
 5.04E04 1     6300.      620.     6300.      570.                    1    1
 5.04E04 1     6300.      570.        0.      570.                    1    1
        0
   11   1        0.        0.      750.        0.
   21   1     1000.        0.     6000.        0.
    1  21        0.        0.        0.     1500.
    0
```

B.5.2 Output for Sample Problem

```
1

   * * * * * * * * * * * * * * * * * * *
   * 2-D STRESS ANALYSIS BY THE BOUNDARY ELEMENT METHOD  *
   *  PLANE STRAIN CONDITIONS,  FICTITIOUS STRIP LOADS   *
   *  INCLUDING FLUID PRESSURE AND TEMPERATURE EFFECTS   *
   * * * * * * * * * * * * * * * * * * *

PROBLEM 1 -- 1-D, INFINITE RESERVOIR,  UNITS- FEET,POUNDS

ROCK PROPERTIES:

   MODULUS OF ELASTICITY =   .216E+07

   POISSON'S RATIO =   .250

   BULK MODULUS =   .144E+07

   SHEAR MODULUS =   .864E+06

   COMPRESSIVE STRENGTH  =   .100E+04

   TENSILE STRENGTH =  -100.

   M   =     10.0
   S   =     1.00

THE ANALYSIS IS IN AN HOMOGENOUS GRAVITATIONAL MEDIUM

UNIT WEIGHT OF ROCK =    144.000

HORIZONTAL STRESS RATIO =      1.000

MAXIMUM NUMBER OF ITERATIONS =    50

TOLERANCE = .10000E-05

X - SYMMETRY:   NO

Z - SYMMETRY:  YES

NUMBER OF SEGMENTS =     9
```

ELEMENT DEFINITION DATA

ELEMENTS	PRESS	CENT X (FIRST-X)	CENT Z (FIRST-Z)	THET1 (LAST-X)	THET2 (LAST-Z)	RADIUS	RATIO	PSI	MAT
4	0.	0.	0.	200.	0.				0
3	0.	200.	0.	500.	0.				0
3	0.	500.	0.	.110E+04	0.				0
4	0.	.110E+04	0.	.270E+04	0.				0
5	0.	.270E+04	0.	.630E+04	0.				0
10	0.	.630E+04	0.	.250E+05	0.				0
1	.504E+05	0.	620.	.630E+04	620.				1
1	.504E+05	.630E+04	620.	.630E+04	570.				1
1	.504E+05	.630E+04	570.	0.	570.				1

THE SYSTEM HAS CONVERGED AFTER 15 ITERATIONS

1 NN = 0

STRESSES AND DISPLACEMENTS , AND FAILURE CRITERION AT CENTERS OF BOUNDARY ELEMENTS

*** ALPH IS THE ANGLE FROM THE ELEMENT NORMAL TO THE MAJOR PRINCIPAL STRESS

I	CX	CZ	PRESSURE	SIG1	SIG3	ALPHA	UX	UZ	F.O.S	BETA	
1	25.0	0.	0.	.100E-03	-311.	.215E-06	.3378E-02	-.5863	.318	0.	TENSILE FAILURE
2	75.0	0.	0.	.100E-03	-311.	.283E-06	.1013E-01	-.5863	.318	0.	TENSILE FAILURE
3	125.	0.	0.	.100E-03	-311.	.258E-06	.1689E-01	-.5862	.318	0.	TENSILE FAILURE
4	175.	0.	0.	.100E-03	-311.	.208E-06	.2365E-01	-.5862	.318	0.	TENSILE FAILURE
5	250.	0.	0.	.100E-03	-312.	.107E-06	.3379E-01	-.5861	.318	0.	TENSILE FAILURE
6	350.	0.	0.	.100E-03	-312.	.673E-07	.4733E-01	-.5860	.317	0.	TENSILE FAILURE
7	450.	0.	0.	.100E-03	-313.	.324E-07	.6090E-01	-.5858	.317	0.	TENSILE FAILURE
8	600.	0.	0.	.100E-03	-314.	-.717E-08	.8130E-01	-.5854	.316	0.	TENSILE FAILURE
9	800.	0.	0.	.100E-03	-316.	-.287E-07	.1087	-.5848	.313	0.	TENSILE FAILURE
10	.100E+04	0.	0.	.100E-03	-319.	-.419E-07	.1362	-.5839	.310	0.	TENSILE FAILURE
11	.130E+04	0.	0.	.100E-03	-324.	-.442E-07	.1781	-.5821	.306	0.	TENSILE FAILURE
12	.170E+04	0.	0.	.100E-03	-334.	-.509E-07	.2353	-.5790	.297	0.	TENSILE FAILURE
13	.210E+04	0.	0.	.100E-03	-347.	-.526E-07	.2945	-.5747	.285	0.	TENSILE FAILURE
14	.250E+04	0.	0.	.100E-03	-366.	-.489E-07	.3566	-.5691	.271	0.	TENSILE FAILURE
15	.306E+04	0.	0.	.100E-03	-396.	-.357E-07	.4496	-.5575	.250	0.	TENSILE FAILURE
16	.378E+04	0.	0.	.100E-03	-459.	-.299E-07	.5842	-.5340	.216	0.	TENSILE FAILURE
17	.450E+04	0.	0.	.100E-03	-557.	-.230E-07	.7458	-.4913	.178	0.	TENSILE FAILURE
18	.522E+04	0.	0.	.100E-03	-679.	-.167E-07	.9501	-.4001	.146	0.	TENSILE FAILURE
19	.594E+04	0.	0.	.100E-03	-426.	-.216E-07	1.184	-.1638	.232	0.	TENSILE FAILURE
20	.724E+04	0.	0.	374.	-.180E-07	-90.0	1.049	.4795	2.67	N.A	NO FAILURE
21	.911E+04	0.	0.	262.	-.273E-07	-90.0	.7326	.6548	3.82	N.A	NO FAILURE
22	.110E+05	0.	0.	152.	-.326E-07	-90.0	.5643	.6945	6.56	N.A	NO FAILURE
23	.128E+05	0.	0.	101.	-.347E-07	-90.0	.4620	.7089	9.93	N.A	NO FAILURE
24	.147E+05	0.	0.	72.3	-.340E-07	-90.0	.3920	.7149	13.8	N.A	NO FAILURE
25	.166E+05	0.	0.	54.8	-.310E-07	-90.0	.3405	.7172	18.3	N.A	NO FAILURE
26	.185E+05	0.	0.	43.1	-.261E-07	-90.0	.3008	.7171	23.2	N.A	NO FAILURE
27	.203E+05	0.	0.	34.9	-.195E-07	-90.0	.2691	.7154	28.6	N.A	NO FAILURE
28	.222E+05	0.	0.	28.7	-.974E-08	90.0	.2432	.7119	34.9	N.A	NO FAILURE
29	.241E+05	0.	0.	22.8	0.	90.0	.2220	.7060	43.9	N.A	NO FAILURE

1 NN = 1

STRESSES AND DISPLACEMENTS, AND FAILURE CRITERION AT OBSERVATION POINTS

*** ALPH IS THE ANGLE FROM THE POSITIVE Z-AXIS TO THE MAJOR PRINCIPAL STRESS

I	CX	CZ	PRESSURE	SIG1	SIG3	ALPHA	UX	UZ	F.O.S	BETA	
1	.100E-09	.100E-09	0.	.504	-314.	.511E-02	.1661E-13	-.5863	.316	0.	TENSILE FAILURE
2	75.0	.100E-09	0.	.100E-03	-311.	.283E-06	.1013E-01	-.5863	.318	0.	TENSILE FAILURE
3	150.	.100E-09	0.	.494	-314.	.272E-01	.2027E-01	-.5862	.315	0.	TENSILE FAILURE
4	225.	.100E-09	0.	-.241E-01	-312.	.184E-01	.3041E-01	-.5862	.318	0.	TENSILE FAILURE
5	300.	.100E-09	0.	1.01	-317.	.101	.4056E-01	-.5861	.312	0.	TENSILE FAILURE
6	375.	.100E-09	0.	.708E-01	-312.	-.164E-01	.5072E-01	-.5859	.317	0.	TENSILE FAILURE
7	450.	.100E-09	0.	.100E-03	-313.	.323E-07	.6090E-01	-.5858	.317	0.	TENSILE FAILURE
8	525.	.100E-09	0.	-.181	-313.	.643E-01	.7110E-01	-.5856	.316	0.	TENSILE FAILURE
9	600.	.100E-09	0.	.100E-03	-314.	-.717E-08	.8130E-01	-.5854	.316	0.	TENSILE FAILURE
10	675.	.100E-09	0.	.376	-315.	-.401E-01	.9153E-01	-.5852	.315	0.	TENSILE FAILURE
11	750.	.100E-09	0.	-.208	-316.	.441E-01	.1018	-.5850	.314	0.	TENSILE FAILURE
12	.100E+04	.100E-09	0.	.100E-03	-319.	-.419E-07	.1362	-.5839	.310	0.	TENSILE FAILURE
13	.125E+04	.100E-09	0.	-.387	-323.	.464E-01	.1711	-.5825	.307	0.	TENSILE FAILURE
14	.150E+04	.100E-09	0.	6.33	-341.	1.94	.2065	-.5807	.274	0.	TENSILE FAILURE
15	.175E+04	.100E-09	0.	.606	-335.	-.434E-01	.2426	-.5785	.295	0.	TENSILE FAILURE
16	.200E+04	.100E-09	0.	-1.38	-344.	.151	.2795	-.5760	.287	0.	TENSILE FAILURE
17	.225E+04	.100E-09	0.	2.76	-354.	-.690E-01	.3174	-.5727	.279	0.	TENSILE FAILURE
18	.250E+04	.100E-09	0.	.100E-03	-366.	-.489E-07	.3566	-.5691	.271	0.	TENSILE FAILURE
19	.275E+04	.100E-09	0.	-6.42	-386.	.953	.3975	-.5651	.257	0.	TENSILE FAILURE
20	.300E+04	.100E-09	0.	-1.64	-392.	.130	.4394	-.5592	.252	0.	TENSILE FAILURE
21	.325E+04	.100E-09	0.	6.32	-411.	-.273	.4829	-.5519	.241	0.	TENSILE FAILURE
22	.350E+04	.100E-09	0.	-9.62	-443.	1.34	.5300	-.5455	.223	0.	TENSILE FAILURE
23	.375E+04	.100E-09	0.	-1.37	-456.	.110	.5783	-.5354	.217	0.	TENSILE FAILURE
24	.400E+04	.100E-09	0.	12.8	-491.	-.562	.6296	-.5228	.202	0.	TENSILE FAILURE
25	.425E+04	.100E-09	0.	-14.0	-537.	2.05	.6872	-.5109	.184	0.	TENSILE FAILURE
26	.450E+04	.100E-09	0.	.100E-03	-557.	-.230E-07	.7458	-.4913	.178	0.	TENSILE FAILURE
27	.475E+04	.100E-09	0.	28.0	-632.	-1.42	.8100	-.4664	.157	0.	TENSILE FAILURE
28	.500E+04	.100E-09	0.	-13.6	-677.	3.90	.8865	-.4389	.146	0.	TENSILE FAILURE
29	.525E+04	.100E-09	0.	3.54	-685.	-.578	.9590	-.3939	.144	0.	TENSILE FAILURE
30	.550E+04	.100E-09	0.	60.2	-852.	-5.11	1.040	-.3311	.116	0.	TENSILE FAILURE
31	.575E+04	.100E-09	0.	78.9	-659.	8.27	1.139	-.2448	.150	0.	TENSILE FAILURE
32	.600E+04	.100E-09	0.	-25.0	-358.	-6.56	1.194	-.1342	.277	0.	TENSILE FAILURE
33	.100E-09	.100E-09	0.	.504	-314.	.511E-02	.1661E-13	-.5863	.316	0.	TENSILE FAILURE
34	.100E-09	75.0	0.	.108E+05	.105E+05	.407E-12	.1776E-13	-.5896	1.92	N.A	NO FAILURE
35	.100E-09	150.	0.	.216E+05	.213E+05	.407E-12	.4974E-13	-.5930	1.66	N.A	NO FAILURE
36	.100E-09	225.	0.	.324E+05	.321E+05	.407E-12	.4974E-13	-.5963	1.54	N.A	NO FAILURE
37	.100E-09	300.	0.	.432E+05	.429E+05	.407E-12	.1350E-12	-.5997	1.47	N.A	NO FAILURE
38	.100E-09	375.	0.	.540E+05	.537E+05	.407E-12	.4263E-13	-.6030	1.42	N.A	NO FAILURE
39	.100E-09	450.	0.	.648E+05	.645E+05	.407E-12	-.1421E-13	-.6062	1.39	N.A	NO FAILURE
40	.100E-09	525.	0.	.756E+05	.753E+05	.407E-12	.2842E-13	-.6094	1.36	N.A	NO FAILURE
41	.100E-09	600.	.504E+05	.120E+06	.864E+05	90.0	0.	-.2929E-01	.967	43.0	SHEAR FAILURE
42	.100E-09	675.	0.	.972E+05	.969E+05	.407E-12	-.5684E-13	.3565	1.32	N.A	NO FAILURE
43	.100E-09	750.	0.	.108E+06	.108E+06	-.147E-10	-.1705E-12	.3534	1.30	N.A	NO FAILURE
44	.100E-09	825.	0.	.119E+06	.119E+06	.407E-120.		.3503	1.29	N.A	NO FAILURE
45	.100E-09	900.	0.	.130E+06	.129E+06	.407E-12	.2842E-13	.3473	1.28	N.A	NO FAILURE
46	.100E-09	975.	0.	.140E+06	.140E+06	.407E-120.		.3444	1.26	N.A	NO FAILURE
47	.100E-09	.105E+04	0.	.151E+06	.151E+06	-.122E-11	-.1705E-12	.3415	1.26	N.A	NO FAILURE
48	.100E-09	.113E+04	0.	.162E+06	.162E+06	.204E-11	.5684E-13	.3387	1.25	N.A	NO FAILURE
49	.100E-09	.120E+04	0.	.173E+06	.173E+06	.204E-11	.5684E-13	.3359	1.24	N.A	NO FAILURE
50	.100E-09	.128E+04	0.	.184E+06	.183E+06	.407E-12	-.3411E-12	.3332	1.23	N.A	NO FAILURE
51	.100E-09	.135E+04	0.	.194E+06	.194E+06	.244E-11	.5684E-13	.3306	1.23	N.A	NO FAILURE
52	.100E-09	.143E+04	0.	.205E+06	.205E+06	-.163E-11	.4547E-12	.3281	1.22	N.A	NO FAILURE
53	.100E-09	.150E+04	0.	.216E+06	.216E+06	-.814E-11	.5684E-12	.3256	1.21	N.A	NO FAILURE

B.6 SOURCE LISTING FOR BIEM2D

```
      PROGRAM BIEM2D(INPUT,OUTPUT,TAPE1=INPUT,TAPE7=OUTPUT)
C
C     ****************************************************************
C     BOUNDARY ELEMENT PROGRAM FOR TWO-DIMENSIONAL STRESS ANALYSIS
C     IN HOMOGENEOUS ISOTROPIC MEDIA   -   J W BRAY 1974
C     STRAIGHT BOUNDARY ELEMENTS WITH STRIP FICTITIOUS LOADS
C     UPDATED AUGUST-1976 TO CALCULATE DISPLACEMENTS   -   G HOCKING
C     UPDATED OCT.-1978 FOR GRAVITATIONAL ANALYSIS AND FAILURE
C     CRITERION   - E A EISSA . IMPERIAL COLLEGE  LONDON
C     UPDATED JULY,1979 FOR PRESSURE CONTOUR ANALYSIS - GOLDER ASSOC.
C     ****************************************************************
C
      DIMENSION CX(60),CZ(60),EX1(60),EX2(60),EZ1(60),EZ2(60),PN(60),
     1 PNM(60),QM(60),QN(60),BMM(60,60),BMN(60,60),BNM(60,60),
     2 BNN(60,60),DM(60,60),DN(60,60),SIG1(60),SIG3(60),
     3 ALPHA(60),SINB(60),COSB(60),UX(60),UZ(60),FOS(60),BETA(60),
     4 FPX(60),FPZ(60),TITLE(20),LPTS(30),XLIN(60,30),ZLIN(60,30),
     5 PR(30),PRESM(60),PRESN(60),PRES(60),PRSS(60),CXN(2),CZN(2)
     6 ,SDAT(2)
      LOGICAL GAUSS,DEBUG,DEBUG1
      DATA SDAT/' NO','YES'/
C
C     READING AND PRINTING OF INPUT DATA
C
      WRITE(7,12)
12    FORMAT('1',///
     .10X,'*  *  *  *  *  *  *  *  *  *  *  *  *  *  *  *  *  *  *'/
     .10X,'* 2-D STRESS ANALYSIS BY THE BOUNDARY ELEMENT METHOD  *'/
     .10X,'*  PLANE STRAIN CONDITIONS,  FICTITIOUS STRIP LOADS   *'/
     .10X,'*  INCLUDING FLUID PRESSURE AND TEMPERATURE EFFECTS   *'/
     .10X,'*  *  *  *  *  *  *  *  *  *  *  *  *  *  *  *  *  *  *'///)
      READ(1,10) (TITLE(I),I=1,20)
   10 FORMAT(20A4)
      WRITE(7,9) (TITLE(I),I=1,20)
9     FORMAT(7X,20A4///)
      DEBUG=.FALSE.
      DEBUG1=.FALSE.
      READ(1,11) ICODE,NSEG,KXS,KZS,NCYC,I,TOL,E,RNU,J,K
   11 FORMAT(6(2X,I3),3F10.3,18X,2I1)
      GAUSS=.FALSE.
      IF(J.NE.0)  DEBUG=.TRUE.
      IF(K.NE.0) DEBUG1=.TRUE.
      IF(I.NE.0)GAUSS=.TRUE.
      IF(ICODE.GE.1.AND.ICODE.LE.2) GO TO 319
      WRITE(7,318)
  318 FORMAT(1H ///,7X,'*** ERROR -CODE OF PROBLEM TYPE IS WRONG')
      GO TO 503
  319 CONTINUE
      READ(1,35) SIGC,SIGT,RM,S
   35 FORMAT(4F10.5)
      BMOD=E/(3.*(1.-2.*RNU))
      SMOD=E/(2.*(1.+RNU))
      WRITE(7,36)  E,RNU,BMOD,SMOD,SIGC,SIGT,RM,S
36    FORMAT(7X,'ROCK PROPERTIES:',//10X,'MODULUS OF ELASTICITY = ',G1
     *0.3,//10X,'POISSON'S RATIO = ',G10.3,//10X,'BULK MODULUS = ',
     *G10.3,//10X,'SHEAR MODULUS = ', G10.3,//10X,'COMPRESSIVE STRENGTH
     * = ',G10.3,//10X,'TENSILE STRENGTH = ',G10.3,//10X,'M    =    ',
     *G10.3,/10X,'S    =    ',G10.3//)
      IF(ICODE.EQ.2) GO TO 322
  320 WRITE(7,321)
  321 FORMAT(1H //,6X,' THE ANALYSIS IS IN AN INFINITE ISOTROPIC MEDI'.
     1'UM')
```

```
      READ(1,21) FPXX,FPZZ
   21 FORMAT(2F10.3)
      WRITE(7,22) FPXX,FPZZ
   22 FORMAT(1H /,7X,'HORIZONTAL FIELD STRESS = ',F10.3,//
     *7X,'VERTICAL FIELD STRESS = ',F10.3)
      GO TO 336
  322 WRITE(7,323)
  323 FORMAT(1H //,6X,' THE ANALYSIS IS IN AN HOMOGENOUS GRAVITATIONAL '
     *,'MEDIUM'  )
      READ(1,324)GAMMA,FSR
  324 FORMAT(2F10.3)
      WRITE(7,325) GAMMA,FSR
  325 FORMAT(1H /,7X,'UNIT WEIGHT OF ROCK = ',F10.3,//
     *7X,'HORIZONTAL STRESS RATIO = ',F10.3)
  336 CONTINUE
      IF(TOL.EQ.0.)  TOL=.000001
      WRITE (7,13) NCYC,TOL,SDAT(KXS+1),SDAT(KZS+1),NSEG
 13   FORMAT(///7X,'MAXIMUM NUMBER OF ITERATIONS = '
     *,I5,//7X,'TOLERANCE = ',G10.5,//7X,'X - SYM',
     *'METRY:  ',A3,//7X,'Z - SYMMETRY:  ',A3,//
     *7X,'NUMBER OF SEGMENTS = ',I5/)
      IF(GAUSS)WRITE(7,23)
 23   FORMAT(7X,'GAUSSIAN AVERAGING WILL BE PERFORMED')
      IF(ABS(SIGT).GE.ABS(SIGC)) WRITE 24
 24   FORMAT(//,7X'**** ERROR - MAGNITUDE OF TENSILE STRENGTH '
     *,'EXCEEDS COMPRESSIVE STRENGTH')
      NN = 0
      PI = ATAN(1.0) * 4.0
      TA = 2.0*(1.0 - RNU)
      TJ = 1.0/(2.0*PI*TA)
      TU=3.0-4.0*RNU
      G=E/(2.0*(1.0+RNU))
      TV=0.5*TJ/G
      DATA QN,QM/120*0.0/
      DATA LPTS/30*0/
      MAT=0
      MAXI=0
      NMAT=0
C
C     INTERPRETATION OF SYMMETRY CODE
C
      KAS = 0
      IF(KZS.EQ.-1) KAS=1
      KXT = 2*KXS + 1
      KZT = 2*(KZS + KAS) + 1
C
C     DIVISISON OF BOUNDARY INTO SEGMENTS
C
      I = 0
      NSEGG = 0
      WRITE(7,16)
 16   FORMAT(///5X,'ELEMENT DEFINITION DATA'//
     *  '      ELEMENTS PRESS      CENT X     CENT Z      THET1      THET2',
     *  '      RADIUS    RATIO      PSI       MAT'/
     *  '                          (FIRST-X) (FIRST-Z)  (LAST-X)  (LAST-Z)
     *'/)
C
  700 IF(NSEGG.EQ.NSEG) GO TO 50
      NSEGG = NSEGG + 1
      NELG = 0
      RELG = NELG
      READ(1,17)PRESS, NELR,XO,ZO,XL,ZL,RDS,RATIO,PSI,NCODE,MAT
   17 FORMAT(G8.2,I2,5G10.3,2G5.1,2I5)
      NMAT=MAXO(MAT,NMAT)
      IF(PRESS.EQ.0..AND.MAX1.NE.I) WRITE 326
      IF(PRESS.EQ.0.)MAXI=MAXI+NELR
```

```
  326 FORMAT(1X,'***  ERROR - ZERO PRESSURE
     *NODES ARE NOT BEING INPUT FIRST'//)
      RELR = NELR
      IF(RDS.EQ.0.0) GO TO 800
C
C     DIVISION OF ELLIPTICAL OR CIRCULAR SEGMENTS INTO ELEMENTS
C
      IF(RATIO.EQ.0.0) RATIO = 1.0
      WRITE(7,18) NELR,PRESS,XO,ZO,XL,ZL,RDS,RATIO,PSI,MAT
   18 FORMAT(1H ,6X,I3,8(1X,G9.3),I7)
      SINPSI = SIN(PSI*PI/180.)
      COSPSI = COS(PSI*PI/180.)
      GD = .1E-10
      GA = RATIO*COS((XL-PSI)*PI/180.)
      IF(ABS(GA).LT.GD) GA=GD
      GB=RATIO*COS((ZL-PSI)*PI/180.)
      IF(ABS(GB).LT.GD) GB=GD
      CHI1=ATAN2(SIN((XL-PSI)*PI/180.),GA)
      CHI2 = ATAN2(SIN((ZL-PSI)*PI/180.),GB)
      DCHI = (CHI2 - CHI1)/RELR
      IF(ABS(DCHI).LT.GD) GO TO 606
      GC = DCHI/ABS(DCHI)
      GO TO 605
  606 GC=-1.0*(ZL-XL)/ABS(ZL-XL)
  605 DCHI = DCHI + ((ZL-XL)/ABS(ZL-XL)-GC)*PI/RELR
  600 I = I + 1
      CHI = CHI1 + RELG*DCHI
      EX1(I) = RDS*(COS(CHI)*SINPSI+SIN(CHI)*COSPSI*RATIO)+XO
      EZ1(I) = RDS*(COS(CHI)*COSPSI - SIN(CHI)*SINPSI*RATIO) + ZO
      CHI = CHI + DCHI
      EX2(I) = RDS*(COS(CHI)*SINPSI + SIN(CHI)*COSPSI*RATIO) + XO
      EZ2(I) = RDS*(COS(CHI)*COSPSI - SIN(CHI)*SINPSI*RATIO) + ZO
      CX(I) = 0.5*(EX1(I) + EX2(I))
      CZ(I) = 0.5*(EZ1(I) + EZ2(I))
      DX = EX2(I) - EX1(I)
      DZ = EZ2(I) - EZ1(I)
      IF(ABS(DX).LT.(.1E-13)*RDS) DX = 0.0
      IF(ABS(DZ).LT.(.1E-13)*RDS) DZ = 0.0
      DS = SQRT(DX*DX + DZ*DZ)
      SINB(I) = -DZ/DS
      COSB(I) = DX/DS
      NELG = NELG + 1
      RELG = NELG
      PRES(I)=PRESS
      IF(PRESS.EQ.0.) GO TO 42
      LPTS(MAT)=LPTS(MAT)+1
      IC=LPTS(MAT)
      XLIN(IC,MAT)=EX1(I)
      ZLIN(IC,MAT)=EZ1(I)
   42 CONTINUE
      IF(NELG.LT.NELR) GO TO 600
      IF(PRESS.EQ.0.) GO TO 700
      IC=IC+1
      XLIN(IC,MAT)=EX2(I)
      ZLIN(IC,MAT)=EZ2(I)
      IF(NCODE.EQ.1) GO TO 43
      XLIN(IC+1,MAT)=XLIN(1,MAT)
      ZLIN(IC+1,MAT)=ZLIN(1,MAT)
      GO TO 44
43    XLIN(IC+1,MAT)=XLIN(IC,MAT)
      ZLIN(IC+1,MAT)=ZLIN(IC,MAT)
44    PR(MAT)=PRESS
      GO TO 700
```

```
C
C     DIVISION OF STRAIGHT LINE SEGMENTS INTO ELEMENTS
C
800   CONTINUE
      WRITE(7,15) NELR,PRESS,XO,ZO,XL,ZL,MAT
   15 FORMAT(1H ,6X,I3,5(1X,G9.3),30X,I7)
      DX = (XL-XO)/RELR
      DZ = (ZL-ZO)/RELR
      DS = SQRT(DX*DX+DZ*DZ)
  900 I = I + 1
      SINB(I) = -DZ/DS
      COSB(I) = DX/DS
      EX1(I) = XO + RELG*DX
      EZ1(I) = ZO + RELG*DZ
      CX(I) = EX1(I) + 0.5*DX
      CZ(I) = EZ1(I) + 0.5*DZ
      EX2(I) = EX1(I) + DX
      EZ2(I) = EZ1(I) + DZ
      PRES(I)=PRESS
      IF(PRESS.EQ.0.) GO TO 49
      LPTS(MAT)=LPTS(MAT)+1
      IC=LPTS(MAT)
      XLIN(IC,MAT)=EX1(I)
      ZLIN(IC,MAT)=EZ1(I)
   49 CONTINUE
      NELG = NELG + 1
      RELG = NELG
      IF(NELG.LT.NELR) GO TO 900
      IF(PRESS.EQ.0.) GO TO 700
      IC=IC+1
      XLIN(IC,MAT)=EX2(I)
      ZLIN(IC,MAT)=EZ2(I)
      IF(NCODE.EQ.1) GO TO 45
      XLIN(IC+1,MAT)=XLIN(1,MAT)
      ZLIN(IC+1,MAT)=ZLIN(1,MAT)
      GO TO 46
45    XLIN(IC+1,MAT)=XLIN(IC,MAT)
      ZLIN(IC+1,MAT)=ZLIN(IC,MAT)
46    PR(MAT)=PRESS
      GO TO 700
  50  MAXJ = I
      IF(I.GT.60) WRITE 53
53    FORMAT(//5X,'*** ERROR - NUMBER OF ELEMENTS EXCEEDS',
     *' DIMENSION OF ARRAYS')
C
      DO 52 II=1,NMAT
 52   LPTS(II)=LPTS(II)+1
      IF(NCODE.EQ.1)  GO TO 51
      IF(KXS+KZS.LT.2)  GO TO 51
      DO 47 II=1,NMAT
      IC=LPTS(II)
      ICM=IC-1
      A1=(XLIN(1,II)-XLIN(2,II))**2+(ZLIN(1,II)-ZLIN(2,II))**2
      A2=(XLIN(IC,II)-XLIN(ICM,II))**2+(ZLIN(IC,II)-ZLIN(ICM,II))**2
      IF(XLIN(1,II)/A1.LT..00001.AND.ZLIN(IC,II)/A2.LT..00001)GO TO 48
      IF(ZLIN(1,II)/A1.GE..00001.OR.XLIN(IC,II)/A2.GE..00001) GO TO 47
48    LPTS(II)=LPTS(II)+1
      IC=IC+1
      XLIN(IC+1,II)=XLIN(IC,II)
      ZLIN(IC+1,II)=ZLIN(IC,II)
      XLIN(IC,II)=0.0
      ZLIN(IC,II)=0.0
47    CONTINUE
51    IF(MAXI.EQ.0)  GO TO 932
```

```
C
C     DETERMINATION OF COEFFICIENTS IN EXPRESSIONS FOR STRESSES
C     INDUCED BY FICTITIOUS LOADS
C
C     THESE COEFFICIENTS, WHEN MULTIPLIED BY THE TRACTIONS, GIVE
C     TWICE THE STRESS CHANGE.
C     DM= 2 * SHEAR STRESS (I) DUE TO SHEAR TRACTION (J)
C     BNM= 2 * NORMAL STRESS (I) DUE TO SHEAR TRACTION (J)
C     DN= 2 * SHEAR STRESS (I) DUE TO NORMAL TRACTION (J)
C     BNN= 2 * NORMAL STRESS (I) DUE TO NORMAL TRACTION (J)
C
C     BMN= 2 * DIRECT STRESS, PARALLEL TO THE ELEMENT, DUE TO SHEAR
C         TRACTION (J)
C     BMM= 2* DIRECT STRESS, PARALLEL TO THE ELEMENT, DUE TO NORMAL
C         TRACTION (J)
C
C
C
105   DO 101 I = 1,MAXI
      CXN(1) = CX(I)
      CZN(1) = CZ(I)
      IF(NN.GT.0) GO TO 104
      COS2BI = 2.0 * (COSB(I))**2 - 1.0
      SIN2BI = 2.0 * SINB(I) * COSB(I)
      IF(.NOT.GAUSS)  GO TO 104
      FAC=-1.0
      DO 990 IGP=1,2
      CXN(IGP)=CX(I)+.288675*(EX2(I)-EX1(I))*FAC
      CZN(IGP)=CZ(I)+.288675*(EZ2(I)-EZ1(I))*FAC
990   FAC=FAC+2.0
  104 DO 118 J = 1,MAXJ
      BMM(I,J)=0.
      BMN(I,J)=0.
      BNM(I,J)=0.
      BNN(I,J)=0.
      DM(I,J)=0.
      DN(I,J)=0.
      DO 991 IGP=1,2
      TK = 0.0
      TL = 0.0
      TM = 0.0
      TN = 0.0
      TO = 0.0
      TP = 0.0
      DO 102  KXU = 1,KXT,2
      KX = 2- KXU
      RX = KX
      DO 102 KZU=1,KZT,2
      KZ = (2-KZU)*(1-KAS)+KAS*KX
      RZ = KZ
      COSBJ = RX*COSB(J)
      SINBJ = RZ*SINB(J)
      EX1J = RZ*EX1(J)
      EX2J = RZ*EX2(J)
      EZ1J = RX*EZ1(J)
      EZ2J = RX*EZ2(J)
      LL = KX+KZ-2+10*(I-J)+1000*NN
      IF(LL.EQ.0) GO TO 135
C
C     RN=LOCAL Z ,RM1=LOCAL X1,  RM2=LOCAL X2, RSQ1= RADIUS 1,
C     RSQ2= RADIUS 2.
C
      RN = (CZN(IGP) - EZ1J)*COSBJ + (CXN(IGP) - EX1J)*SINBJ
      RM1 = (CXN(IGP) - EX1J)*COSBJ - (CZN(IGP) - EZ1J)*SINBJ
      RM2 = (CXN(IGP) -EX2J)*COSBJ - (CZN(IGP) - EZ2J)*SINBJ
      IF(RN.NE.0.)  GO TO 1352
      IF(RM1.EQ.0.)   GO TO 1353
       IF(RM2.NE.0.)  GO TO 1352
      RM2=-.0001*RM1*RX*RZ
      RM1=(1.0+RZ*RX*.0001)*RM1
      GO TO 1352
```

```
1353  RM1=0.0001*RM2*RZ*RX
      RM2=(1.0-RZ*RX*.0001)*RM2
1352  RSQ1 = RM1*RM1 + RN*RN
      RSQ2 = RM2*RM2 + RN*RN
      TB=RN*RN+RM1*RM2
      IF(DEBUG1) WRITE 140,I,J,RN,RM1,RM2,EZ1J,EX1J,
     *EZ2J,EX2J,TB
140   FORMAT(1X,2I5,1P8E12.4)
      IF((TB).NE.0.0)  GO TO 138
      TB=SIGN(PI,(RM1-RM2)*RN)
      GO TO 139
138   TB = 2.0*ATAN2((RM1 - RM2)*RN,(TB))
139   TC = 2.0 *RN * (RM1/RSQ1 - RM2/RSQ2)
      TD = (RN**2 - RM1**2)/RSQ1 - (RN**2 - RM2**2)/RSQ2
      TE = ALOG(RSQ1/RSQ2)
      COS2F = 2.0*(COS2BI*(COSBJ**2 - 0.5) + SIN2BI*SINBJ*COSBJ)
      SIN2F = 2.0*(SIN2BI*(COSBJ**2 - 0.5) - COS2BI*SINBJ*COSBJ)
      GO TO 137
  135 TB = 2.0*PI
1351  TC = 0.0
      TD = 0.0
      TE = 0.0
      COS2F = 1.0
      SIN2F = 0.0
  137 CONTINUE
      TK = TK + TB*RX*RZ
      TL = TL + TE
      TM = TM + (TD + TA*TE)*COS2F + (TC - TA*TB)*SIN2F
      TN = TN + (((1.0-TA)*TB-TC)*COS2F + (TD+(1.0-TA)*TE)*SIN2F)*RX*RZ
      TO = TO+(TD+TA*TE)*SIN2F-(TC-TA*TB)*COS2F
      TP = TP + (((1.0-TA)*TB-TC)*SIN2F - (TD+(1.0-TA)*TE)*COS2F)*RX*RZ
  102 CONTINUE
      BMM(I,J) = BMM(I,J)+(TL + TM) * TJ
      BMN(I,J) = BMN(I,J)+(TK + TN) * TJ
      BNM(I,J) = BNM(I,J)+(TL - TM) *TJ
      BNN(I,J) = BNN(I,J)+(TK -TN) * TJ
      DM(I,J) = DM(I,J)+TO *TJ
      DN(I,J) = DN(I,J)+TP *TJ
      IF(.NOT.GAUSS)  GO TO 118
  991 CONTINUE
      BMM(I,J)=BMM(I,J)/2.
      BMN(I,J)=BMN(I,J)/2.
      BNM(I,J)=BNM(I,J)/2.
      BNN(I,J)=BNN(I,J)/2.
      DM(I,J)=DM(I,J)/2.
      DN(I,J)=DN(I,J)/2.
  118 CONTINUE
      IF(.NOT.DEBUG1) GO TO 101
      WRITE 98,I,(BMM(I,J),J=1,10)
      WRITE 98,I,(BMN(I,J),J=1,10)
      WRITE 98,I,(BNM(I,J),J=1,10)
      WRITE 98,I,(BNN(I,J),J=1,10)
      WRITE 98,I,(DM(I,J),J=1,10)
      WRITE 98,I,(DN(I,J),J=1,10)
98    FORMAT(1X,I5,1P10E12.4,)
  101 CONTINUE
      M = 0
C
C
      IF(DEBUG) WRITE 112,(I,LPTS(I),PR(I),(XLIN(J,I),ZLIN(J,I),J=1,
     *5),I=1,30)
112   FORMAT(//5X,'MATERIAL ZONE DEFINITIONS',/5X,2I5,11G10.4)
```

```
C
C     DETERMINATION OF PRESSURE DIFFERENCE
      DO 435 I=1,MAXI
      CALL SZONE(CX(I),CZ(I),PRESS,XLIN,ZLIN,LPTS,PR)
  435 PRSS(I)=PRESS
C
      IF(DEBUG) WRITE 113,(PRSS(I),I=1,MAXI)
113    FORMAT(//5X,'PRESSURE OF BOUNDARY ELEMENT OR INTER',
     *'IOR POINT',/5X,10G10.3)
C
C
C     DETERMINATION OF BOUNDARY TRACTIONS EQUIVALENT TO FIELD STRESSES
C     ADD THE CHANGE IN PRESSURE TO THE FIELD STRESS
C
      DO 100 I = 1,MAXI
      IF(ICODE.EQ.1) GO TO 328
      FPZ(I) = GAMMA*CZ(I)+PRSS(I)
      FPX(I) = FSR*(FPZ(I)-PRSS(I))+PRSS(I)
      GO TO 329
  328 FPZ(I) = FPZZ+PRSS(I)
      FPX(I) = FPXX+PRSS(I)
329   IF(NN.GT.0) GO TO 100
      PN(I) = 2.0*((FPZ(I))*(COSB(I))**2 + (FPX(I))
     **(SINB(I))**2)
      PNM(I) = 2.0*(FPX(I) -FPZ(I))*SINB(I)*COSB(I)
      QM(I) = PNM(I)
      QN(I) = PN(I)
  100 CONTINUE
      IF(NN.GT.0)  GO TO 108
C
C     ADDITION OF BOUNDARY TRACTIONS DUE TO BOUNDARY LOADS
C
  106 READ(1,19) LP1,LP2,BPX,BPZ
   19 FORMAT(5X,I5,5X,I5,2F10.0)
      IF(LP1.EQ.0) GO TO 404
      WRITE(7,20) LP1,LP2,BPX,BPZ
20    FORMAT(///7X,'ELEMENTS',I5,' TO',I5,' HAVE HORIZONTAL APPLIED TRA'
     *,'CTIONS OF',F10.3,' AND APPLIED VERTICAL TRACTIONS OF',F10.3///)
      DO 107 I = LP1,LP2
      PN(I) = PN(I)-2.0*((BPX-BPZ)*(SINB(I))**2+BPZ)
      PNM(I) = PNM(I) - 2.*(BPX-BPZ)*SINB(I)*COSB(I)
  107 CONTINUE
      GO TO 106
C
C     ADDITION OF EFFECT OF TRACTIONS FROM THE PRESSURE CONTOUR
C
404   IF(MAXI.EQ.MAXJ)  GO TO 400
      MM=MAXI+1
      DO 111 I=1,MAXI
      PRESM(I)=0.
      PRESN(I)=0.
      DO 110 J=MM,MAXJ
      PRESM(I)=DN(I,J)*PRES(J)+PRESM(I)
  110 PRESN(I)=BNN(I,J)*PRES(J)+PRESN(I)
      IF(DEBUG) WRITE 109,I,PRESN(I),PRESM(I)
  109 FORMAT(1X,I5,'  NORMAL STRESS = ',G10.3,'  SHEAR STRESS = ',G10.3)
      PNM(I)=PNM(I)+PRESM(I)
  111  PN(I)=PN(I)+PRESN(I)
C
C
C     DETERMINATION OF FICTITIOUS LOADS
C
      TOL1=0.
  400 DO 401 I = 1,MAXI
      QMI = PNM(I)
      QNI = PN(I)
      DO 402 J = 1,MAXI
      IF(I.EQ.J) GO TO 402
      QMI = QMI - DM(I,J)*QM(J) - DN(I,J)*(QN(J))
      QNI = QNI - BNM(I,J)*QM(J) -BNN(I,J)*(QN(J))
  402 CONTINUE
```

```
C     EQUATION 1: DM * QM1 + DN * QN1 = QMI
C     EQUATION 2: BNM * QM1 + BNN * QN1 = QNI
C     SOLVE THE TWO EQUATIONS FOR THE FICTITIOUS TRACTIONS
C          WHICH ARE TWICE THE APPLIED STRESS
C     QM1 AND QN1 ARE THE FICTITIOUS TRACTIONS
      DENOM = BNN(I,I)*DM(I,I) - DN(I,I)*BNM(I,I)
      QM1 = (QMI*BNN(I,I) - QNI*DN(I,I))/DENOM
      QN1 = (QNI*DM(I,I) - QMI*BNM(I,I))/DENOM
      TOLM=ABS(QM(I)-QM1)
      TOLN=ABS(QN(I)-QN1)
      QM(I)=QM1
      QN(I)=QN1
      TOL1=AMAX1(TOLN,TOLM)
  401 CONTINUE
      M = M + 1
      IF((TOL1.GT.TOL).AND.M.LT.NCYC) GO TO 400
      IF(TOL1.GT.TOL)WRITE 980,TOL1
 980  FORMAT(///7X,'THE SYSTEM DID NOT CONVERGE:  MAXIMUM '
     *'ERROR IS ',G10.4//)
      IF(TOL1.LE.TOL) WRITE 981,M
981   FORMAT(///7X,'THE SYSTEM HAS CONVERGED AFTER',I5,' ITERATIONS'//)
C
C     DETERMINATION OF STRESS COMPONENTS, PRINCIPAL STRESSES
C     AND DIRECTIONS
C
  108 DO 500 I = 1,MAXI
      SMI = 2.0*(FPX(I))
      SNI = 2.0*(FPZ(I))
      SNMI = 0.0
      IF(NN.GT.0) GO TO 405
      SMI = 2.0*((FPX(I) - FPZ(I))*(COSB(I))**2 + FPZ(I))
      SNI = 2.0*((FPX(I) - FPZ(I))*(SINB(I))**2 + FPZ(I))
      SNMI = 2.0*(FPX(I) - FPZ(I))*SINB(I)*COSB(I)
  405 DO 501 J = 1,MAXJ
C      ADD EFFECTS OF FICTITIOUS LOADS AND PRESSURE TRACTIONS
      SNI = SNI - BNM(I,J)*QM(J) - BNN(I,J)*(QN(J)-PRES(J))
      SMI = SMI-BMM(I,J)*QM(J)-BMN(I,J)*(QN(J)-PRES(J))
      SNMI = SNMI - DM(I,J)*QM(J) - DN(I,J) *(QN(J)-PRES(J))
  501 CONTINUE
      SDI = 0.5*(SMI-SNI)
      TAUMAX = 0.5*SQRT(SDI**2 + SNMI**2)
      SIG1(I) = 0.25*(SMI+SNI) + TAUMAX
      SIG3(I) = 0.25*(SMI+SNI) - TAUMAX
      TR = 2.0*TAUMAX + SNMI - SDI
      IF(TR.EQ.0.0) TR = 0.00001
      ALPHA (I) = (180./PI)*ATAN(1.0 + 2.*SDI/TR)
  500 CONTINUE
C
C     DETERMINATION OF INDUCED DISPLACEMENTS
C
      DO 601 I=1,MAXI
      CXI=CX(I)
      CZI=CZ(I)
      UXX=0.0
      UZZ=0.0
      DO 602 J=1,MAXJ
      DO 603 KXU=1,KXT,2
      KX=2-KXU
      RX = KX
      DO 603 KZU=1,KZT,2
      KZ=(2-KZU)*(1-KAS)+KAS*KX
      RZ = KZ
      COSBJ = RX*COSB(J)
      SINBJ = RZ*SINB(J)
```

```
      EX1J = RZ*EX1(J)
      EX2J = RZ*EX2(J)
      EZ1J = RX*EZ1(J)
      EZ2J = RX*EZ2(J)
      RN = (CZI-EZ1J)*COSBJ+(CXI-EX1J)*SINBJ
      LL=KX+KZ-2+10*(I-J)+1000*NN
      IF(LL.EQ.0) RN = 0.0001
      IF(ABS(RN).LT.0.0001)  RN=0.0001
      RM1 = (CXI - EX1J)*COSBJ - (CZI - EZ1J)*SINBJ
      RM2 = (CXI - EX2J)*COSBJ - (CZI - EZ2J)*SINBJ
      RSQ1 = SQRT(RM1*RM1 + RN*RN)
      RSQ2 = SQRT(RM2*RM2 + RN*RN)
      RNO = -EZ1J*COSBJ - EX1J*SINBJ
      IF(ABS(RNO).LT.0.0001) RNO = 0.0001
      RM10 = EX1J*COSBJ - EZ1J*SINBJ
      RM20 = EX2J*COSBJ - EZ2J*SINBJ
      RSQ10 = SQRT(RM10*RM10 + RNO*RNO)
      RSQ20 = SQRT(RM20*RM20 + RNO*RNO)
      IF(RSQ10.LT.0.001) RSQ10 = 0.001
      IF(RSQ20.LT.0.001) RSQ20 = 0.001
      IF(ABS(RNO).LT.0.0001.AND.RSQ20.LT.0.001) RSQ20 = 0.001
      TS = RNO*ALOG(RSQ20/RSQ10)-RN*ALOG(RSQ2/RSQ1)
      TR = RNO*ATAN2((RM20 - RM10)*RNO,(RNO*RNO + RM10*RM20))
     1 - RN*ATAN2((RM2 - RM1)*RN,(RN*RN + RM1*RM2))
      TT = TU*(RM20*ALOG(RSQ20) - RM10*ALOG(RSQ10) - RM2*ALOG(RSQ2)
     .   +RM1*ALOG(RSQ1)-RM20+RM10+RM2-RM1+TR)
      UM = TV*(TS*(QN(J)-PRES(J))*RX*RZ - (TT+TR)*QM(J))
      UN = TV*(TS*QM(J) - (TT+RM20-RM10-RM2+RM1-TR)*RX*RZ*(QN(J)-
     *PRES(J)))
      UXX = UXX-UM*COSBJ-UN*SINBJ
      UZZ = UZZ + UM*SINBJ - UN*COSBJ
  603 CONTINUE
  602 CONTINUE
      UX(I) = UXX
      UZ(I) = UZZ
  601 CONTINUE
      WRITE(7,119) NN
119   FORMAT('1',5X,'NN =',I3)
      IF(SIGC.EQ.0.0) GO TO 420
      IF(NN.GT.0) GO TO 611
      WRITE(7,612)
  612 FORMAT(1H ///,4X,82HSTRESSES AND DISPLACEMENTS , AND FAILURE CRITE
     1RION AT CENTERS OF BOUNDARY ELEMENTS)
      WRITE (7,316)
  316 FORMAT(/7X,'*** ALPH IS THE ANGLE FROM THE ELEMENT NORMAL TO THE MAJO
     *AJOR PRINCIPAL STRESS')
      GO TO 613
  611 WRITE(7,614)
  614 FORMAT(1H ///,4X,'STRESSES AND DISPLACEMENTS, AND FAILURE CRITER'
     1,'ION AT OBSERVATION POINTS')
      WRITE(7,315)
  315 FORMAT(/7X,'*** ALPH IS THE ANGLE FROM THE POSITIVE Z-AXIS TO THE
     8 MAJOR PRINCIPAL STRESS'/)
 613  WRITE(7,25)
   25 FORMAT(1H //,3X,2H I,6X,2HCX,9X,2HCZ,4X,8HPRESSURE,4X,4HSIG1,
     1 6X,4HSIG3,5X,5HALPHA,6X,3H UX,7X,3H UZ,7X,5HF.O.S,6X,4HBETA)
C
C     FAILURE CRITERION AND FACTOR OF SAFETY DETERMINATIONS
C
      DO 620 I=1,MAXI
      IF(ABS(SIG1(I)).LT.0.0001) SIG1(I) = 0.0001
      PSRAT = SIG3(I)/SIG1(I)
      IF(PSRAT.LE.(-RM/150.0).OR.SIG3(I).LE.SIGT) GO TO 622
```

```
C
C     CHECK FOR SHEAR FAILURE
C
      TSC = SQRT(RM*SIGC*SIG3(I)+S*SIGC*SIGC)
      FOS(I) = (SIG3(I) + TSC)/SIG1(I)
      IF(FOS(I).GT.1.0) GO TO 621
      TAUM = 0.5*(SIG1(I) - SIG3(I))
      TCM = 0.25*SIGC*RM
      TCM1 = SQRT(TAUM*TAUM + TAUM*TCM)
      TCM2 = 0.5*TCM
      BETA(I) = 0.5*(180.0/PI)*ATAN(TCM1/TCM2)
      WRITE(7,616) (I,CX(I),CZ(I),PRSS(I),SIG1(I),SIG3(I),ALPHA(I),
     1 UX(I),UZ(I),FOS(I),BETA(I))
  616 FORMAT(1H ,I4,6(1X,G9.3),2G10.4,2(1X,G9.3),4X,13HSHEAR FAILURE)
      GO TO 620
C
C     CHECK FOR TENSILE FAILURE
C
  622 TCT = RM - SQRT(RM*RM + 4.0*S)
      FOS(I) = SIGC*TCT/(2.0*SIG3(I))
      IF(FOS(I).GT.1.0) GO TO 621
      BETA(I) = 0.0
      WRITE(7,617) (I,CX(I),CZ(I),PRSS(I),SIG1(I),SIG3(I),ALPHA(I),
     1 UX(I),UZ(I),FOS(I),BETA(I))
  617 FORMAT(1H ,I4,6(1X,G9.3),2G10.4,2(1X,G9.3),4X,15HTENSILE FAILURE)
      GO TO 620
621   WRITE(7,625)(I,CX(I),CZ(I),PRSS(I),SIG1(I),SIG3(I),ALPHA(I),
     1 UX(I),UZ(I),FOS(I))
  625 FORMAT(1H  ,I4,6(1X,G9.3),2G10.4,1X,G9.3,7X,3HN.A,6X,11HNO  FAILUR
     *E)
  620 CONTINUE
      GO TO 450
  420 IF(NN.GT.0) GO TO 422
      WRITE(7,421)
  421 FORMAT(1H ///,4X,58HSTRESSES AND DISPLACEMENTS AT CENTERS OF BOUND
     1ARY ELEMENTS)
      GO TO 425
  422 WRITE(7,423)
  423 FORMAT(1H ///,4X,45HSTRESSES AND DISPLACEMENTS AT INTERIOR POINTS)
  425 WRITE(7,430)
  430 FORMAT(1H ///,3X,2H I,6X,2HCX,9X,2HCZ,4X,8HPRESSURE,4X,4HSIG1,6X
     1 ,4HSIG3,5X,5HALPHA,6X,3H UX,7X,3H UZ)
      WRITE(7,440)(I,CX(I),CZ(I),PRSS(I),SIG1(I),SIG3(I),ALPHA(I),UX(I),
     .      UZ(I),I=1,MAXI)
  440 FORMAT(1H ,I4,6(1X,G9.3),2G10.4)
  450 CONTINUE
      IF(NN.GT.0) GO TO 503
C
C     GENERATION OF INTERIOR POINTS, STRESSES AND DISPLACEMENTS
C     DETERMINED BY LOOPING TO 105
C
932   NN = NN + 1
      IF(NN.GT.1) GO TO 503
      COS2BI = 1.0
      SIN2BI = 0.0
      NP=0
  504 READ 474,NXP,NZP,XMIN,ZMIN,XMAX,ZMAX
      IF(NXP.LE.0) GO TO 505
  474 FORMAT(2I5,4F10)
      DX=0.
      DZ=0.
      IF(NXP.EQ.1) GO TO 475
      DX=(XMAX-XMIN)/(NXP-1)
  475 IF(NZP.EQ.1) GO TO 476
      DZ=(ZMAX-ZMIN)/(NZP-1)
  476 CONTINUE
      DO 502 I=1,NXP
      DO 502 J=1,NZP
      NP=NP+1
```

```
      CX(NP)=XMIN+(I-1)*DX
      CZ(NP)=ZMIN+(J-1)*DZ
      IF(KXS+KZS.EQ.0)  GO TO 502
      IF(CX(NP).EQ.0.) CX(NP)=.0000000001
      IF(CZ(NP).EQ.0.)CZ(NP)=.0000000001
502   CONTINUE
      GO TO 504
  505 MAXI=NP
      GAUSS=.FALSE.
      GO TO 105
  503 CONTINUE
      STOP
      END
      SUBROUTINE SZONE(X,Y,PRESS,XLIN,YLIN,LPTS,PR)
      DIMENSION XLIN(60,30),YLIN(60,30),LPTS(30),PR(30)
C
C
C S/R TO DETERMINE THE SOIL ZONE OF A POINT.
C
C  LOOP THRU ALL THE LINES.
      PRESS=0.
      DO 40  M=1,30
      LINE = M
      IF(LPTS(LINE).LE.0) GO TO 40
      NUMCRS=0
      ACRSS=1.E30
C     LOOP THRU THE SEGMENTS WHICH MAKE UP THE LINE.
      ISEGS=LPTS(LINE)
      DO 30 ILINE=1,ISEGS
C     CROSS DRAWS A VERTICAL LINE THROUGH X,Y. ON RETURN,
C     IFABOV=1 IF THE VERTICAL LINE INTERSECTS THE SEGMENT ABOVE X,Y
C     IFABOV=-1 IF THE VERTICAL LINE INTERSECTS THE SEGMENT BELOW X,Y
C     IFABOV=0 IF THE VERTICAL LINE DOES NOT INTERSECT THE SEGMENT.
C     YCROSS = THE Y-VALUE OF THE INTERCEPTION.
      CALL CROSS(IFABOV,YCRSS,X,Y,XLIN(ILINE,LINE),YLIN(ILINE,LINE))
      IF(IFABOV)20,30,10
C     CROSSING ABOVE X,Y*IS IT LOWER THAN THE PREVIOUS LOWEST FOR THIS
C         ZONE
10    ACRSS=AMIN1(YCRSS,ACRSS)
      GO TO 30
C     CROSSING BELOW X,Y* INCREMENT THE CROSSING-COUNTER.
20    NUMCRS=NUMCRS+1
30    CONTINUE
      IF(MOD(NUMCRS,2).EQ.0) GO TO 40
C     THE POINT IS WITHIN THE CLOSED LOOP.
C     FIND THE CUMULATIVE PRESSURE.
      PRESS=PRESS+PR(LINE)
40    CONTINUE
   50 RETURN
      RETURN
      END
```